Combining machine learning and mathematical models of disease dynamics to guide development of novel malaria interventions

Authors: Monica Golumbeanu[1,2]†, Guojing Yang[1,2]†, Flavia Camponovo[1,2,3], Erin M. Stuckey[4], Nicholas Hamon[5], Mathias Mondy[5], Sarah Rees[5], Nakul Chitnis[1,2], Ewan Cameron[6,7,8], and Melissa A. Penny[1,2]*

Affiliations:

[1]Swiss Tropical and Public Health Institute, Basel, Switzerland

[2]University of Basel, Basel, Switzerland

[3]Center for Communicable Disease Dynamics, Department of Epidemiology, Harvard T. H. Chan School of Public Health, Boston, MA 02115, USA

[4]The Bill and Melinda Gates Foundation, Seattle, WA, USA

[5]Innovative Vector Control Consortium, Liverpool, United Kingdom

[6]Malaria Atlas Project, Big Data Institute, University of Oxford, Oxford, UK

[7]Curtin University, Perth, Australia

[8]Telethon Kids Institute, Perth Children's Hospital, Perth, Australia

†These authors contributed equally.

Email: *Correspondence to: melissa.penny@unibas.ch

One Sentence Summary: Defining quantitative profiles of novel malaria interventions by combining machine learning with mathematical models of disease transmission

Keywords:

Infectious disease, malaria, novel interventions, mathematical modelling, machine learning

This PDF file includes:

Main Text

Figures 1 to 6

Supplementary Materials

Abstract

While progress to reduce malaria burden appears to be stalling, substantial research is underway to develop next-generation interventions addressing current malaria control challenges. However, due to limited testing early in development, it is currently difficult to predefine optimal intervention specifications to achieve target health goals or prioritize investment in novel candidate interventions. Mathematical models of malaria transmission can provide quantitative evidence to guide this process. Models can simulate deployment and predict the potential impact of a new intervention before testing by considering operational, health-system, population, and disease characteristics. Here, we present a quantitative approach to guide intervention development. Our method relies on consultation with product development stakeholders to define the putative space of novel intervention specifications. Coupling malaria transmission dynamics models with machine learning enables searching this multi-dimensional space and efficiently identifying optimal properties of candidate interventions to reach a specified target health goal. We demonstrate the power of our approach by application to five malaria interventions currently under development. Aiming for health goals of malaria prevalence reduction, we quantify and rank intervention characteristics which are key determinants of health impact. Furthermore, we identify minimal requirements and tradeoffs between operational factors, intervention efficacy and duration to achieve different levels of impact and show how these vary across disease transmission settings. When single interventions cannot achieve significant impact, our method allows finding optimal combinations of interventions fulfilling the desired health goals. Enabling efficient use of disease transmission dynamics models, our approach supports decision-making and resource investment to develop new malaria interventions.

Significance Statement

Novel interventions are needed to reduce malaria burden and tackle insecticide and drug resistance. Developing these interventions entails optimizing their specifications against target health goals. Because clinical evidence is limited early in development, these specifications are defined with little quantitative considerations. Mathematical models simulating disease dynamics can quantify intervention impact; however, their complexity hinders exploring the high-dimensional space of putative intervention characteristics. We established a quantitative approach to guide intervention development through dialogue with product development stakeholders and leveraging models of malaria dynamics with machine learning. Our analysis identifies requirements of efficacy, coverage and duration of effect for five novel malaria interventions to achieve targeted reductions in malaria prevalence, highlighting the role of mathematical models to support intervention development.

.

Introduction

Significant efforts to deploy malaria interventions worldwide over the last decades have led to considerable progress and reduced global malaria prevalence in Africa by half between years 2000 and 2015 (1). Reductions were achieved through a diverse range of interventions (sometimes referred to as “tools” or “products”) including mass distributions of insecticide-treated mosquito nets, indoor residual spraying, rapid diagnosis, as well as efficient artemisinin-based combination therapies (2). However, since 2015, progress has stalled, and several countries have seen an increase in malaria incidence of over 40% (3). Current interventions and malaria control programs are facing major challenges due to funding, spread of drug and insecticide resistance, diagnostic-resistant parasites, as well as supply chain and deployment difficulties (4-6). Strategic investment and timely development of novel interventions is crucial to maintain the progress made and advance towards malaria elimination (3, 7). Two recent reports issued by the World Health Organization (WHO) (8) and the Lancet Commission (9) emphasize the need for novel malaria products, calling for a sustained investment in research and development (R&D).

The malaria product development space has steadily expanded over the last 15 years; these novel products cover a diverse panel, ranging from therapeutic and immunological interventions such as drugs or vaccines to new vector control. Here we provide a brief overview of these novel malaria interventions and illustrate a subset whose properties we explore in detail in our study.

With over 13 new drug compounds under early clinical development (3, 10) and successful collaborative initiatives accelerating drug target discovery (11), new antimalarial therapies are hopefully expected to be rolled out in the next five years (9, 12). Nevertheless, emergence of drug resistance remains a threat for novel drugs, advocating for novel products which ensure a long, sustained protection.

Several malaria vaccine candidates are currently under development, targeting various stages of the malaria transmission cycle, including pre-erythrocytic, blood-stage, and transmission-blocking vaccines (13-15). After 30 years of development, the RTS,S/AS01 pre-erythrocytic vaccine is currently being evaluated in three pilot implementation programs in Malawi, Ghana and Kenya (16, 17). In phase 3 clinical trials in Africa, RTS,S was shown to have a clinical

101 efficacy of 36 - 50% in children aged 5-17 months old (18) with potential to avert mortality in
102 children, suggesting that tailored, regional implementation in combination with other
103 interventions may be impactful to reduce burden in moderate to high transmission intensities
104 (19-22). Several other vaccines are in Phase 2 clinical studies, and recently the protein-based
105 vaccine R21 demonstrated a clinical efficacy of up to 77% (23). More recently, biological
106 alternatives to vaccines include passive immunization with injectable small molecules (24, 25) or
107 monoclonal antibodies (26-28). Conferring protection against malaria during several months and
108 safe to administer during pregnancy, monoclonal antibodies are seen as potential interventions
109 for seasonal malaria chemoprevention and protection of risk groups such as travelers to endemic
110 regions. While promising, they are still at early development stages and their future is open-
111 ended. The first human trials of monoclonal antibodies are currently ongoing (9, 28).

112 Like for malaria medicines, the area of vector control has equally seen an active development
113 over the past years, with over 10 different categories of novel products aiming to reduce both
114 indoor and outdoor mosquito biting (29-31). These include new insecticides (32, 33), vector traps
115 (34, 35), as well as genetically-altered mosquitoes or gene drives (36-38). Furthermore,
116 improved housing has been shown to significantly reduce indoor mosquito biting (39, 40), and a
117 new R&D area has emerged with innovative house traps or lures to supplement classical indoor
118 interventions (41). An example of a novel intervention in this category are eave tubes treated
119 with insecticide to kill host-seeking mosquitoes, which has been evaluated across several
120 locations in Africa and shown efficacy and superior cost-effectiveness to existing interventions
121 (42). As interventions targeting indoor biting are less effective in areas where transmission is
122 mainly caused by outdoor mosquito biting, development of novel vector control targeting
123 outdoor transmission is increasingly needed (43). Attractive targeted sugar baits have
124 demonstrated a reduction of *Anopheles gambiae* outdoor density of 90% in field trials, being an
125 affordable and scalable prospective tool for reducing outdoor transmission (44, 45).

126 The current pipeline for malaria interventions is supported by several stakeholders, with the
127 Medicines for Malaria Venture (MMV) driving innovation for medicines, and the Innovative
128 Vector Control Consortium (IVCC) overseeing development for vector control, both sides
129 receiving continuous support from other entities such as the Program for Appropriate

130 Technology in Health - Malaria Vaccine Initiative (PATH-MVI), the Bill and Melinda Gates
131 Foundation (BMGF) and the WHO (9).

132 Malaria products under development are defined through Target Product Profiles (TPPs) which
133 guide R&D investments. Target Product Profiles (TPPs) are dynamic documents commonly used
134 during the development of a cutting-edge medical product, defining its required characteristics to
135 fulfill an unmet health need (46). By offering a comprehensive snapshot of the development
136 process at any given point in time, a TPP constitutes a vital reference for dialogue between
137 various stakeholders to guide decisions on the development direction to be pursued (46-50). A
138 well-constructed TPP is thus essential for efficient resource allocation and success during the
139 development phase (46, 50). However, the process of establishing TPPs relies on minimal
140 clinical or quantitative evidence. They are often set by expert opinion and consensus based on
141 limited quantitative consideration of the complex dynamics of disease or predictions of the likely
142 intervention impact while achieving the identified unmet health need (51). Furthermore, few
143 malaria TPPs consider operational aspects such as deployment coverage in addition to product-
144 specific characteristics such as efficacy or half-life. This has implications for the appropriate
145 definition of intervention effectiveness characteristics according to local health systems and
146 health targets (46, 51, 52). Given the large amount of malaria interventions currently in the
147 development pipeline, a systematic approach is essential to inform development decisions and
148 prioritization of novel interventions to ensure a sustainable investment of resources and a fast
149 pace of innovation. Currently, there is no approach incorporating quantitative evidence and the
150 aforementioned operational aspects in malaria product development from early development
151 stages.

152 Mathematical models of malaria transmission dynamics can be used to bridge this gap, as they
153 quantitatively estimate the impact of interventions while including considerable evidence of
154 disease progression and transmission, host immunity, as well as environmental or health system
155 dynamics and their interaction with interventions (53, 54) (Fig. 1). These models have been used
156 extensively to estimate the impact of malaria interventions and to optimize intervention packages
157 for specific geographies (55-59).

158 One example of an established malaria model is OpenMalaria (60), an open source, stochastic,
159 individual-based model which simulates malaria epidemiology and transmission dynamics across
160 humans and mosquitoes (Fig. 1, Tables S1.1-S1.3). In this model, the pattern of yearly malaria
161 infection in the absence of interventions is determined by the input entomological inoculation
162 rate (EIR) (Fig. S2.1). Each infected human host in the simulated population has an associated
163 parasite density and duration of infection. Each infection is modelled individually, and follows a
164 modelled transmission cycle which captures effects such as immunity, infectiousness to
165 mosquitoes, morbidity or mortality. During the simulation, a wide range of human and vector
166 interventions can be applied, affecting the transmission cycle at various stages. Setting-specific
167 characteristics such as population demographics, mosquito species entomological characteristics
168 or seasonality are explicitly modelled. Various health outcomes are monitored over time
169 including Plasmodium falciparum prevalence of infections (*Pf*PR), uncomplicated clinical
170 disease, severe disease in and out of hospital, and malaria mortality. The disease dynamics
171 assumptions of the model have been extensively described and validated with field data in
172 previous studies, notably in a dedicated issue of The American Journal of Tropical Medicine and
173 Hygiene (60) and very recently revisited in (61). In addition, several major consensus modeling
174 studies have shown the validity of the OpenMalaria predictions with regard to the public health
175 impact of the RTS,S vaccine (55), mass drug administration (62) or vector control (63).
176 Additional validation studies conducted using published data on various malaria indicators such
177 as EIR, *Pf*PR, incidence and mortality have shown that OpenMalaria accurately captures the
178 seasonally-dependent relationships between these indicators (64). An overview of the key model
179 components is depicted in Fig. 1 and is accompanied by a description of the disease model
180 assumptions and parameters in Materials and Methods and in Tables S1.1- S1.3.

181 Due to absence of data at early intervention development stages and computational limitations in
182 exploring a highly combinatorial parameter space of presumed intervention characteristics,
183 mathematical models such as OpenMalaria have been mainly used at late stages during the
184 development of a new intervention; for example, to predict likely impact or cost-effectiveness
185 from data collected in Phase 3 clinical trials (55, 65-69). As yet, mathematical models have only
186 been minimally applied in directing the design of new interventions, or in understanding how
187 intervention-specific, epidemiological and systems factors jointly contribute to impact. Model
188 investigations are usually informed by scenario analysis accounting for the delivery and target

age groups, as well as properties of the new intervention pre-defined or informed by late clinical trials (62, 70-72). In these constrained scenarios, high model and parameter complexity tend to obscure the complex relationships between intervention parameters, operational factors, health outcomes and public health impact (73). Exhaustive scenario analyses are computationally expensive, rendering the full exploration of all possible interventions for a disease, in conjunction with all possible delivery scenarios, combinatorically infeasible. Previous approaches using disease models to inform TPPs have tackled the combinatorically-complex parameter space by only exploring a discrete, constrained set of parameters (74-76). These approaches have provided insightful knowledge and emphasized the importance of using disease models for defining TPPs. Nevertheless, they have provided a constrained view of intervention specifications.

Here we propose a different approach (Fig. 2), where epidemiological models guide from early stages the development of novel disease interventions designed to achieve quantified health goals, placing the end goal of public health impact at the center of decision making. To do this efficiently, we undertook an engaging, iterative exchange with malaria product development stakeholders to define desired outcomes and the likely delivery use-cases of new malaria interventions. Then, we used machine learning combined with mathematical models to perform a directed search of the entire space of intervention profiles, to define properties of new interventions that will achieve the desired health goals. We used Gaussian processes (GPs) (77) to generate computationally light emulators of the established OpenMalaria model of malaria dynamics. These emulators accurately captured the non-linear relationships between properties of deployed interventions, operational factors and resulting health outcomes. They allowed us to efficiently perform sensitivity analyses of intervention and health system parameters on predicted public health impacts at low computational cost. Furthermore, by coupling emulators with nonlinear optimization techniques, we constructed a predictive framework that identified key determinants of intervention impact as well as the minimal intervention profiles required for achieving a given health goal (Fig. 2).

We covered a diverse spectrum of interventions in the malaria development space, pertaining to 1) anti-infective monoclonal antibodies, 2) anti-infective vaccines, 3) transmission-blocking vaccines, 4) outdoor attractive targeted sugar baits, and 5) eave tubes. We used our approach to

1) understand the link between their characteristics and the resulting impact and 2) to define the requirements of these interventions in terms of coverage, efficacy and duration of their effect to reach desired prevalence reduction goals contingent on operational constraints (Fig. 2). Our approach illustrates how the use of mathematical models enables translation of R&D efforts into potential impact. In this paper, we show how modelling can support this process, and introduce a framework that quantitatively defines malaria product characteristics within TPPs.

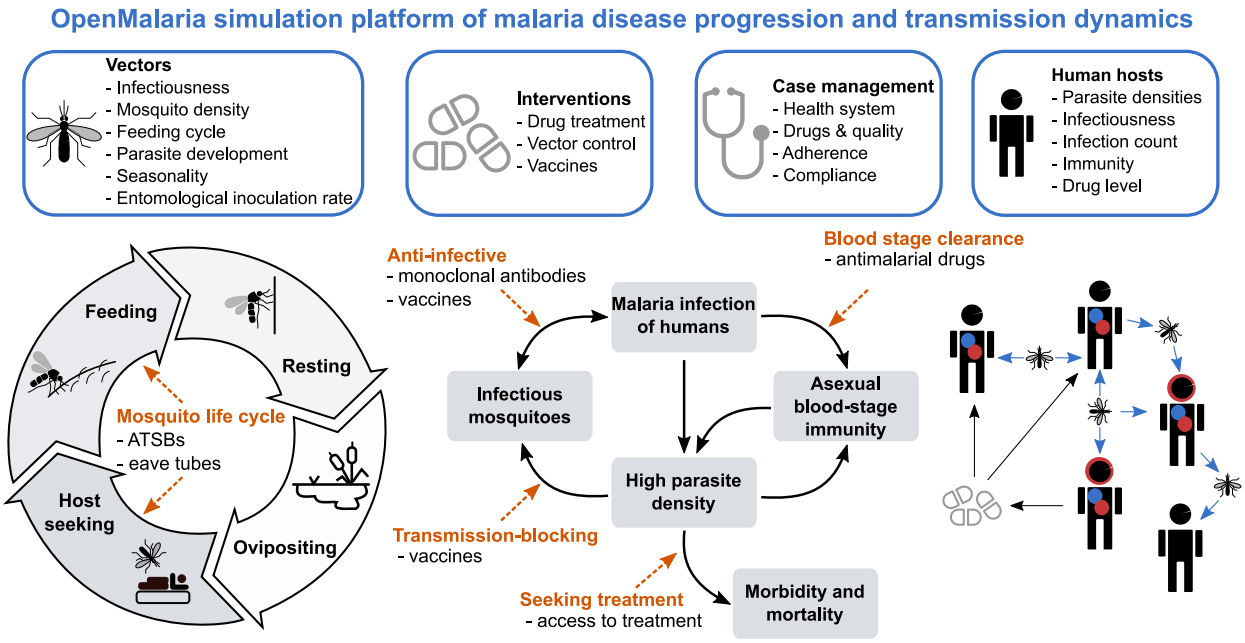

Fig. 1 Simulation of malaria transmission dynamics with OpenMalaria: model schematic
The key components specified in the model are displayed on the top row including vector, intervention, case management and human host-specific factors. Below, a detailed representation of the intrinsic modelled mosquito feeding and host transmission cycles are provided. The dotted, orange arrows mark the action and targets of the modelled interventions in this study which are also indicated below the arrows. ATSBs stands for attractive targeted sugar baits. A detailed overview of model assumptions and parameters is provided in Tables S1.1-S1.3, and in Materials and Methods.

Results

A disease model and machine learning approach to quantitatively define malaria interventions

Our approach (Fig. 2) started with an iterative consultation with product development experts to build sensibly informed TPP simulation scenarios, i.e. to define the breadth, range and intervention profiles to simulate with OpenMalaria for the five considered malaria interventions. Accordingly, we collaborated with the BMGF and the product development partnerships PATH-MVI and IVCC. For each new intervention in the portfolio of PATH-MVI, IVCC and others, we undertook several expert discussion groups to catalogue the ranges of potential intervention effectiveness; potential delivery strategies; parasite or vector targets; the likely properties in terms of action (target), efficacy, duration and decay; and use cases/delivery consisting of age target, mass intervention, and yearly deployment (see Section 1 of Materials and Methods for a detailed description of the setup for iterative dialogue with malaria product development stakeholders).

The defined health goals in the present analysis were true Plasmodium falciparum malaria prevalence reductions (denoted as $Pf\mathrm{PR}_{0\text{-}99}$ when evaluated in all ages and $Pf\mathrm{PR}_{2\text{-}10}$ when evaluated in 2-10-year-old individuals) observed in the first year and in the third year following intervention deployment (Fig. 3A). We modelled each intervention by identifying their action on parasite or vector targets during the malaria transmission cycle (orange arrows in Fig. 1). Accordingly, each intervention was defined by its target, the ranges of the deployment coverage, initial efficacy, half-life or duration of effect as well as the type of decay (see Section 2 of Materials and Methods, Fig. S2.2, and Table 1 for detailed intervention specifications). For simplification, the words ‘half-life and ‘duration’ are used interchangeably to describe the longevity of an intervention effect. The simulated malaria transmission settings were defined by the yearly EIR, seasonality level, access to treatment, as well as proportion of indoor mosquitoes. Table 1 summarizes the results of the discussions with stakeholders to set up the OpenMalaria simulation scenarios and presents a comprehensive description of all the subsequent intervention characteristics explored in our study as well as the simulated malaria transmission settings.

Next, within the *“Disease model”* component of our approach (Fig. 2A), malaria transmission was modeled by the means of the established, stochastic, individual-based model OpenMalaria

265 (60) (Fig. 1, Fig. 3A, Tables S1.1 – S1.3). In our analysis, we used a previously published
266 calibration of OpenMalaria which reflects demographics, epidemiology, entomology, health
267 system and seasonality (Fig. S2.1) of a health facility catchment area in Tanzania (78-80).
268 Intervention impact in the current study was assessed through predicted reduction in *Pf*PR$_{0\text{-}99}$,
269 corresponding to true infection prevalence and not patent (detected with a diagnostic such as
270 rapid diagnostic test (RDT), or polymerase chain reaction (PCR), Fig. 3A, S2.3, S3.1-S3.4). We
271 simulated malaria epidemiology and transmission dynamics within various transmission settings
272 based on the Tanzanian calibration. These settings cover a broad spectrum of transmission and
273 mosquito biting behavior archetypes relevant for attaining general guiding principles in the early
274 development phase of new malaria interventions. A comprehensive set of simulated scenarios
275 was built by uniformly sampling the parameter space defined by intervention and transmission
276 setting characteristics (defined by the parameters emphasized in bold under *"Tool*
277 *specifications"* and *"Setting"* components in Fig. 2A and detailed in Table 1). These scenarios
278 were simulated with OpenMalaria, yielding an extensive database of disease outcomes for the
279 defined scenarios.

280 In the machine learning part of the approach (illustrated in the *"Machine learning"* panel of
281 Figure 2A), the database of simulated scenarios and corresponding outcomes (*Pf*PR$_{0\text{-}99}$
282 reductions following intervention deployment) was used to train predictive models for the
283 OpenMalaria simulation results (for an example of simulated *Pf*PR$_{0\text{-}99}$ time series with
284 OpenMalaria see Fig. 3A and S3.1). For this purpose, we trained a Heteroskedastic Gaussian
285 process (GP) model for each intervention and transmission setting (see detailed training
286 procedure in Section 3 of Materials and Methods). The trained GP models accurately captured
287 the dependencies between the disease model input parameters and the output intervention impact
288 (Fig. 3B-C), and were thus able to reliably predict the reduction in *Pf*PR$_{0\text{-}99}$ attributable to any
289 input intervention characteristics in a given malaria transmission setting. Precisely, the
290 correlation between true and predicted *Pf*PR$_{0\text{-}99}$ reduction on out-of-sample test sets exceeded
291 95% while the absolute mean error was below 3% for all trained GP models (Fig. 3B, S4.1-S4.3,
292 Table S4.1). As a result, the trained predictive GP models acted as emulators of the complex
293 modelled parameter dynamics and non-linear relationships within the individual-based
294 mathematical model of malaria transmission (Fig. 3C, S4.5-S4.6) and could predict the disease
295 outcome for the given health goal and any set of input parameters.

Due to the significantly less intensive computational requirements of our emulator-based approach compared to OpenMalaria, we could reduce the analysis execution time by several orders of magnitude. This allowed conducting elaborate sensitivity and optimization analyses which required a large number of parameter set evaluations and would otherwise not have been possible (Fig. 3D, S4.7). Thus, the trained GP emulators could be efficiently and promptly used in downstream analyses to explore the multi-dimensional space of intervention properties to design TPPs of new malaria interventions (panel *"Target product profiles"* on Fig. 2A), i.e., to identify the drivers of their impact and their quantitative properties meeting the health goals previously defined (Fig. 2B-C). Specifically, through global sensitivity analysis, we identified the key determinants of intervention impact (Fig. 2B). In addition, we performed a constrained search for intervention and delivery profiles (TPPs) that maximized impact under a particular health goal, given concrete, expert-informed, operational constraints such as possible deployment coverage, or feasible intervention properties such as efficacy or duration of protection (Fig. 2C). The results of these analyses are detailed in the following sections and illustrated for seasonal transmission settings with high indoor mosquito biting. Results for the other simulated transmission settings (perennial settings and for other mosquito biting patterns) are provided in the supplement (additional sensitivity analysis results presented in Fig. S5.1-S5.2, additional optimization results presented in Fig. S6.1 – S6.6 and S7.1-S7.5) and summarized in Table 2.

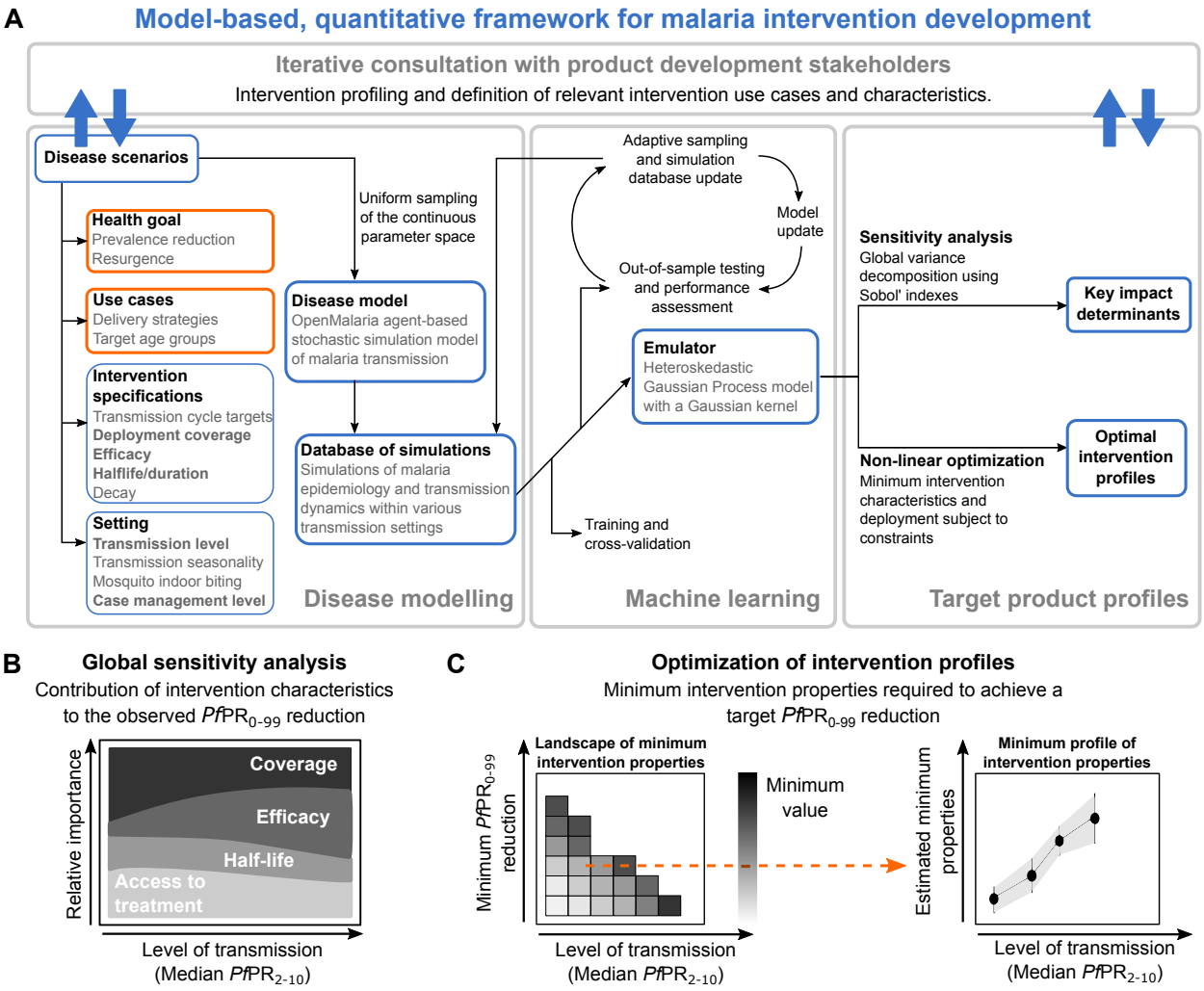

Fig. 2 Overview of the approach to quantitatively define TPPs of novel malaria interventions. ***(A)*** *Schematic description of the proposed model-based, quantitative framework to guide malaria product development. The results of applying this framework to guide development of five novel malaria interventions are provided for a range of median simulated, true* $PfPR_{2\text{-}10}$ *(before intervention deployment) and are schematically described as follows:* ***(B)*** *Global sensitivity analysis for identifying the determinants of intervention impact: colors define the intervention specifications, deployment coverage, and health system access levels varied in the analysis; the magnitude of the colored area at different levels of transmission (x axis) represent the relative importance (y axis) attributable to those factors driving the observed* $PfPR_{0\text{-}99}$ *reductions following intervention deployment.* ***(C)*** *Optimization of intervention properties to achieve desired health goals: the heatmap (left side) displays, for a given intervention property (coverage, efficacy or half-life), the landscape of minimum required values to achieve various target* $PfPR_{0\text{-}99}$ *reductions. Each row of the heatmap corresponds to a target of* $PfPR_{0\text{-}99}$ *reduction and constitutes a minimum profile of the considered intervention characteristic (right side).*

335 **Table 1. Description and ranges of OpenMalaria simulation variables (interventions and**
336 **transmission settings) defined by consultation with product development stakeholders.**

	Intervention	Coverage	Initial efficacy	Half-life or duration (years)	Decay type
Simulated malaria intervention properties	Preventing infection				
	Anti-infective vaccine	0 – 1	0.3 – 0.95	0.5 – 5	Weibull (k = 0.8) (Sigmoidal)
	Anti-infective monoclonal antibody	0 – 1	0.3 – 0.95	0.167 – 0.667	Weibull (k = 3) (Biphasic)
	Blood stage clearance				
	Antimalarial drugs	0 – 1	0.8 – 1	0 – 0.1667	Exponential
	Transmission blocking				
	Vaccine	0 – 1	0.3 – 0.95	0.5 – 5	Weibull (k = 0.8) (Biphasic)
	Preprandial killing effect (affects indoor mosquito biting)				
	Eave tubes	0 – 1	0.3 – 0.99	0.5 – 5	Weibull (k = 3) (Sigmoidal)
	Preprandial and postprandial killing effect (affects outdoor mosquito biting)				
	Attractive targeted sugar baits	0 – 1	0.7 – 0.99	0.167 – 0.667	Step
Simulated malaria transmission settings	EIR range: 1 – 25, representing a *Pf*PR$_{0\text{-}99}$ of 13-88% and a *Pf*PR$_{0\text{-}2}$ of 7.2-74% Case management (baseline scenario) range: 0 – 0.8, corresponding to a probability range of seeking care within 5 days from the onset of fever of 0 - 0.5 Seasonality levels: 1. high seasonal setting with one transmission peak over a year 2. perennial setting with constant yearly transmission Proportion of indoor-biting mosquitoes, out of total indoor and outdoor biting mosquitoes: 3. high (0.8) 4. medium (0.5) 5. low (0.2)				

337 *The varied parameters within the OpenMalaria simulations include the characteristics of*
338 *applied malaria interventions (see also Fig S2.2 for visual ranges of these parameters), as well*
339 *as malaria transmission setting characteristics.*
340
341

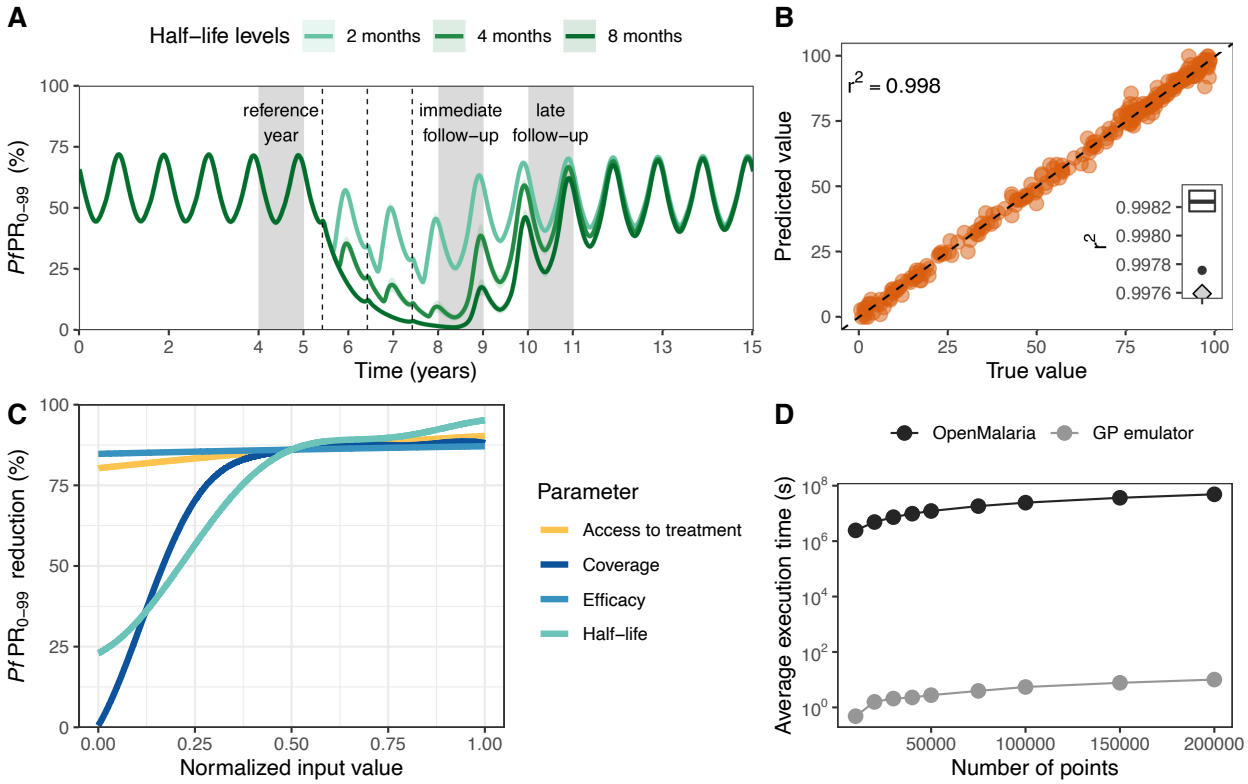

Fig. 3: Training predictive GP emulators of simulated intervention impact with OpenMalaria. *Examples are shown for attractive targeted sugar baits (ATSBs); results for other interventions are shown in the Supplement in Fig. S3.1, S4.2-S4.7, Table S4.1.* ***(A)*** *Simulated malaria $PfPR_{0\text{-}99}$ time series at EIR=10 where ATSBs were deployed at a coverage of 70% and had an efficacy of 70%. Results are shown for three intervention half-life levels. The dotted lines indicate when interventions were applied (beginning of June). The effect of the interventions was assessed by evaluating the yearly average $PfPR_{0\text{-}99}$ reduction in all ages relative to the year prior deployment (first grey block). Two outcomes were assessed, depending on whether the average prevalence was calculated across the next year after deployment (immediate follow-up), or across the third year after deployment (late follow-up).* ***(B)*** *Correlation between simulated true (x axis) and predicted (y axis) $PfPR_{0\text{-}99}$ reduction with a GP emulator trained to predict the immediate impact of ATSBs. The GP emulator was trained in a cross-validation scheme (distribution of the Pearson correlation coefficient r^2 shown in boxplot) and validated on an out-of-sample test set (r^2 left upper corner and grey diamond on the boxplot in the right lower corner).* ***(C)*** *Relationship between each normalized input parameter and the resulting $PfPR_{0\text{-}99}$ reduction predicted with the trained GP emulator. Each parameter was in turn varied within its defined ranges (Table 1) while the other parameters were set to their average values.* ***(D)*** *Estimated CPU execution time for varying sizes of input parameter sets evaluated with OpenMalaria (black) and with the trained GP emulator (grey).*

363
364 *Impact of malaria interventions and the importance of their characteristics*

365 Following simulation with OpenMalaria of deployment of each of the studied interventions
366 through mass administration campaigns over several years (see Materials and Methods), we first
367 analyzed the predicted distributions of reduction in true *Pf*$PR_{0\text{-}99}$. We found that, in general,
368 when aiming for substantial, prompt reductions in prevalence for this particular health target,
369 vector control was by far the most impactful intervention across all settings. Conversely,
370 monoclonal antibodies, anti-infective and transmission-blocking vaccines had a more
371 pronounced impact in low-transmission settings compared to endemic settings (Fig. 4A, S3.1-
372 S3.4, Table 2).

373 Sensitivity analysis indicated that the impacts of these interventions on malaria prevalence were
374 driven by different characteristics of their efficacy profiles, deployment strategies, or access to
375 care for treatment of clinical cases, for either short and long impact follow-up. Across a large
376 proportion of the simulated scenarios, over all parasite and vector targets and interventions,
377 coverage of the deployed intervention was overwhelmingly the primary driver of impact
378 especially in low transmission settings (Fig. 4B-F, S5.1-S5.2). For immunological interventions,
379 the impact of short-term passive immunizations such as monoclonal antibodies relied on their
380 deployment coverage and the health system (Fig. 4B, S5.1). In contrast, for long-acting
381 interventions such as vaccines, impact was driven by deployment coverage and efficacy (Fig.
382 4C-D, S5.1). Highly-efficient vector control interventions such as attractive targeted sugar baits
383 had a strong effect on prevalence (Fig. 4A), and their duration of effect was the most important
384 determinant (Fig. 4E, S5.2). The immediate impact of long-term vector control interventions
385 such as eave tubes was driven by deployment coverage, while their half-life was a key
386 determinant for preventing resurgence (Fig. 4F, S5.2). Determinants of impact were identified
387 for both immediate and late follow-up, when interventions were applied once per year for three
388 years (full intervention specifications are provided in Materials and Methods and results for other
389 settings and interventions are shown in Fig. S5.1-5.2 and Table 2).

390

391

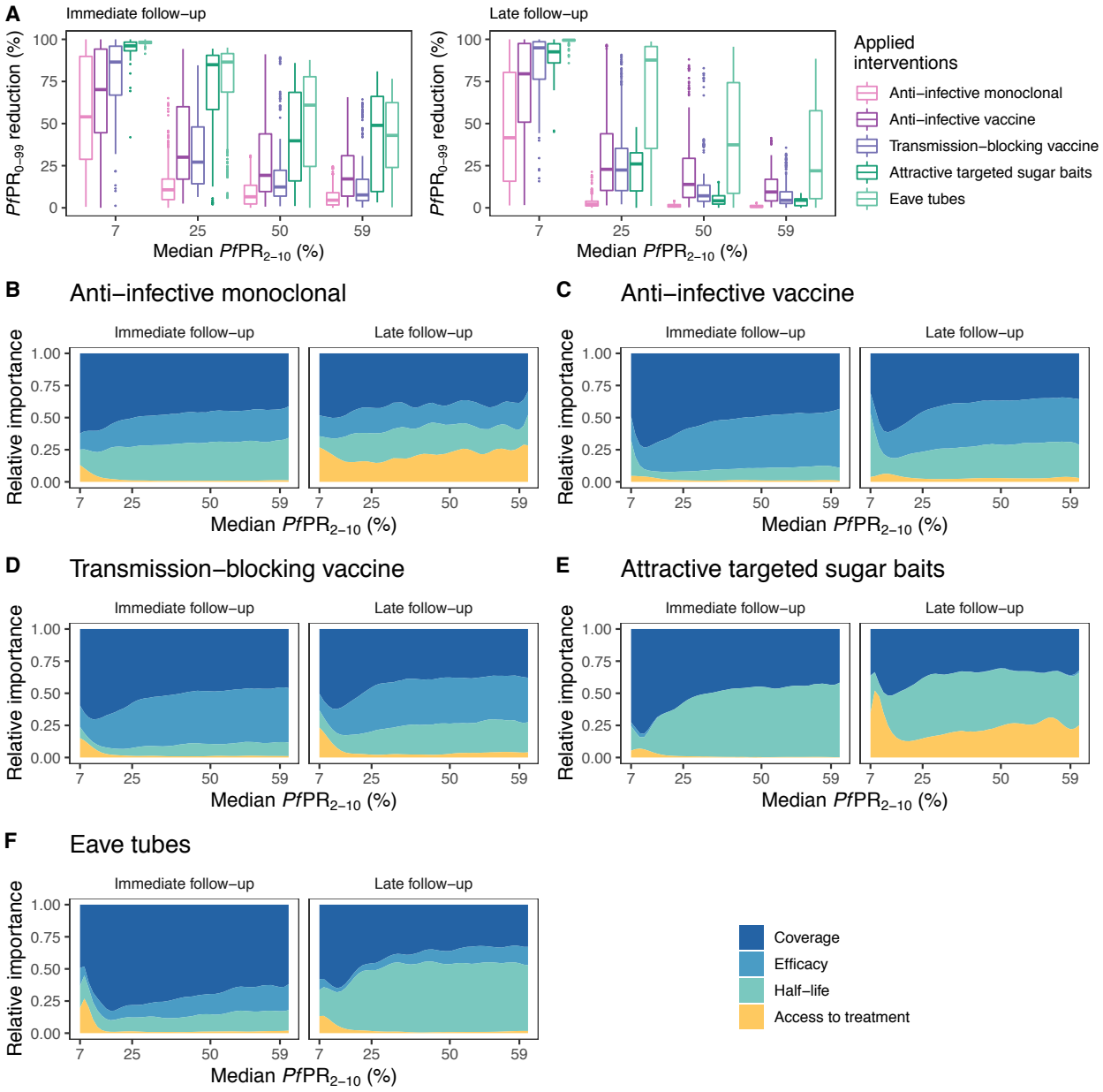

Fig. 4: Effects of novel malaria interventions on *Pf*PR$_{0\text{-}99}$ and their key drivers of impact
(A) *Distribution of obtained reduction in PfPR$_{0\text{-}99}$ across the simulated scenarios with OpenMalaria following deployment of various malaria interventions under development (shown with different colors) for a range of simulated transmission settings (specified by median true PfPR$_{2\text{-}10}$ rounded values, x axis). Each boxplot displays the interquartile range (box), the median value (horizontal line), the largest and smallest values within 1.5 times the interquartile range (whiskers), and the remaining outside values (points) of the PfPR$_{0\text{-}99}$ reduction values obtained across all the simulations for each given setting. The remaining figures present the results of global sensitivity analysis showing, across the same simulated PfPR$_{2\text{-}10}$ settings, the contribution of intervention characteristics to the resulting PfPR$_{0\text{-}99}$ reduction for anti-infective monoclonal antibodies* ***(B)****, anti-infective vaccines* ***(C)****, transmission-blocking vaccines* ***(D)****, attractive targeted sugar baits* ***(E),*** *and eave tubes* ***(F)****.*

405 *Minimal requirements of novel malaria interventions to achieve a defined health goal*

406 For the five aforementioned malaria interventions, we explored their optimal properties for a
407 broad set of *Pf*PR$_{0\text{-}99}$ reduction targets, creating landscapes of intervention profiles according to
408 their minimal characteristics across various transmission settings (Fig. 5-6, S6.1-S6.6, S7.1-
409 S7.5). These landscapes provide a comprehensive overview of the intervention potential
410 capabilities and limitations in achieving a desired health goal. For example, as opposed to an
411 anti-infective monoclonal antibody which required high efficacy and duration to achieve large
412 *Pf*PR$_{0\text{-}99}$ reductions in only a limited number of settings (Fig. 5A-B, S6.1-S6.2), attractive
413 targeted sugar baits that kill mosquitoes achieved a wider range of target *Pf*PR$_{0\text{-}99}$ reductions in
414 high-transmission settings as well (Fig. 6A-B, S6.5). Similarly, while anti-infective and
415 transmission-blocking vaccines had comparable requirements in achieving similar *Pf*PR$_{0\text{-}99}$
416 reduction targets in settings with lower transmission (*Pf*PR$_{2\text{-}10}$ < 30%), anti-infective vaccines
417 showed a higher potential and reached additional targets in high-transmission, endemic settings
418 (Fig. 5C-F).

419 For a detailed overview of landscapes of intervention profiles for all simulated settings and
420 interventions see Fig. S6.1-S6.6. These landscapes together with the results of the sensitivity
421 analysis offer an evidence-based prioritization of resources during the product development
422 process. For example, we found that while both efficacy and half-life were important for
423 immediate prevalence reductions with monoclonal antibodies, their effect was limited in
424 preventing resurgence and was only supported by high case-management levels (Fig. 4-5, S5.1,
425 S6.1-S6.2). Conversely, the efficacy of anti-infective vaccines determined their immediate
426 impact, whereas half-life of effect had greater importance for achieving and maintaining *Pf*PR$_{0\text{-}99}$
427 reductions (Fig. 4-5, S5.1, S6.3-S6.4). These results suggest that if monoclonal antibodies were
428 to support preventing resurgence, then R&D efforts should focus on increasing and establishing
429 antibody longevity.

430 Our analysis showed that coverage was a primary driver of impact (Fig. 4B-F, S5.1-S5.2). This
431 result has important implications for interventions requiring multiple applications to achieve high
432 efficacy, indicating that it is of crucial importance to target both vulnerable populations and the
433 proportion of the population missed by the intervention. While, for some interventions, high

434 coverage deployment might be very difficult or impossible to achieve, our analysis showed that
435 this can be alleviated by increasing the deployment frequency or through deploying
436 combinations of interventions, which may also have cost implications (Fig. 5B, 5D, 5F, 6B,
437 S6.1-S6.5, S7.1-7.4).

438 We found that combining several interventions targeting different stages in the transmission
439 cycle can strongly affect the minimum requirements of a putative new intervention, potentially
440 increasing the impact of an otherwise weaker intervention. For example, for an anti-infective
441 monoclonal antibody with an initial half-life of 4 months and deployed at a coverage of 60%
442 reflecting completion of multiple doses, achieving a prevalence reduction of 80% was impossible
443 when deployed once yearly for three years (Fig. 5A, S6.1). Furthermore, achieving the
444 aforementioned health goal required an efficacy of over 80% when the intervention was
445 deployed twice per year for three years (Fig. S6.2). However, when deployment of the
446 monoclonal antibody was coupled with a short half-life blood-stage parasite treatment such as
447 dihydroartemisinin-piperaquine or artemether-lumefantrine, its minimum required efficacy was
448 considerably reduced for both delivery frequencies (Fig. 5B, S6.1-S6.2, S7.1). Conversely, if we
449 assumed an initial efficacy of 85% for the monoclonal antibody, we found that its minimal
450 required half-life could be reduced if we deployed this intervention in combination with a blood-
451 stage parasite clearing drug (Fig. 5B, S6.1-S6.2, S7.1). These results partly motivated the current
452 development of anti-infective monoclonal antibodies; use-cases will likely include deployment
453 with existing or new antimalarial treatment.

454 When coupled with a short half-life blood-stage parasite treatment, requirements of coverage,
455 efficacy and half-life were reduced also for anti-infective and transmission blocking vaccines to
456 achieve the targeted reductions of $Pf\mathrm{PR}_{0\text{-}99}$ (Fig. 5C-F, S6.3-6.4, S7.2-S7.3). In particular, for
457 high-transmission settings ($Pf\mathrm{PR}_{2\text{-}10} > 30\%$), given an RTS,S-like half-life of 7 months, both
458 anti-infective and transmission-blocking vaccines could not achieve a defined prevalence
459 reduction goal of 70% if deployed singly (Fig. 5D, 5F). This was the case for any deployment
460 coverage given an initial efficacy of 85% as well as for any efficacy given a deployment
461 coverage of 60%. Combining vaccine deployment with a blood-stage drug not only significantly
462 expanded the achievable health targets also to high-transmission settings, but also reduced
463 vaccine properties requirements. Our analysis revealed that anti-infective vaccines had a higher

potential than transmission-blocking vaccines, requiring less performance and achieving higher prevalence reductions targets also in higher transmission settings. When combined with blood-stage parasite treatment, the coverage, efficacy and half-life requirements of anti-infective vaccines were lower compared to those of transmission-blocking vaccines for the same prevalence reduction targets (Fig. 5, S6.3, S6.4, S7.2, S7.3).

We also showed that a modified deployment schedule could reduce requirements for properties of some interventions. For example, for highly-efficacious attractive targeted sugar baits, higher coverage and half-life were required when implemented once per year for three years compared with an accelerated delivery schedule of twice per year for three years (Fig. 6A-B). Except for high transmission settings ($Pf\mathrm{PR}_{2\text{-}10} > 41\%$), a minimum required efficacy of 70% was sufficient to attain the desired health goal for the majority of settings and for both delivery schedules (Fig. 6A-B, Fig. S6.5, Fig. S7.4). This result was also reflected by the sensitivity analysis (Fig. 4E). Accordingly, the variation in intervention efficacy in the ranges investigated had little importance in driving the intervention impact. This result suggests that, once a vector control intervention such as attractive targeted sugar baits has achieved a high killing efficacy (here equal to or greater than 70%), a next step of optimizing other intervention characteristics such as deployment coverage or duration would lead to higher impact. These results demonstrate the strength of our analysis in identifying the intervention characteristics to be prioritized for R&D.

Our comprehensive analysis was applied to explore determinants of impact and required profiles of interventions across two seasonal settings (seasonal and perennial) and three types of mosquito biting patterns (low, medium and high indoor biting). A detailed overview of impact determinants and optimal intervention profiles is presented in the Supplementary Materials (Fig. S6.1-S6.6, S7.1 – S7.5) and additional key results are summarized in Table 2.

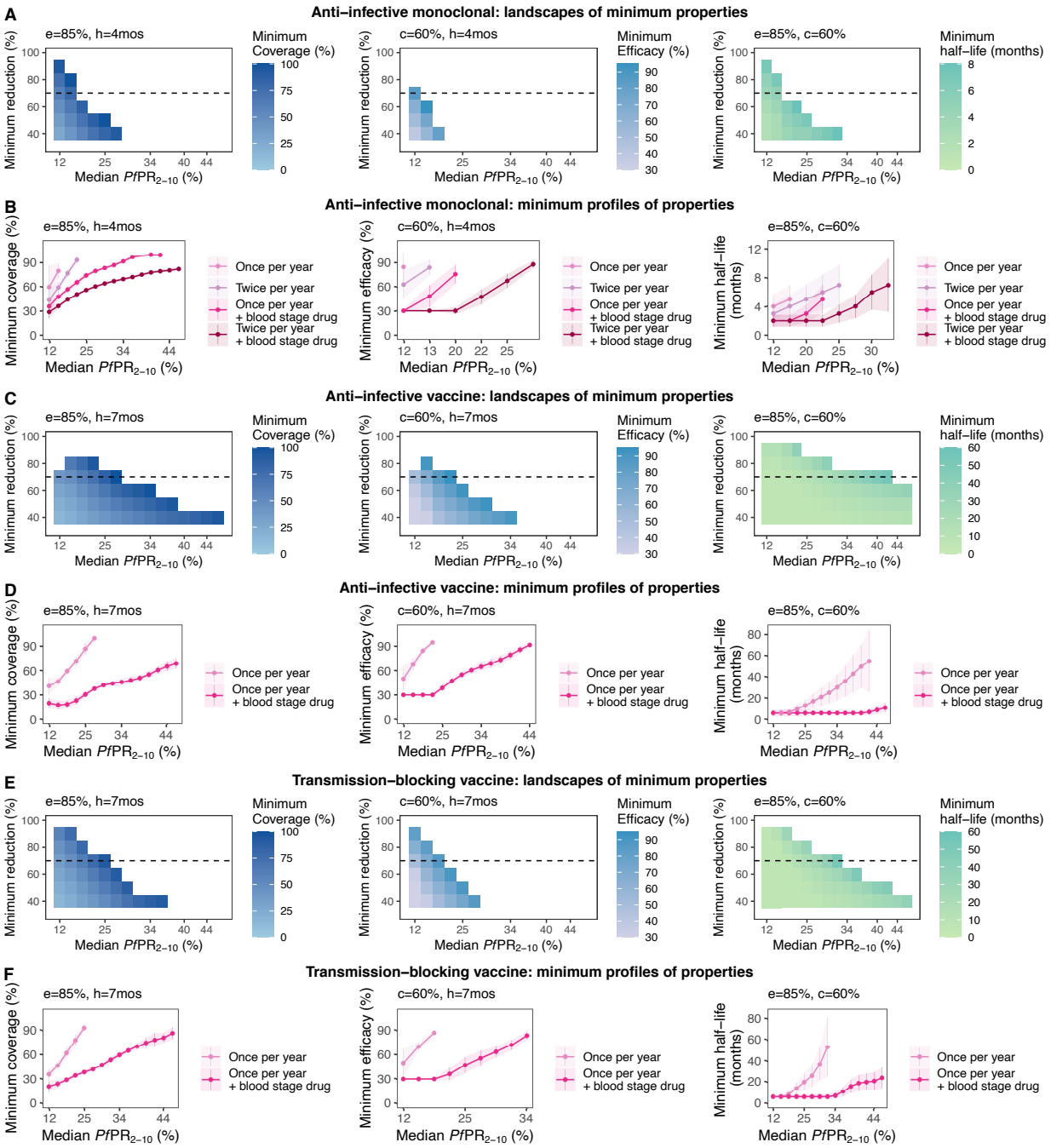

Fig. 5: Estimated optimal intervention profiles (TPPs) for immunological interventions. *The heatmaps in figures **(A)**, **(C)** and **(E)** display, for each intervention property (coverage, efficacy or half-life), the landscape of minimum required values to achieve various target $PfPR_{0-99}$ reductions (y axis) across different simulated transmission settings (true $PfPR_{2-10}$ rounded values, x axis). Each row of the heatmap corresponds to a target of $PfPR_{0-99}$ reduction and constitutes the minimum required profile of the considered intervention. For a selected health goal of 70% $PfPR_{0-99}$ reduction (dotted line on each heatmap), figures **(B)**, **(D)** and **(F)** present in detail how the minimum profile changes with transmission intensity. Each intervention characteristic was minimized in turn, while keeping the other characteristics fixed (values*

marked on each figure where c = coverage, e = efficacy, and h = half-life). The simulated access to treatment, corresponding to a probability of seeking care within 5 days, was 25%.

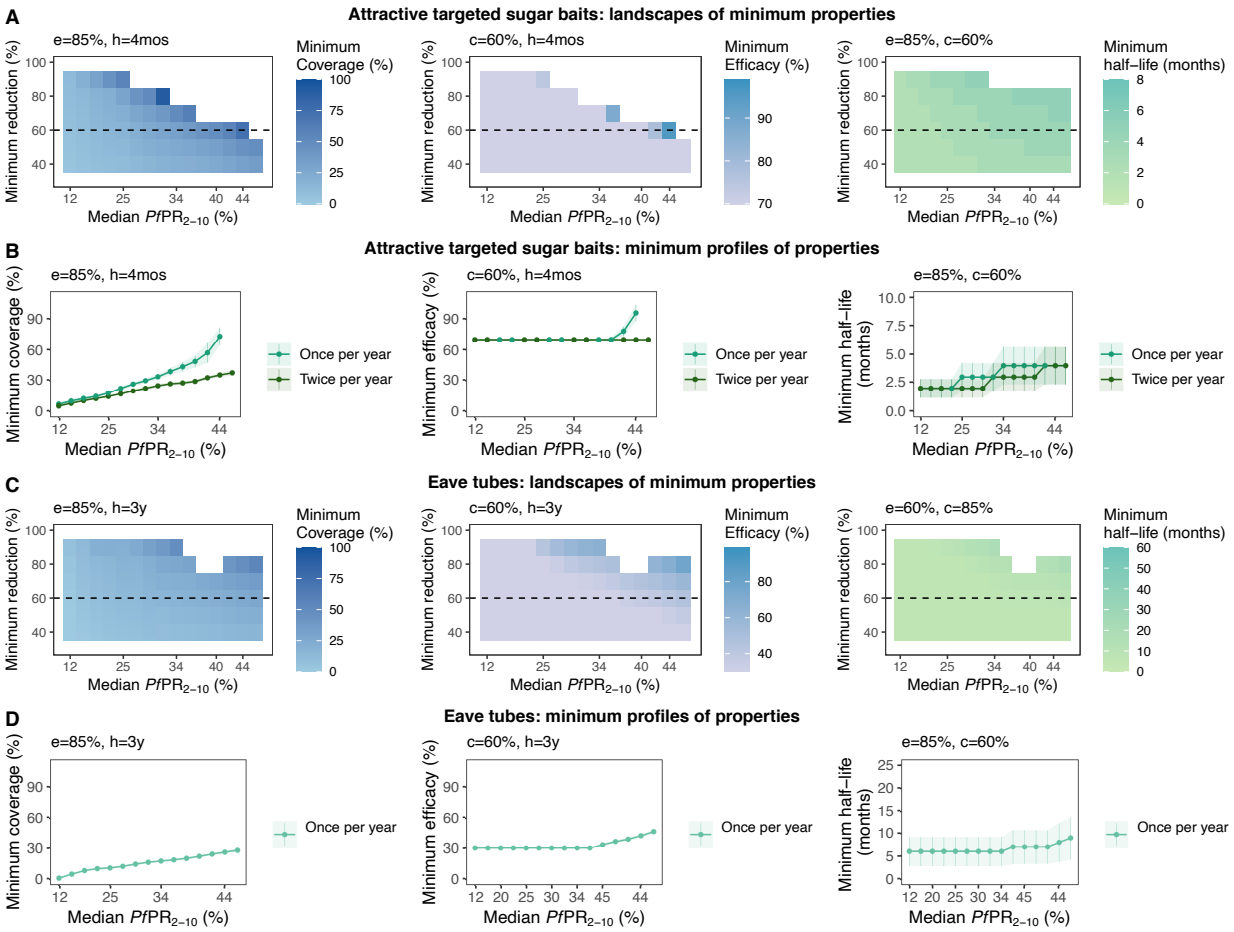

Fig. 6. Estimated optimal intervention profiles (TPPs) for vector control interventions
*The heatmaps in figures **(A)** and **(C)** display, for each intervention property (coverage, efficacy or half-life), the landscape of minimum required values to achieve various target $PfPR_{0\text{-}99}$ reductions (y axis) across different simulated transmission settings (true $PfPR_{2\text{-}10}$ rounded values, x axis). Each row of the heatmap corresponds to a target of $PfPR_{0\text{-}99}$ reduction and constitutes the minimum required profile of the considered intervention. For a selected health goal of 60% $PfPR_{0\text{-}99}$ reduction (dotted line on each heatmap), figures **(B)** and **(D)** present in detail how the minimum profile changes with transmission intensity. Each intervention characteristic was minimized in turn, while keeping the other characteristics fixed (values marked on each figure where c = coverage, e = efficacy, and h = half-life). The simulated access to treatment, corresponding to a probability of seeking care within 5 days, was 25%.*

518 **Table 2. Key findings of our quantitative approach guiding target product profiles of new**
519 **malaria interventions.**

Intervention	Summary of analysis results
Immunological interventions - Anti-infective monoclonal antibodies - Anti-infective vaccines - Transmission-blocking vaccines	**Key determinants of impact** (Fig. 2, Fig. S5.1) - The main driver of intervention impact was coverage - The second determinant of intervention impact depended on intervention half-life. For interventions with short half-lives such as monoclonal antibodies, the half-life was the second driver, while for long-term interventions such as vaccines, efficacy played a key role. - As opposed to long-term vaccines whose impact was mainly driven by coverage and efficacy, interventions with short half-life (e.g., anti-infective monoclonal antibodies) relied on the case management to prevent resurgence - The various biting patterns of mosquitoes did not influence the intervention determinants of impact
	Optimal intervention profiles (Fig. 3, Fig. S6.1-S6.4, S7.1-S7.3) - As opposed to vaccines, anti-infective monoclonal antibodies required high efficacy and deployment coverage while achieving limited reduction in *Pf*PR_{0-99} with very little impact in perennial settings - Increasing the deployment frequency for anti-infective monoclonal antibodies from once to twice per year, extended the landscape of feasible health targets mainly in seasonal settings - Combination with a blood-stage drug proved more impactful as compared to increasing the deployment frequency for anti-infective monoclonal antibodies, extending the achievable health goals in perennial settings as well
Vector control interventions - Attractive targeted sugar baits - Eave tubes	**Key determinants of impact** (Fig. 2, Fig. S5.2) - As with short-term immunological interventions, attractive targeted sugar baits relied on case management to prevent resurgence - We saw limited difference between key drivers for attractive targeted sugar baits in different biting settings because mosquitoes sugar feed before indoor or outdoor biting. - We observed that intervention properties of eave tubes rather than health system access to treatment were larger drivers of impact in high indoor biting settings, as mosquitoes in those settings will be more likely to contact the eave tube.
	Optimal intervention profiles (Fig. S7.5-S7.6, S8.4-S8.55 and Fig. 3) - Increasing deployment frequency from once to twice per year for attractive targeted sugar baits, resulted in a significant increase in

	intervention impact and less requirements in terms of coverage and half-life - Increasing efficacy of attractive targeted sugar baits did not have a significant impact

Summary of key results concerning impact determinants and minimal intervention profiles.

Discussion

In this study, we introduced a quantitative framework, using detailed simulation models of malaria transmission dynamics, that enables for the first time a quantitative differentiation between operational, transmission setting, and intervention parameters to understand the potential impact of novel interventions against malaria. The framework consists of (i) a comprehensive disease progression and transmission simulation model applied on a discrete, uniformly sampled set of input parameters; (ii) training of a GP emulator on the sampled set of parameters and corresponding impact outcomes; (iii) using sensitivity analysis to understand drivers of intervention impact; and (iv) applying a non-linear constrained optimization algorithm to explore intervention operational and effectiveness characteristics meeting various targets and deployment use-cases specified following iterative consultation with product development experts. Our work thus builds on recent applications of GPs in disease modelling and burden prediction for malaria (81).

In this work, we provided mathematical tools for efficiently and quantitatively defining the minimum profiles of malaria interventions as well as delivery approaches required to reach a desired health goal. Our framework can be extended and used for any disease where a valid model of disease progression or natural history of disease is available. It can be used to direct the design of novel interventions and understand how intervention-specific, epidemiological and systems factors jointly contribute to impact. Most immediately, this approach is highly relevant to define successful interventions against emerging diseases such as SARS-CoV-2, and to support efficient, fast development of operational strategies. As uncertainties in disease progression and epidemiology can be incorporated in our approach by accordingly adjusting the putative parameter space of intervention characteristics, it also provides a way to systematically

546 sort through large complex landscapes of unknowns and refine properties of interventions
547 following clinical trials as more knowledge is available.

548 Our framework tackles and moves beyond current challenges in product development. On one
549 hand, it allows us to rigorously define TPPs by efficiently exploring highly complex parameter
550 spaces of mathematical disease models, and on the other hand it identifies the determinants of
551 desired public health impact to inform tradeoffs between product characteristics and use-cases.

552 The value of our approach is realized through iterative collaboration with product development
553 experts, to perform model-based guidance throughout the development process, and refine
554 feedback on model predictions as interventions progress through development. For malaria,
555 where multiple interventions are in development, it also offers an approach for product
556 developers from diverse fields (such as therapeutics and insecticide development) to collaborate
557 and incorporate knowledge of other interventions into their TPP development. Coordinated by
558 BMGF, the exchanges with stakeholders ensured a crucial discussion environment, guiding and
559 supporting the methodology at various levels, from intervention profiling and defining relevant
560 intervention use cases to shaping research questions and subsequent analyses. The framework
561 has been presented and validated in the presence of the stakeholders in successive meetings.
562 These discussions contributed towards refining the investigation of various intervention profiles
563 and led to an exploration of intervention combinations. Subsequently, the iterative exchanges
564 with the stakeholders have not only shaped but also proven the value of our methodological
565 framework in its versatility to adapt addressing relevant questions along the product development
566 pathway.

567 Using a complex, individual-based malaria transmission model like OpenMalaria brings
568 significant advantages compared to a simpler and computationally less intensive Ross-
569 MacDonald model. Individual-based models capture the interactions between hosts, vectors and
570 parasites at individual level which provides a more realistic representation of the nonlinear
571 transmission and epidemiological processes in the population as well as of the stochasticity of
572 the modelled system (82). Second, it allows a realistic implementation of interventions, allowing
573 for explicitly modeling intervention characteristics relevant for defining TPPs such as
574 deployment regimes, efficacy, half-life, or shape of decay as well as explicit action at the
575 different stages of the transmission cycle. Conversely, in Ross-MacDonald models, the modelled

interventions have a very simplified representation through their effect only on transmission rates and this representation does not scale to the required detailed specifications of interventions in TPP documents.

The machine learning layer of our approach builds a simplified approximation of the relationships between intervention characteristics and resulting intervention impact. This approximation is very specific to the varied components across the model simulations (intervention characteristics, access to treatment and EIR) and to the resulting $Pf\mathrm{PR}_{0\text{-}99}$ reduction and does not explicitly provide a low-dimensional representation of all the processes captured by OpenMalaria. The complex disease dynamics processes captured by OpenMalaria (for a detailed description see Table S1.1) are intrinsically captured when training the GP emulator and cannot be disentangled from the observed effects of the interventions per se. Furthermore, these relationships are non-linear and change with the transmission intensity (EIR) as shown in Figures S4.5 and S4.6. Therefore, to allow translation with product development processes, our approach for guiding novel interventions requires a model of disease transmission which is able to capture the non-linear disease dynamics processes and offer a realistic representation of interventions and their effects.

Although in our analysis we used reduction of $Pf\mathrm{PR}_{0\text{-}99}$ as a health goal, our method can be applied to other continuous disease burden statistics as required (see Fig. S4.4 for performance predicting malaria incidence reduction). The same rationale applies for investigation of other deployment strategies, required doses of interventions or further intervention combinations. However, our approach using a smooth GP model is not tailored for classification and categorical health goals. Nevertheless, it could be adapted to these types of outputs by replacing the GP emulator with a predictive model/alternative algorithm suited for categorical data such as support vector machines. While sensitivity analysis would still be applicable for identifying the drivers of the categorical outcomes, the optimization questions and analyses would need to be reformulated to be relevant for the chosen categorical outcomes.

While bringing valuable quantitative insights to guide product development, our analysis of novel malaria interventions reproduces previous findings concerning intervention characteristics which are key drivers of impact. Previous studies have shown that intervention coverage is a major determinant of impact in the context of mass drug administration (62), of vaccines (83) as

606 well as vector control (31). Furthermore, our analysis reaffirms previous work showing the
607 ability of vector control interventions to achieve substantial reductions in malaria burden (84).

608 Our approach constitutes a powerful tool to help address the challenges of current malaria
609 strategies and develop new interventions to progress towards malaria elimination. While
610 currently promising interventions such as insecticide treated nets, seasonal malaria
611 chemoprevention (SMC) and intermittent preventative treatment (IPT) have been very successful
612 at reducing malaria incidence and saving lives, their improved burden reduction and future
613 success is currently challenged by limited adherence, resource and time constraints to increase
614 coverage and usage in underserved populations, as well as resistance (85). Furthermore, for
615 settings where SMC has not been implemented or not recommended (for example in East Africa
616 or in perennial settings), there remains a gap in available interventions to protect vulnerable
617 populations who experience the highest burden of malaria. Similarly, for settings with outdoor
618 biting mosquitoes, the development and rollout of novel vector control interventions is needed.
619 New therapeutics and immune therapies suitable for seasonal delivery such as long-acting
620 injectables or monoclonal antibodies are currently being developed and may close one of these
621 gaps (26, 27). However, to efficiently make decisions on their development, guidance on their
622 key performance characteristics and definition of their TPP documents is needed from early
623 stages.

624 Our quantitative framework can support the development of interventions from the beginning by
625 generating the evidence to inform and define evaluation criteria ensuring new products meet
626 relevant health targets, while considering how these products may affect disease burden and
627 epidemiology within a population. As we show, this relies on iterative dialogue with
628 stakeholders, to first define health targets, simulated scenarios, achievable intervention properties
629 and operational settings. The modelling part of the framework incorporates all this information
630 as well as relevant disease transmission dynamics, building an *in-silico* system for testing the
631 developed intervention. Next, the sensitivity analysis part of the framework informs which
632 intervention characteristics drive impact and are thus crucial in achieving the defined health goal,
633 providing insights on the development processes to be prioritized. Finally, the optimization
634 analysis part of the framework reveals the potential of the developed intervention and how its
635 efficacy and coverage requirements change according to the defined health targets and
636 deployment setting. The landscapes of intervention profiles help product developers to gauge

development and investment efforts and select promising products. Furthermore, our approach allows investigating combinations of new and existing interventions, identifying alternatives to alleviate shortcomings such as coverage limitations. To achieve a final TPP, several iterations of the analysis are required, to ensure that the optimal tradeoffs between intervention capabilities and target goals for a given setting are achieved.

As with all modelling studies, our approach is subject to several limitations. While the emulators capture not just the mean tendency of complex disease models dynamics, but also the inherent output variance caused by the stochasticity in the models (86), the provided estimations in this study are dependent on the performance of the trained emulator. We addressed this challenge with extensive adaptive sampling and testing to ensure a high level of accuracy of the trained emulators (Fig. 3, S4.1-S4.3, Table S4.1). Despite the intrinsic uncertainty, the framework is intended to provide guiding principles and an efficient means of exploring the space of intervention characteristics which otherwise would not be possible. Evidently, our analysis relies on the disease model assumptions of disease and transmission dynamics as well as expert opinion of likely intervention parameterizations in absence of clinical knowledge. Lastly, the current analysis explored a subset of use-cases, transmission settings and intervention combinations. Future work should focus on the likely settings and relevant use cases as the interventions are being developed and their TPP documents refined.

Moving beyond the work presented in this paper, our framework would allow combining simulation models with other sources of data describing geographical variation in disease, for example, modelled health systems or modelled prevalence (87, 88) and to incorporate interactions of interventions with novel interventions for surveillance. Clinical trials for new interventions could thereby be prioritized to geographical settings, where public health impact is likely to be maximized and where appropriate, to inform decisions on achieving non-inferiority or superiority endpoints (89, 90). A significant extension is incorporating economic considerations which may affect development decisions, including both costs of R&D, as well as implementation and systems costs for final deployment.

Materials and Methods

The approach introduced here combines infectious disease modeling with machine learning to understand determinants and define quantitative properties of target product profiles of new malaria interventions. The building blocks and methodology of the approach are schematically outlined in Fig. 2 which guides the following sections of Materials and Methods.

1 Iterative communication with malaria product development stakeholders

We actively engaged in regular communication exchanges with different expert groups during the development of our methodological framework for guiding TPPs of novel malaria interventions. The aims of these exchanges were to:

1. Create a communication environment with stakeholders to be able to incorporate their feedback for ensuring a realistic representation of novel malaria interventions and of the simulated disease transmission settings in our modeling approach;
2. Continuously shape our methodology to enable generating the relevant quantitative evidence to inform TPPs of novel malaria interventions from early stages of product development;
3. Define and refine the priority research questions to address with our analysis.

The stakeholders involved in these discussions were the Bill and Melinda Gates Foundation (BMGF), the Innovative Vector Control Consortium (IVCC) and the Program for Appropriate Technology in Health - Malaria Vaccine Initiative (PATH-MVI). The exchanges with these stakeholders have been coordinated and guided by BMGF through regular meetings as follows:

1. Initial convening with all the stakeholders to frame the key questions of the study, to establish a network for iterative dialogue and to inform the partners about OpenMalaria, about its components, features, and validity of assumptions. At this meeting, there were over 15 participants from BMGF, IVCC, PATH-MVI and Swiss TPH. The health goal of malaria prevalence reduction in all ages was chosen during this meeting, as well as the five malaria interventions to focus our analysis on;
2. Several one-to-one iterative meetings with each stakeholder to define the way the five chosen interventions are implemented in OpenMalaria and the relevant aspects to consider for their deployment (e.g., targets in the malaria transmission cycle, shape of

696 decay, mass deployment, assessing impact at early and late follow-up), as well as putative
697 ranges of their characteristics. We consulted with BMGF and PATH-MVI to refine the
698 modeled vaccine, monoclonal antibodies and drugs, and with IVCC for attractive targeted
699 sugar baits and eave tubes. The set of simulated transmission settings (seasonality, indoor
700 biting) were also defined during these meetings.

701 3. Interim meetings with several stakeholders where we presented proof-of-concept and
702 intermediate analyses. These meetings ensured building trust and a high level of
703 confidence of our stakeholders in our analysis while shaping the research questions. For
704 example, an intermediate result was that the determinants of impact of novel
705 interventions were different in low as compared to moderate transmission settings. This
706 motivated exploring a wide range of EIR settings to ascertain how impact determinants
707 were modulated as transmission increased. Another early result was that the efficacy,
708 coverage and half-life requirements of monoclonal antibodies and vaccines were
709 significantly high, that it was infeasible to reach high targets of prevalence reduction in
710 high transmission settings deploying these interventions alone. The subsequent
711 discussions led to the exploration of deploying combinations of these interventions with
712 an antimalarial drug and to refining target health goals based on the capabilities of the
713 interventions to reduce burden.

714 4. Final presentation of results via meetings or reports with the stakeholders where the final
715 results of the analysis were presented and prospects of future work were defined.

716 We provided regular presentations of our ongoing analysis to BMGF. These presentations
717 covered the relevant model assumptions for implementing the different interventions, focusing
718 on the aspects where the stakeholder feedback was needed as well as intermediary results where
719 the model predictions of the interventions were shown. This ensured an iterative dynamic of our
720 exchanges where stakeholders were directly involved in shaping the intervention characteristics,
721 allowing them to see how their input was incorporated in our methodology (Table 1) and how
722 these assumptions influenced the impact predictions of our analysis. These exchanges helped us
723 design and refine the means of communication of our methodological approach and the model
724 predictions to a stakeholder audience. For this purpose, we used communication elements such
725 as tables summarizing the key quantitative results of discussions (e.g., Table 2), clear definitions
726 of modeled intervention properties (see definition of the components of an intervention profile in

727 section 2.3 of Materials and Methods and summary in Table 1), schematic diagrams offering an
728 intuitive representation for the methodological processes (Fig. 1-2), and a standardized system of
729 plots communicating the results of our analysis for the different interventions explored in our
730 study (Fig. 2 - 6). These standardized plots were of three types:

731 1. Sensitivity analysis plot (Fig. 2B, 4) displaying, for each intervention, the relative
732 importance of the intervention characteristics in determining the resulting impact on
733 *Pf*PR$_{0\text{-}99}$ reduction. The relative importance was calculated following global sensitivity
734 analysis using Sobol' indices (see section 4 of Materials and Methods for a detailed
735 description and calculation). These figures allowed for a visual communication of the key
736 drivers of intervention impact and importantly how these drivers changed across various
737 transmission settings, across immediate versus late follow-up of intervention impact as
738 well as across interventions.

739 2. Landscapes of minimum intervention properties plot (Fig. 2C - left panel, Fig. 5A, C, E
740 and 6 A, C) displaying for different malaria transmission levels, an overview of the
741 minimum intervention requirements in terms of coverage, efficacy, and half-life for a
742 wide range of target *Pf*PR$_{0\text{-}99}$ reductions (see section 5 of Materials and Methods for a
743 detailed description of the optimization process). These figures allowed for
744 communication of overall intervention capabilities in reducing malaria prevalence, as
745 well as their minimal requirements across different malaria transmission settings and for
746 a wide range of *Pf*PR$_{0\text{-}99}$ reduction goals. These requirements defined the profiles of
747 intervention characteristics.

748 3. Minimum profiles of properties plot (Fig. 2C – right panel, Fig. 5B, D, F and 6B, D)
749 displaying for different malaria transmission levels, the estimated minimum intervention
750 requirements in terms of coverage, efficacy, and half-life for a chosen target of *Pf*PR$_{0\text{-}99}$
751 reduction (see section 5 of Materials and Methods for a detailed description of the
752 optimization process). These figures allowed for a visual communication of the minimal
753 intervention profiles and their variance across a range of different transmission settings
754 for a chosen target of *Pf*PR$_{0\text{-}99}$ reduction. Furthermore, they allowed a direct comparison
755 of the required intervention profiles between immediate and long follow-up, across
756 different deployment regimes (once versus twice per year) as well as across different

757 intervention strategies (medical interventions deployed single or in combination with an
758 antimalarial drug).
759
760 **2 Description of the OpenMalaria model of malaria transmission dynamics**
761 **2.1 Individual-based model of malaria transmission**
762 We used OpenMalaria (60, 91), an open source stochastic individual-based model to
763 simulate malaria epidemiology and transmission dynamics across humans and mosquitoes in
764 various settings. OpenMalaria considers the natural history of malaria in humans linked with a
765 deterministic, entomological model of the mosquito oviposition cycle and malaria transmission
766 in mosquitoes (92, 93) (Table S1.1). The modelled transmission cycle (Fig. 1) considers the
767 chain of processes following infection of a human host, simulating malaria infection in
768 individuals and modelling infection characteristics such as parasite density, duration of infection,
769 infectivity to mosquitoes, and health outcomes such as morbidity, mortality or anemia.
770 OpenMalaria specifically captures heterogeneity in host exposure, susceptibility and immune
771 response, taking into consideration the effects of several factors such as acquired immunity,
772 human demography structure, or seasonality (80, 94-96). Furthermore, the model includes a
773 detailed representation of the health system (79), and of a wide range of human and vector
774 control interventions while tracking multiple health outcomes over time (Fig. 1, Table S1.1).
775 OpenMalaria has been widely documented and validated against a multitude of field
776 studies, compared to existing models and used in extensive studies to provide evidence for the
777 epidemiological effects of various interventions (55, 56, 60, 82, 97, 98). It comprises 14 model
778 variants based on distinct sets of assumptions on its epidemiology and transmission components
779 (91). For the present analysis, the "base" simulation model was used. The mathematical
780 equations of the OpenMalaria model, its assumptions, calibration and validation have been
781 thoroughly described in numerous previous publications (see the Results section), therefore are
782 not specified here, however, an overview of the key modelled disease processes and assumptions
783 along with the corresponding references where they are elaborated are provided in Table S1.1. In
784 the sections below, we provide an overview of the calibration and simulation settings used for
785 the current study.
786

2.2 Calibration of the disease model and description of simulation experiments

OpenMalaria has been calibrated and validated in previous studies using historical epidemiological data (56, 60, 91). The present analysis is based on a previously-calibrated version of the model which reflects demographics, epidemiology, entomology, health system and seasonality of a health facility catchment area in Tanzania (78-80). The core parameters of this calibration have been previously estimated using a genetic algorithm approach, optimizing a weighted sum over 10 objective functions (91). These objective functions represent key epidemiological relationships captured form available study survey and study site data and are listed below (along with the figures displaying data and model fits from the reference studies):

- Age patterns of incidence after interventions (Fig. 5 from (99))
- Age patterns of prevalence (Fig. 4 in (94))
- Age patterns of parasite density (Fig. 6 in (94))
- Age patterns of the multiplicity of infections (Fig. 5 in (94))
- Age patterns of clinical malaria incidence (Fig. 1 in (96))
- Age patterns of the parasite density threshold for clinical attacks (Fig. 4 in (96))
- Hospitalization rate in relation to prevalence in children (Fig. 2 in (80))
- Age patterns of hospitalization in relation to severe malaria (Fig. 4 in (80))
- Malaria specific mortality in children less than 5 years old (Fig. 7-8 in (80))
- Indirect malaria infant mortality rate (Fig. 9 in (80))

The full details of the calibration procedure have been described in (91), and in (61) and the estimated parameters have been previously summarized in Table 1 in (60), in Table 3 in (91), and in Table S1 in (61). We include a summary of the model parameters in Tables S1.2 and S1.3.

The simulated human population size in this analysis was 10’000 individuals, with its age structure informed by data collected from a health and demographic surveillance site in Ifakara, Tanzania, available through the INDEPTH network (100). For all simulations, we assumed there were no imported infections during the whole study period.

Health system characteristics (Table S1.1) were defined through parameterization of a case management model based on data provided by the Tanzanian National Malaria Control Program (79). To define the simulated case management level, the probability of effective cure within two weeks from the onset of fever (E_{14}) was varied within the interval [0 - 0.8] corresponding to a probability of seeking care (access to treatment) within 5 days from the onset of fever (E_5) within

818 the interval [0.04 - 0.5] (97). During the model simulations, the case management level was
819 constant over time.
820 Mosquito entomological parameters and seasonal exposure patterns were estimated from
821 field studies conducted in the Namawala and Michenga villages located nearby Ifakara in
822 Tanzania (101, 102). Two archetypal seasonal settings were simulated: a seasonal exposure
823 setting with one transmission peak in September estimated from the mentioned field studies (Fig.
824 S2.1), and a perennial setting with uniform, constant exposure throughout the year. Two
825 mosquito species were present in the simulated settings: endophagic (indoor-biting, human blood
826 index equal to 0.99) and exophagic (outdoor-biting, human blood index is 0.5), respectively. The
827 ratios between the population sizes of indoor and outdoor mosquito species were classified into
828 three levels corresponding to high (indoor proportion is 0.8 out of total mosquito population),
829 mid (indoor proportion is 0.5) and low indoor biting (indoor proportion is 0.2). The extent of
830 malaria transmission in each simulation was defined by the yearly entomological inoculation rate
831 (EIR). For each simulation, EIR was sampled from the interval [1, 25] leading to a simulated
832 range of *Plasmodium falciparum* parasite rate or prevalence (*Pf*PR) distributions across the
833 various transmission settings (Figures S2.1, S2.3, Table S2.1).
834
835 **2.3 Definition of intervention profiles**
836 We built a standardized representation for each malaria intervention. Accordingly, a
837 malaria intervention was characterized through the targets of the transmission life cycle it affects,
838 along with the efficacy, half-life and decay of its effect (Figure 1, S2.2, Table 1). The efficacy of
839 a therapeutic or immunologic intervention was quantified by its ability to clear parasites or
840 prevent infection, while for mosquito-targeted interventions (vector control) it corresponded to
841 the ability of the intervention to kill or prevent mosquitoes from biting human hosts. For each
842 intervention, its efficacy decayed over time according to a specific decay type (defined in Fig.
843 S2.2). The coverage of interventions was quantified by the percentage of the population affected
844 by the respective intervention. Where interventions were applied to individual humans, in the
845 present analysis this was equally applied across ages, and not targeted to certain populations.
846 Geographical setting characteristics such as entomological inoculation rates (EIR), seasonality,
847 case-management coverage, as well as transmission and vector characteristics were also included
848 in the simulation specifications (Fig. 1, Table 1).

We defined the following intervention targets in the transmission cycle (Fig. 1):

- **Anti-infective:** acts at the liver stage and prevents occurrence of a new infection
- **Blood stage clearance:** clears blood-stage parasites by administration of a drug
- **Transmission blocking:** prevents parasite development into gametocytes
- **Mosquito life-cycle killing effect:** kills mosquitoes during different stages of their life cycle, such as, for example, before a blood meal (pre-prandial killing) and/or after a blood meal (post-prandial killing). Furthermore, mosquitoes are affected by vector control interventions according to their indoor and outdoor biting patterns.

The length of the intervention effect was described via either half-life for exponential, sigmoidal or biphasic decay profiles, or by duration for step-like decay profiles. Generally, half-life refers to half-life of intervention efficacy decay, representing the time in which the initial intervention efficacy has been reduced by 50% (Fig. S2.2, Table 1). As opposed to half-life, the duration of effect is equivalent to the entire decay time. For simplicity, since only one intervention had a step-like decay, we used the words half-life and duration interchangeably.

In our current study, each intervention or combination of interventions was applied as mass intervention targeting all ages equally, along with continuous case management. In this analysis, we did not examine targeting particular populations or age groups to develop our approach. The deployed mass intervention packages followed a long period of model warm up (150 years), and were implemented in June and/or December for three years (Fig. 3, S3.1). Coverage at deployment time refers to the percentage of the population covered by the intervention's initial efficacy, irrespective of how many doses/applications are required to reach that coverage, assuming that the necessary doses have previously occurred. The base scenario xml files used for the simulations can be found at https://github.com/SwissTPH/TPP_workflow/tree/master/Intervention_scenarios.

2.4 Translation of input EIR to *Pf*PR$_{2\text{-}10}$ and *Pf*PR$_{0\text{-}99}$

For each simulation, OpenMalaria requires the definition of the intensity and seasonality of malaria exposure specified through the input EIR level and its yearly profile in the absence of interventions (Fig. S2.1). EIR is an appropriate measure for reflecting transmission intensity (103), however it is difficult to measure in the field and its interpretation in the context of intervention impact is difficult to apprehend when looking at the effects of drugs and vaccines

880 (104, 105). For this reason, although EIR is the force of infection input to all OpenMalaria
881 simulations, we reported simulation outcomes and downstream analyses at the corresponding
882 median *Pf*PR$_{2-10}$ before the interventions are deployed. We report true infection prevalence and
883 not patent PCR or RDT-detected. To do so, we discretized the continuous EIR space into discrete
884 unit-wide intervals and the median *Pf*PR was calculated across the obtained *Pf*PR for all
885 simulations in each discrete interval (Fig. S2.3).
886
887 **2.5 Definition of intervention impact and health goals**
888 A comprehensive set of simulated scenarios was built by sampling uniformly the
889 parameter space of setting and intervention characteristics. To estimate the impact of the
890 deployed interventions, in each simulation, we calculated the reduction in *Pf*PR$_{0-99}$ attributable to
891 the deployed intervention. *Pf*PR$_{0-99}$ reduction was calculated by comparing the initial average
892 prevalence in the year before any interventions were deployed to the average yearly prevalence
893 obtained in the first year (short follow-up) and in the third year (long follow-up) after
894 deployment of interventions (Fig. 3, S3.1). Consequently, the defined health goals corresponded
895 to a given minimum threshold of *Pf*PR$_{0-99}$ reduction that the deployed interventions should
896 achieve.
897 Figures S3.2 – S3.4 present the distributions of obtained *Pf*PR$_{0-99}$ reduction for the
898 OpenMalaria simulation experiments covering all the interventions and deployments investigated
899 in the present study. In seasonal, low transmission settings (EIR < 2) a high proportion of
900 simulations reached elimination before any intervention was deployed and were removed from
901 the analysis (Fig. S3.5). Since this happened for over 75% of simulations at EIR<2, we did not
902 investigate optimal intervention profiles for transmission settings with EIR<2. Arguably, for
903 these settings close to elimination, a different health goal, such as probability of elimination,
904 would be more appropriate which is not within the scope of the present study focusing on the
905 reduction of *Pf*PR$_{0-99}$.
906
907 **<u>3 Building a disease model emulator with Gaussian processes</u>**
908 As it was computationally intensive and challenging to run an exhaustive number of
909 simulations in order to explore with OpenMalaria all the parameter space for diverse
910 combinations of interventions, settings and deployments, we applied machine learning

911 techniques and kernel methods. Precisely, starting from a training dataset of simulations
912 generated with OpenMalaria, we used Gaussian process (GP) models (77) to infer the
913 relationship between simulation variables (e.g., intervention coverage, half-life, efficacy, etc.)
914 and corresponding intervention impact (*Pf*PR$_{0\text{-}99}$ reduction). This approach allowed us to build a
915 fast, simplified predictive model that could provide estimates of the disease model output for any
916 new inputs without running new OpenMalaria model simulations.
917 Gaussian process models are non-parametric models which define a prior probability
918 distribution over a collection of functions using a kernel, smooth function. Precisely, given the
919 relationship

920 $$y = f(\boldsymbol{x}) + \varepsilon$$

921 where y in our case is the *Pf*PR$_{0\text{-}99}$ reduction and $\boldsymbol{x}$ represents the set of intervention parameters
922 $x_1, \ldots, x_n$, the main assumption of a GP is that

923 $$P\big(f(x_1), f(x_2), \ldots, f(x_n)\big) \sim N(\mu, \Sigma)$$

924 where

925 $$\Sigma_{x_i,x_j} = K\big(x_i, x_j\big)$$

926 is the covariance matrix of the Gaussian distribution, μ is its mean and K is a kernel function
927 (77). Once data is observed, the posterior probability distribution of the functions consistent with
928 the observed data can be derived which is then used to infer outcomes at unobserved locations in
929 the parameter space (77). The intuition behind a GP model is based on the "smoothness"
930 relationship between its components. Accordingly, points which are close in the input parameter
931 space will lead to close points in the output space.
932

933 **3.1 Training data**

934 For each intervention and setting, a training dataset was built using discrete Latin hypercube
935 uniform sampling (106) across the input parameter space (defined in Table 1). This sampling
936 scheme ensured a uniform cover of the parameter space and a representative set of points
937 spanning the variability of the predicted output across the entire space. Ten stochastic
938 realizations (replicates) of each sampled data point were considered. OpenMalaria was run on the
939 sampled data points and *Pf*PR$_{0\text{-}99}$ was calculated for both short and long follow-up. The size of
940 the training set was varied between 10 and 1000 points (100 – 10000 including replicates) for
941 several simulation experiments (Fig. S4.1) and the performance of the trained GP was assessed

via the Pearson correlation coefficient r^2. The minimum training set size which led to $r^2 > 0.95$ was selected for the remaining simulation experiments.

3.2 Gaussian process emulators

For each transmission setting and intervention, a GP model with a Gaussian kernel was trained in a 5-fold cross-validation scheme using the training set with OpenMalaria simulations. For training the GP, we used the R package *HetGP* version 1.1.1 (107, 108). HetGP is a powerful implementation of GP models, featuring heteroskedastic GP modeling embedded in a fast and efficient maximum-likelihood-based inference scheme.

GP performance was assessed by calculating the correlation between true and predicted outputs on out-of-sample test sets as well as the mean squared error (Fig. S4.2 – 4.3, Table S4.1). Precisely, the training set was split in 5 subsets and, iteratively, 4 of these subsets were used for training the GP, while the remaining one was used as an out-of-sample test set during the cross-validation procedure. After assessing the prediction error during the cross-validation procedure, the GP was trained using the entire training set.

Furthermore, since the trained GP model provides the mean and variance of each predicted output, we used this probabilistic representation to assess the uncertainty of the trained model across the entire parameter space and to refine the GP model through adaptive sampling (109-111). Accordingly, we iteratively sampled new training points from high-uncertainty regions of the parameter space and updated the model with the new training samples. Precisely, we sampled 100’000 points using Latin hypercube sampling and evaluated the variance of the predicted output with the previously trained GP emulator. We prioritized samples from “rare” regions of the parameter space containing fewer outputs. To do so, we binned the output $Pf\mathrm{PR}_{0\text{-}99}$ range in 4 bins and calculated how many of the predicted outcomes corresponding to the sampled 100’000 points fell in each bin (output density). Out of the sampled points, we chose 30 points (300 including replicates) proportional to the output density in each bin and with the highest predicted variance. We repeated the procedure five times, to ensure that the correlation between true and predicted values on an out-of-sample test set had reached a plateau. Finally, a separate out-of-sample test set was built to assess the overall performance of the GP (Fig. S4.2 – 4.3, Table S4.1).

4 Identifying impact determinants through sensitivity analysis

To estimate the contribution of each model input and its interactions with the other inputs to the variance of the model outcome, we conducted a global sensitivity analysis based on variance decomposition (112). This analysis shows which input parameters have higher impact on the model outcome. It relies on the decomposition of the output variance in a sum of individual input parameter conditional variances:

$$\mathrm{Var(Y)} = \sum_{i} V_i + \sum_{i}\sum_{j>i} V_{ij} + \cdots + V_{12\ldots d}$$

where Y is the model outcome (in our case, *Pf*$PR_{0\text{-}99}$ reduction), d corresponds to the number of model inputs, and the conditional variances are defined as:

$$V_i = \mathrm{Var}(E(Y|x_i))$$

$$V_{ij} = \mathrm{Var}\left(E\left(Y\middle|x_i, x_j\right)\right) - V_i - V_j$$

$$V_{ijk} = \mathrm{Var}\left(E\left(Y\middle|x_i, x_j, x_k\right)\right) - V_{ij} - V_{jk} - V_{ik} - V_i - V_j - V_k$$

$$\ldots$$

with $x_1, \ldots, x_n$ representing the model input parameters.

Based on the above decomposition of output variance, the first order sensitivity index is defined as:

$$S_i = \frac{V_i}{\mathrm{Var(Y)}}$$

and corresponds to the proportion of output variance assigned to the main effect of X_i, i.e., regardless its interactions with other model inputs (112, 113).

To account for the contribution of each model input as well as the variance of its interactions with other inputs to the variability of the model output, the total effect sensitivity index is used:

$$T_i = 1 - \frac{\mathrm{Var}(E(Y|x_{\sim i}))}{\mathrm{Var(Y)}}$$

where the notation ~i stands for all indices except i (112, 113).

In the above decomposition of model output variance, by replacing the expressions of the sensitivity indexes, the following properties can be deduced:

$$\sum_{i} S_i + \sum_{i}\sum_{j>i} S_{ij} + \cdots + S_{12\ldots d} = 1$$

and

$$\sum_{i} T_i \geq 1 .$$

To compute the sensitivity indexes, we use the function "soboljansen" from the R package "sensitivity" (114). The function estimates the sensitivity indices through MCMC sampling, using a Monte Carlo approximation for computing conditional expectations. Within the sampling scheme, we sampled 100'000 points to estimate the sensitivity indices.

Calculating the sensitivity indices defined above, the variance of the GP emulator output was thus decomposed into proportions attributable to intervention characteristics, i.e., intervention efficacy, half-life and deployment coverage, as well as access to care. Using the main effects, we defined the relative importance r_i of each characteristic as a proxy for impact determinants as follows:

$$r_i = \frac{S_i}{\sum_{i=1}^{d} Si}$$

where d is the number of intervention characteristics and $\sum_{i=1}^{d} r_i = 1$.

5 Finding minimal intervention properties

The trained GP models for each transmission setting and intervention were used within a general-purpose optimization scheme to identify minimum intervention properties that reach a defined *Pf*PR$_{0\text{-}99}$ reduction goal given operational and intervention constraints.

Let

$$g(\boldsymbol{x}) = g(x_1, x_2, x_3, x_4)$$

denote the GP model predicting the mean prevalence reduction obtained after deploying an intervention with given characteristics in a transmission setting, with

$$x_1 = tool\ coverage$$

$$x_2 = tool\ half - life$$

$$x_3 = tool\ efficacy$$

$$x_4 = access\ to\ treatment.$$

For various levels of *Pf*PR$_{0\text{-}99}$ denoted with p_k, each intervention characteristic was optimized separately, keeping the remaining characteristics as well as the level of case management fixed to pre-set levels. Precisely, the optimization procedure searches for

$$\min(x_i)|\ x_{\sim i}$$

such as

$$g(\boldsymbol{x}) \geq p_k$$

with the constraints:

$$l_i \leq\ x_i \leq\ u_i,$$

where l_i and u_i are the lower and upper bounds of x_i, respectively and the notation $\sim i$ is used to represent all the characteristics except i. A detailed description of the parameter specifications during optimization for each intervention is provided in Table S2.1.

To solve the above optimization problem, we used a general nonlinear augmented Lagrange multiplier method (115, 116) implemented in the R package "*Rsolnp*" (117). To ensure optimality of the obtained solutions and avoid local minima, 10 random restarts were chosen among 1000 uniformly-sampled input parameter sets and the optimization procedure was run separately for each restart (implemented in function "*gosolnp*" in the same R package). To capture the variance of the optimal intervention profile, since the output of a GP model is a distribution, we solved the above optimization problem for several cases and we report the distribution of the obtained minima when:

$$(i)\ \ g(\boldsymbol{x}) =\ \mu$$

$$(ii)\ \ g(\boldsymbol{x}) =\ \mu \pm\ \sigma$$

$$(iii)\ g(\boldsymbol{x}) =\ \mu \pm\ 2\sigma$$

where μ is the predicted mean of the GP model and σ is the standard deviation. Where the nonlinear optimization algorithm did not find any solutions, we performed an additional fine grid search of 10000 uniformly-sampled data points.

In seasonal settings, at low transmission (simulated EIR < 2, corresponding simulated true $Pf\mathrm{PR}_{2\text{-}10}$ < 11.7%), over 75% of simulations reached malaria elimination ($Pf\mathrm{PR}_{0\text{-}99}$ = 0) under the simulated levels of case management, before intervention deployment (Fig. S3.5). For this reason, the space of obtained prevalence reductions following intervention deployment was rather sparse and the obtained optima were not reliable and often did not converge. Therefore, we chose to report minimum intervention profiles for settings with true $Pf\mathrm{PR}_{2\text{-}10}$ >= 11.7% (with RDTs this yields a patent $Pf\mathrm{PR}_{2\text{-}10}$ >= 5.8%).

Acknowledgments:
We would like to thank Lydia Burgert, Theresa Reiker, Andrew Shattock, Thomas Smith, and Dylan Muir for insightful discussions and feedback on the developed methodology and the manuscript. We would also like to thank Thomas van Boeckel and Amalio Telenti for providing useful feedback on the manuscript. Calculations were performed at sciCORE (http://scicore.unibas.ch/) scientific computing core facility at University of Basel. We would further like to thank collaborators at the Innovative Vector Control Consortium (IVCC), PATH's Malaria Vaccine Initiative (MVI) and Joerg Moehrle from Medicines for Malaria Venture (MMV) for their insightful discussions and feedback on the model scenarios. This work has been possible thanks to the Malaria Team at the Bill and Melinda Gates Foundation (BMGF) who facilitated exchanges with the product development partners and supported model scenarios and interpretations. In particular, we would like to thank Scott Miller, Jean-Luc Bodmer, Laura Norris, Bruno Moonen, Dan Strickman, and Philip Welkhoff.

Funding: This work was supported by the Bill and Melinda Gates Foundation (OPP1170505 to MAP) and the Swiss National Science Foundation (PP00P3_170702 to MAP);

Author contributions: M.G., G.Y. and M.A.P conceived the study, designed the simulation experiments, developed methodology and analyzed the results. F.C., E.C., and N.C. provided methodological expertise. E.M.S., N.H., M.M., and S.R contributed with their expertise regarding product development, intervention properties and guided analysis. M.G., G.Y., M.A.P. wrote the manuscript. All authors provided continuous feedback and approved the final manuscript;

Competing interests: All authors declare no competing interests;

Data and materials availability: All the analysis code used in the paper as well as corresponding documentation, parameterizations and configuration files for the software workflow necessary to generate the simulation data with OpenMalaria and reproduce the analysis are available at https://github.com/SwissTPH/TPP_workflow.

Supplementary Materials are included after the references.

List of Supplementary Figures and Tables

The following supplementary Figures and Tables complement the analysis and results reported in the main manuscript and are organized as follows:

- Description of the malaria disease transmission dynamics (OpenMalaria) model components and assumptions:
  - **Table S1.1.** Overview of the OpenMalaria model components.
  - **Table S1.2.** Estimated core parameters of OpenMalaria describing the natural history of the disease in human hosts.
  - **Table S1.3** OpenMalaria model parameters describing the dynamics of the mosquito feeding cycle.
- Simulated malaria transmission dynamics in the presented analysis together with parameterizations of simulated malaria interventions and their optimization setup:
  - **Fig. S2.1.** Illustration of the yearly malaria transmission and prevalence patterns in simulated seasonal settings.
  - **Fig. S2.2.** Representation of decay and the range of efficacy and half-life against different parasite or vector targets for intervention-agnostic malaria interventions.
  - **Fig. S2.2.** Simulated distributions of true and patent (detected with PCR or RDT) $Pf\mathrm{PR}_{0\text{-}99}$ and $Pf\mathrm{PR}_{2\text{-}10}$ for various input EIR levels in absence of interventions.
  - **Table S2.1.** Specifications of the optimization procedure for TPP development.
- Simulation outputs:
  - **Fig. S3.1.** Examples of OpenMalaria simulation outputs.
  - **Fig. S3.2.** Distributions of prevalence reduction following yearly deployment of single interventions.
  - **Fig. S3.3.** Distributions of prevalence reduction following yearly deployment of combinations of interventions.
  - **Fig. S3.4.** Distributions of prevalence reduction following deployment of single and combinations of interventions twice per year.
  - **Fig. S3.5.** Simulations reaching malaria elimination before intervention deployment.
- Emulator training and evaluation:
  - **Fig. S4.1.** Assessment of the performance of the trained GP depending on the training set size.
  - **Fig. S4.2.** Performance of the trained GP emulators predicting immediate intervention impact.
  - **Fig. S4.3.** Performance of the trained GP emulators predicting long-term intervention impact.
  - **Fig. S4.4.** Performance of trained GP emulators predicting incidence reduction
  - **Fig. S4.5.** Relationships between input intervention parameters and the predicted immediate $Pf\mathrm{PR}_{0\text{-}99}$ reduction with the trained GP emulator
  - **Fig. S4.6.** Relationships between input intervention parameters and the predicted long-term $Pf\mathrm{PR}_{0\text{-}99}$ reduction with the trained GP emulator
  - **Fig. S4.7.** Execution time of OpenMalaria simulations and GP emulator training

- **Table S4.1.** Performance of the trained Gaussian Process emulators predicting immediate and long-term intervention impact.

- Sensitivity analyses and impact determinants of interventions:
  - **Fig. S5.1.** Key drivers of impact for therapeutic malaria interventions across different transmission settings.
  - **Fig. S5.2.** Key drivers of impact for vector control malaria interventions across different transmission settings.
- Feasible landscapes of optimal, constrained intervention profiles (TPPs) for achieving a desired health goal across different transmission settings and operational factors:
  - **Fig. S6.1** Feasible landscapes of optimal, constrained intervention profiles (TPPs) for an anti-infective monoclonal antibody deployed once per year.
  - **Fig. S6.2.** Feasible landscapes of optimal, constrained intervention profiles (TPPs) for an anti-infective monoclonal antibody deployed twice per year.
  - **Fig. S6.3.** Feasible landscapes of optimal, constrained intervention profiles (TPPs) for an anti-infective vaccine deployed once per year.
  - **Fig. S6.4.** Feasible landscapes of optimal, constrained intervention profiles (TPPs) for a transmission-blocking vaccine deployed once per year.
  - **Fig. S6.5.** Feasible landscapes of optimal, constrained intervention profiles (TPPs) for attractive targeted sugar baits deployed once or twice per year.
  - **Fig. S6.6.** Feasible landscapes of optimal, constrained intervention profiles (TPPs) for eave tubes deployed once per year.
- Minimum profiles of interventions for achieving a desired health goal across different transmission settings and operational factors:
  - **Fig. S7.1.** Optimal intervention profiles (TPPs) for anti-infective monoclonal antibodies under various deployment regimes to achieve a $Pf\mathrm{PR}_{0\text{-}99}$ reduction of at least 70%.
  - **Fig. S7.2.** Optimal intervention profiles (TPPs) for anti-infective vaccines under various deployment regimes to achieve a $Pf\mathrm{PR}_{0\text{-}99}$ reduction of at least 70%.
  - **Fig. S7.3.** Optimal intervention profiles (TPPs) for transmission-blocking vaccines under various deployment regimes to achieve a $Pf\mathrm{PR}_{0\text{-}99}$ reduction of at least 70%.
  - **Fig. S7.4.** Optimal intervention profiles (TPPs) for attractive targeted sugar baits under various deployment regimes to achieve a $Pf\mathrm{PR}_{0\text{-}99}$ reduction of at least 70%.
  - **Fig. S7.5.** Optimal intervention profiles (TPPs) for eave tubes to achieve a $Pf\mathrm{PR}_{0\text{-}99}$ reduction of at least 70%.

References and Notes:

1. S. Bhatt *et al.*, The effect of malaria control on Plasmodium falciparum in Africa between 2000 and 2015. *Nature* **526**, 207 (2015).
2. P. L. Alonso, M. Tanner, Public health challenges and prospects for malaria control and elimination. *Nature Medicine* **19**, 150 (2013).
3. WHO, World malaria report 2020: 20 years of global progress and challenges. (2020).

1179 4. WHO, World Health Organization: Global report on insecticide resistance in malaria
1180 vectors: 2010–2016 accessed at
1181 https://www.who.int/malaria/areas/vector_control/insecticide_resistance/en/. (2018).
1182 5. L. J. Espinoza, Malaria Resurgence in the Americas: An Underestimated Threat.
1183 *Pathogens* **8** (2019).
1184 6. C. J. M. Whitty, E. Ansah, Malaria control stalls in high incidence areas. *BMJ* **365**, l2216
1185 (2019).
1186 7. P. Alonso, A. M. Noor, The global fight against malaria is at crossroads. *The Lancet* **390**,
1187 2532-2534 (2017).
1188 8. WHO, Malaria eradication: benefits, future scenarios & feasibility. (2020).
1189 9. R. G. Feachem *et al.*, Malaria eradication within a generation: ambitious, achievable, and
1190 necessary. *The Lancet* **394**, 1056-1112 (2019).
1191 10. G. T. Edwin, M. Korsik, M. H. Todd, The past, present and future of anti-malarial
1192 medicines. *Malaria journal* **18**, 1-21 (2019).
1193 11. T. Yang *et al.*, MalDA, accelerating malaria drug discovery. *Trends in Parasitology*
1194 (2021).
1195 12. R. H. van Huijsduijnen, T. N. Wells, The antimalarial pipeline. *Current opinion in*
1196 *pharmacology* **42**, 1-6 (2018).
1197 13. WHO, Tables of malaria vaccine projects globally" The Rainbow Tables. *World Health*
1198 *Organization, Geneva, Switzerland. http://www. who.*
1199 *int/vaccine_research/links/Rainbow/en* (2013).
1200 14. P. E. Duffy, Transmission-blocking vaccines: harnessing herd immunity for malaria
1201 elimination. *Expert Review of Vaccines*, 1-14 (2021).
1202 15. P. E. Duffy, J. P. Gorres, Malaria vaccines since 2000: progress, priorities, products. *NPJ*
1203 *vaccines* **5**, 1-9 (2020).
1204 16. WHO, Q&A on the malaria vaccine implementation programme (MVIP). (2019).
1205 17. A. Maxmen, First proven malaria vaccine rolled out in Africa--but doubts linger. *Nature*
1206 **569**, 14-16 (2019).
1207 18. S. C. T. P. RTS, Efficacy and safety of RTS, S/AS01 malaria vaccine with or without a
1208 booster dose in infants and children in Africa: final results of a phase 3, individually
1209 randomised, controlled trial. *The Lancet* **386**, 31-45 (2015).
1210 19. M. van den Berg, B. Ogutu, N. K. Sewankambo, N. Biller-Andorno, M. Tanner, RTS, S
1211 malaria vaccine pilot studies: addressing the human realities in large-scale clinical trials.
1212 *Trials* **20**, 1-4 (2019).
1213 20. B. Greenwood, New tools for malaria control–using them wisely. *Journal of Infection* **74**,
1214 S23-S26 (2017).
1215 21. S. Mahmoudi, H. Keshavarz, Efficacy of phase 3 trial of RTS, S/AS01 malaria vaccine:
1216 the need for an alternative development plan. *Human vaccines & immunotherapeutics* **13**,
1217 2098-2101 (2017).
1218 22. M. A. Penny, F. Camponovo, N. Chitnis, T. A. Smith, M. Tanner, Future use-cases of
1219 vaccines in malaria control and elimination. *Parasite epidemiology and control* **10**,
1220 e00145 (2020).
1221 23. M. S. Datoo *et al.*, Efficacy of a low-dose candidate malaria vaccine, R21 in adjuvant
1222 Matrix-M, with seasonal administration to children in Burkina Faso: a randomised
1223 controlled trial. *The Lancet* (2021).

24. R. P. Bakshi *et al.*, Long-acting injectable atovaquone nanomedicines for malaria prophylaxis. *Nature communications* **9**, 1-8 (2018).
25. Y. Yuthavong *et al.*, Malarial dihydrofolate reductase as a paradigm for drug development against a resistance-compromised target. *Proceedings of the National Academy of Sciences* **109**, 16823-16828 (2012).
26. L. T. Wang *et al.*, A Potent Anti-Malarial Human Monoclonal Antibody Targets Circumsporozoite Protein Minor Repeats and Neutralizes Sporozoites in the Liver. *Immunity* **53**, 733-744. e738 (2020).
27. F. Macintyre *et al.*, Injectable anti-malarials revisited: discovery and development of new agents to protect against malaria. *Malaria journal* **17**, 402 (2018).
28. N. K. Kisalu *et al.*, A human monoclonal antibody prevents malaria infection by targeting a new site of vulnerability on the parasite. *Nature medicine* **24**, 408 (2018).
29. WHO, New tools, technologies and approaches for vector control (2020).
30. G. F. Killeen *et al.*, Developing an expanded vector control toolbox for malaria elimination. *BMJ Global Health* **2** (2017).
31. A. L. Wilson *et al.*, The importance of vector control for the control and elimination of vector-borne diseases. *PLoS neglected tropical diseases* **14**, e0007831 (2020).
32. K. Raghavendra *et al.*, Chlorfenapyr: a new insecticide with novel mode of action can control pyrethroid resistant malaria vectors. *Malaria Journal* **10**, 1-7 (2011).
33. S. Camara *et al.*, Efficacy of Interceptor® G2, a new long-lasting insecticidal net against wild pyrethroid-resistant Anopheles gambiae ss from Côte d'Ivoire: a semi-field trial. *Parasite* **25** (2018).
34. WHO, Efficacy-testing of traps for control of Aedes spp. mosquito vectors. (2018).
35. A. E. Eiras, M. C. Resende, J. L. Acebal, K. S. Paixão, "New cost-benefit of Brazilian technology for vector surveillance using trapping system" in Malaria. (IntechOpen, 2018).
36. R. Carballar-Lejarazú *et al.*, Next-generation gene drive for population modification of the malaria vector mosquito, Anopheles gambiae. *Proceedings of the National Academy of Sciences* **117**, 22805-22814 (2020).
37. T. Nolan, Control of malaria-transmitting mosquitoes using gene drives. *Philosophical Transactions of the Royal Society B* **376**, 20190803 (2021).
38. A. M. Hammond, R. Galizi, Gene drives to fight malaria: current state and future directions. *Pathogens and global health* **111**, 412-423 (2017).
39. R. Carter, N. D. Karunaweera, The role of improved housing and living environments in malaria control and elimination. *Malaria Journal* **19**, 1-6 (2020).
40. R. L. Nguela *et al.*, The effect of improved housing on indoor mosquito density and exposure to malaria in the rural community of Minkoameyos, Centre Region of Cameroon. *Malaria journal* **19**, 1-16 (2020).
41. WHO, Keeping the vector out: housing improvements for vector control and sustainable development. (2017).
42. E. D. Sternberg *et al.*, Impact and cost-effectiveness of a lethal house lure against malaria transmission in central Côte d'Ivoire: a two-arm, cluster-randomised controlled trial. *The Lancet* **397**, 805-815 (2021).
43. S. Sougoufara, E. C. Ottih, F. Tripet, The need for new vector control approaches targeting outdoor biting Anopheline malaria vector communities. *Parasites & Vectors* **13**, 1-15 (2020).

44. G. C. Müller *et al.*, Successful field trial of attractive toxic sugar bait (ATSB) plant-spraying methods against malaria vectors in the Anopheles gambiae complex in Mali, West Africa. *Malaria journal* **9**, 1-7 (2010).
45. J. M. Fiorenzano, P. G. Koehler, R.-D. Xue, Attractive toxic sugar bait (ATSB) for control of mosquitoes and its impact on non-target organisms: a review. *International journal of environmental research and public health* **14**, 398 (2017).
46. P. Cocco, A. Ayaz-Shah, M. P. Messenger, R. M. West, B. Shinkins, Target Product Profiles for medical tests: a systematic review of current methods. *BMC medicine* **18**, 1-12 (2020).
47. A. Brooks *et al.*, Aligning new interventions with developing country health systems: Target product profiles, presentation, and clinical trial design. *Global Public Health* **7**, 931-945 (2012).
48. R. Chin, B. Y. Lee, *Principles and practice of clinical trial medicine* (Elsevier, 2008).
49. J. N. Burrows *et al.*, New developments in anti-malarial target candidate and product profiles. *Malaria journal* **16**, 26 (2017).
50. U. F. a. D. Administration., Guidance for industry and review staff Target Product Profile — a strategic development process tool. available at https://www.fda.gov/media/102657/download. (2007).
51. B. Y. Lee, D. S. Burke, Constructing target product profiles (TPPs) to help vaccines overcome post-approval obstacles. *Vaccine* **28**, 2806-2809 (2010).
52. K. B. Ebels *et al.* (2014) Incorporating user needs into product development for improved infection detection for malaria elimination programs. in *IEEE Global Humanitarian Technology Conference (GHTC 2014)* (IEEE), pp 555-560.
53. H. Heesterbeek *et al.*, Modeling infectious disease dynamics in the complex landscape of global health. *Science* **347** (2015).
54. R. M. Anderson, B. Anderson, R. M. May, *Infectious diseases of humans: dynamics and control* (Oxford university press, 1991).
55. M. A. Penny *et al.*, Public health impact and cost-effectiveness of the RTS, S/AS01 malaria vaccine: a systematic comparison of predictions from four mathematical models. *The Lancet* **387**, 367-375 (2016).
56. T. Smith *et al.*, Towards a comprehensive simulation model of malaria epidemiology and control. *Parasitology* **135**, 1507-1516 (2008).
57. P. Winskill, P. G. T. Walker, J. T. Griffin, A. C. Ghani, Modelling the cost-effectiveness of introducing the RTS,S malaria vaccine relative to scaling up other malaria interventions in sub-Saharan Africa. *BMJ Global Health* **2**, e000090 (2017).
58. P. Winskill, P. G. Walker, R. E. Cibulskis, A. C. Ghani, Prioritizing the scale-up of interventions for malaria control and elimination. *Malaria Journal* **18**, 122 (2019).
59. E. Korenromp *et al.*, Malaria intervention scale-up in Africa: effectiveness predictions for health programme planning tools, based on dynamic transmission modelling. *Malaria Journal* **15**, 417 (2016).
60. T. Smith *et al.*, Mathematical modeling of the impact of malaria vaccines on the clinical epidemiology and natural history of Plasmodium falciparum malaria: overview. *The American Journal of Tropical Medicine and Hygiene* **75**, 1-10 (2006).
61. T. Reiker *et al.*, Machine learning approaches to calibrate individual-based infectious disease models. *medRxiv* (2021).

62. O. J. Brady *et al.*, Role of mass drug administration in elimination of Plasmodium falciparum malaria: a consensus modelling study. *The Lancet Global Health* **5**, e680-e687 (2017).
63. M. L. Gatton *et al.*, The importance of mosquito behavioural adaptations to malaria control in Africa. *Evolution: international journal of organic evolution* **67**, 1218-1230 (2013).
64. E. M. Stuckey, T. Smith, N. Chitnis, Seasonally Dependent Relationships between Indicators of Malaria Transmission and Disease Provided by Mathematical Model Simulations. *PLOS Computational Biology* **10**, e1003812 (2014).
65. H. C. Slater *et al.*, Assessing the impact of next-generation rapid diagnostic tests on Plasmodium falciparum malaria elimination strategies. *Nature* **528**, S94-S101 (2015).
66. J. Gerardin *et al.*, Optimal Population-Level Infection Detection Strategies for Malaria Control and Elimination in a Spatial Model of Malaria Transmission. *PLOS Computational Biology* **12**, e1004707 (2016).
67. M. Walker *et al.*, Designing antifilarial drug trials using clinical trial simulators. *Nature Communications* **11**, 1-11 (2020).
68. H. Kimko, J. Pinheiro, Model-based clinical drug development in the past, present and future: a commentary. *Br. J. Clin. Pharmacol.* **79**, 108-116 (2015).
69. C. Vegvari *et al.*, Using clinical trial simulators to analyse the sources of variance in clinical trials of novel therapies for acute viral infections. *PloS one* **11** (2016).
70. P. Selvaraj, J. Suresh, E. A. Wenger, C. A. Bever, J. Gerardin, Reducing malaria burden and accelerating elimination with long-lasting systemic insecticides: a modelling study of three potential use cases. *Malaria journal* **18**, 307-307 (2019).
71. M. Kretzschmar, Disease modeling for public health: added value, challenges, and institutional constraints. *Journal of public health policy* **41**, 39-51 (2020).
72. K. Panayidou *et al.*, GetReal in mathematical modelling: a review of studies predicting drug effectiveness in the real world. *Research synthesis methods* **7**, 264-277 (2016).
73. L. Rychetnik, M. Frommer, P. Hawe, A. Shiell, Criteria for evaluating evidence on public health interventions. *Journal of Epidemiology and Community Health* **56**, 119 (2002).
74. A. B. Hogan, P. Winskill, R. Verity, J. T. Griffin, A. C. Ghani, Modelling population-level impact to inform target product profiles for childhood malaria vaccines. *BMC medicine* **16**, 1-11 (2018).
75. G. F. Killeen, N. Chitnis, S. J. Moore, F. O. Okumu, Target product profile choices for intra-domiciliary malaria vector control pesticide products: repel or kill? *Malaria journal* **10**, 207 (2011).
76. W. Pan-Ngum *et al.*, Predicting the relative impacts of maternal and neonatal respiratory syncytial virus (RSV) vaccine target product profiles: A consensus modelling approach. *Vaccine* **35**, 403-409 (2017).
77. C. E. Rasmussen, C. K. I. Williams, *Gaussian Processes for Machine Learning (Adaptive Computation and Machine Learning)* (The MIT Press, 2005).
78. N. Maire, F. Tediosi, A. Ross, T. Smith, Predictions of the epidemiologic impact of introducing a pre-erythrocytic vaccine into the expanded program on immunization in sub-Saharan Africa. *The American Journal of Tropical Medicine and Hygiene* **75**, 111-118 (2006).

79. F. Tediosi *et al.*, An approach to model the costs and effects of case management of plasmodium falciparum malaria in sub-saharan Africa. *The American Journal of Tropical Medicine and Hygiene* **75**, 90-103 (2006).
80. A. Ross, N. Maire, L. Molineaux, T. Smith, An epidemiologic model of severe morbidity and mortality caused by Plasmodium falciparum. *The American journal of tropical medicine and hygiene* **75**, 63-73 (2006).
81. E. Cameron *et al.*, Defining the relationship between infection prevalence and clinical incidence of Plasmodium falciparum malaria. *Nature Communications* **6**, 8170 (2015).
82. N. R. Smith *et al.*, Agent-based models of malaria transmission: a systematic review. *Malaria journal* **17**, 1-16 (2018).
83. C. E. Utazi *et al.*, Mapping vaccination coverage to explore the effects of delivery mechanisms and inform vaccination strategies. *Nature communications* **10**, 1-10 (2019).
84. N. M. Ferguson, Challenges and opportunities in controlling mosquito-borne infections. *Nature* **559**, 490-497 (2018).
85. J. Gutman, S. Kovacs, G. Dorsey, A. Stergachis, F. O. ter Kuile, Safety, tolerability, and efficacy of repeated doses of dihydroartemisinin-piperaquine for prevention and treatment of malaria: a systematic review and meta-analysis. *The Lancet infectious diseases* **17**, 184-193 (2017).
86. D. Ríos Insua, F. Ruggeri, M. P. Wiper, *Bayesian analysis of stochastic process models* (Wiley, Chichester, 2012).
87. D. J. Weiss *et al.*, Mapping the global prevalence, incidence, and mortality of Plasmodium falciparum, 2000–17: a spatial and temporal modelling study. *The Lancet* **394**, 322-331 (2019).
88. M. Sahu, F. Tediosi, A. M. Noor, J. J. Aponte, G. Fink, Health systems and global progress towards malaria elimination, 2000–2016. *Malaria journal* **19**, 1-12 (2020).
89. R. Ristl, S. Urach, G. Rosenkranz, M. Posch, Methods for the analysis of multiple endpoints in small populations: A review. *Journal of biopharmaceutical statistics* **29**, 1-29 (2019).
90. Food, D. Administration, Multiple endpoints in clinical trials: guidance for industry. *College Park, Maryland: Food and Drug Administration* (2017).
91. T. Smith *et al.*, Ensemble Modeling of the Likely Public Health Impact of a Pre-Erythrocytic Malaria Vaccine. *PLOS Medicine* **9**, e1001157 (2012).
92. N. Chitnis, T. Smith, R. Steketee, A mathematical model for the dynamics of malaria in mosquitoes feeding on a heterogeneous host population. *Journal of Biological Dynamics* **2**, 259-285 (2008).
93. N. Chitnis, D. Hardy, T. Smith, A Periodically-Forced Mathematical Model for the Seasonal Dynamics of Malaria in Mosquitoes. *Bulletin of Mathematical Biology* **74**, 1098-1124 (2012).
94. N. Maire *et al.*, A model for natural immunity to asexual blood stages of Plasmodium falciparum malaria in endemic areas. *The American journal of tropical medicine and hygiene* **75**, 19-31 (2006).
95. A. Ross, G. Killeen, T. Smith, Relationships between host infectivity to mosquitoes and asexual parasite density in Plasmodium falciparum. *The American journal of tropical medicine and hygiene* **75**, 32-37 (2006).

96. T. Smith *et al.*, An epidemiologic model of the incidence of acute illness in Plasmodium falciparum malaria. *The American journal of tropical medicine and hygiene* **75**, 56-62 (2006).
97. M. A. Penny *et al.*, Distribution of malaria exposure in endemic countries in Africa considering country levels of effective treatment. *Malaria Journal* **14**, 384 (2015).
98. T. Reiker, N. Chitnis, T. A. Smith, Modelling reactive case detection strategies for interrupting transmission of Plasmodium falciparum malaria. *Malaria Journal* **18**, 259 (2019).
99. T. Smith *et al.*, Relationship between the entomologica inoculation rate and the force of infection for Plasmodium Falciparum malaria. *The American Journal of Tropical Medicine and Hygiene* **75**, 11-18 (2006).
100. A. M. Ekström *et al.*, INDEPTH Network: contributing to the data revolution. *The Lancet Diabetes & Endocrinology* **4**, 97 (2016).
101. G. F. Kileen, A. Ross, T. Smith, Infectiousness of malaria-endemic human populations to vectors. *The American Journal of Tropical Medicine and Hygiene* **75**, 38-45 (2006).
102. T. C. Smith *et al.*, Absence of seasonal variation in malaria parasitaemia in an area of intense seasonal transmission. *Acta tropica* **54 1**, 55-72 (1993).
103. C. Drakeley *et al.*, An estimation of the entomological inoculation rate for Ifakara: a semi-urban area in a region of intense malaria transmission in Tanzania. *Tropical Medicine & International Health* **8**, 767-774 (2003).
104. A. M. Shaukat, J. G. Breman, F. E. McKenzie, Using the entomological inoculation rate to assess the impact of vector control on malaria parasite transmission and elimination. *Malaria journal* **9**, 122 (2010).
105. L. S. Tusting, T. Bousema, D. L. Smith, C. Drakeley, "Measuring changes in Plasmodium falciparum transmission: precision, accuracy and costs of metrics" in Advances in parasitology. (Elsevier, 2014), vol. 84, pp. 151-208.
106. M. Stein, Large Sample Properties of Simulations Using Latin Hypercube Sampling. *Technometrics* **29**, 143-151 (1987).
107. M. Binois, R. B. Gramacy, M. Ludkovski, Practical heteroscedastic gaussian process modeling for large simulation experiments. *Journal of Computational and Graphical Statistics* **27**, 808-821 (2018).
108. M. Binois, R. Gramacy, hetGP: Heteroskedastic Gaussian Process Modeling and Design under Replication. *R package version* **1** (2017).
109. A. M. Gopakumar, P. V. Balachandran, D. Xue, J. E. Gubernatis, T. Lookman, Multi-objective optimization for materials discovery via adaptive design. *Scientific reports* **8**, 3738 (2018).
110. R. Dehghannasiri *et al.*, Optimal experimental design for materials discovery. *Computational Materials Science* **129**, 311-322 (2017).
111. M. Binois, J. Huang, R. B. Gramacy, M. Ludkovski, Replication or Exploration? Sequential Design for Stochastic Simulation Experiments. *Technometrics* **61**, 7-23 (2019).
112. I. M. Sobol′, Global sensitivity indices for nonlinear mathematical models and their Monte Carlo estimates. *Mathematics and Computers in Simulation* **55**, 271-280 (2001).
113. A. Saltelli, S. Tarantola, F. Campolongo, M. Ratto, *Sensitivity Analysis in Practice: A Guide to Assessing Scientific Models* (Halsted Press, 2004).

114. R. C. Team (2013) R: A language and environment for statistical computing. (Vienna, Austria).
115. M. R. Hestenes, Multiplier and gradient methods. *Journal of Optimization Theory and Applications* **4**, 303-320 (1969).
116. Y. Ye (1987) Interior algorithms for linear, quadratic, and linearly constrained non-linear programming. (Ph. D. thesis, Department of ESS, Stanford University).
117. A. Ghalanos, S. Theussl, Rsolnp: general non-linear optimization using augmented Lagrange multiplier method. *R package version* **1** (2012).
118. W. E. Collins, G. M. Jeffery, A retrospective examination of the patterns of recrudescence in patients infected with Plasmodium falciparum. *The American journal of tropical medicine and hygiene* **61**, 44-48 (1999).
119. G. F. Killeen, A. Ross, T. Smith, Infectiousness of malaria-endemic human populations to vectors. *The American journal of tropical medicine and hygiene* **75**, 38-45 (2006).
120. A. Ross, T. Smith, The effect of malaria transmission intensity on neonatal mortality in endemic areas. *The American journal of tropical medicine and hygiene* **75**, 74-81 (2006).
121. J. O. Yukich, N. Chitnis, Modelling the implications of stopping vector control for malaria control and elimination. *Malaria journal* **16**, 1-16 (2017).
122. F. Camponovo, C. F. Ockenhouse, C. Lee, M. A. Penny, Mass campaigns combining antimalarial drugs and anti-infective vaccines as seasonal interventions for malaria control, elimination and prevention of resurgence: a modelling study. *BMC infectious diseases* **19**, 920 (2019).

Supplementary Materials:

Title: Combining machine learning and mathematical models of disease dynamics to guide development of novel disease interventions

Authors: Monica Golumbeanu[1,2]†, Guojing Yang[1,2]†, Flavia Camponovo[1,2,3], Erin M. Stuckey[4], Nicholas Hamon[5], Mathias Mondy[5], Sarah Rees[5], Nakul Chitnis[1,2], Ewan Cameron[6,7,8], and Melissa A. Penny[1,2]*

Affiliations:
[1]Swiss Tropical and Public Health Institute, Basel, Switzerland
[2]University of Basel, Basel, Switzerland
[3]Center for Communicable Disease Dynamics, Department of Epidemiology, Harvard T. H. Chan School of Public Health, Boston, MA 02115, USA
[4]The Bill and Melinda Gates Foundation, Seattle, WA, USA
[5]Innovative Vector Control Consortium, Liverpool, United Kingdom
[6]Malaria Atlas Project, Big Data Institute, University of Oxford, Oxford, UK
[7]Curtin University, Perth, Australia
[8]Telethon Kids Institute, Perth Children's Hospital, Perth, Australia
*Correspondence to: melissa.penny@unibas.ch
†These authors contributed equally.

One Sentence Summary: Defining quantitative profiles of novel disease interventions by combining machine learning with mathematical models of disease transmission

Short title: Quantitatively defining new disease interventions

Table of contents

1 Disease model 56
Table S1.1 Overview of the OpenMalaria model components. 57
Table S1.2 Estimated core parameters of OpenMalaria describing the natural history of the disease in human hosts. 59
Table S1.3 OpenMalaria model parameters describing the dynamics of the mosquito feeding cycle. 60
2 Disease scenarios 61
Figure S2.1 Illustration of the yearly malaria transmission and prevalence patterns in simulated seasonal settings. 61
Figure S2.2 Representation of decay and the range of efficacy and half-life against different parasite or vector targets for intervention-agnostic malaria interventions. 62
Figure S2.3 Simulated distributions of true and patent (detected with PCR or RDT) $Pf\mathrm{PR}_{0\text{-}99}$ and $Pf\mathrm{PR}_{2\text{-}10}$ for various input EIR levels in absence of interventions. 64
Table S2.1 Specifications of the optimization procedure for TPP development. 65
3 Results: Disease model simulations 67
Figure S3.1. Examples of OpenMalaria simulation outputs. 67
Figure S3.2. Distributions of prevalence reduction following yearly deployment of single interventions. 68
Figure S3.3. Distributions of prevalence reduction following yearly deployment of combinations of interventions. 69

Figure S3.4. Distributions of prevalence reduction following deployment of single and combinations of interventions twice per year. 70
Figure S3.5. Simulations reaching malaria elimination before intervention deployment. 71
4 Results: Emulator performance..... 72
Figure S4.1. Assessment of the performance of the trained GP depending on the training set size. 72
Figure S4.2. Performance of the trained GP emulators predicting immediate intervention impact. 73
Figure S4.3. Performance of the trained GP emulators predicting long-term intervention impact. 74
Figure S4.4 Performance of trained GP emulators predicting incidence reduction 75
Figure S4.5 Relationships between input intervention parameters and the predicted immediate *Pf*PR$_{0\text{-}99}$ reduction with the trained GP emulator..... 76
Figure S4.6 Relationships between input intervention parameters and the predicted long-term *Pf*PR$_{0\text{-}99}$ reduction with the trained GP emulator..... 77
Figure S4.7 Execution time of OpenMalaria simulations and GP emulator training 78
Table S4.1. Performance of the trained GP emulators predicting immediate and long-term intervention impact. 79
5 Results: Key determinants of impact 80
Figure S5.1. Key drivers of impact for immunological malaria interventions across different transmission settings. 80
Figure S5.2. Key drivers of impact for vector control malaria interventions across different transmission settings. 82
6 Results: Feasible landscapes of optimal, constrained intervention profiles 83
Figure S6.1. Feasible landscapes of optimal, constrained intervention profiles (TPPs) for an anti-infective monoclonal antibody deployed once per year..... 83
Figure S6.2. Feasible landscapes of optimal, constrained intervention profiles (TPPs) for an anti-infective monoclonal antibody deployed twice per year. 84
Figure S6.3 Feasible landscapes of optimal, constrained intervention profiles (TPPs) for an anti-infective vaccine deployed once per year. 85
Figure S6.4. Feasible landscapes of optimal, constrained intervention profiles (TPPs) for a transmission-blocking vaccine deployed once per year..... 86
Figure S6.5. Feasible landscapes of optimal, constrained intervention profiles (TPPs) for attractive targeted sugar baits deployed once or twice per year..... 87
Figure S6.6. Feasible landscapes of optimal, constrained intervention profiles (TPPs) for eave tubes deployed once per year. 88
7 Results: Optimal intervention profiles 89
Figure S7.1 Optimal intervention profiles (TPPs) for anti-infective monoclonal antibodies under various deployment regimes to achieve a *Pf*PR$_{0\text{-}99}$ reduction of at least 70%. 89
Figure S7.2 Optimal intervention profiles (TPPs) for anti-infective vaccines under various deployment regimes to achieve a *Pf*PR$_{0\text{-}99}$ reduction of at least 70%. 90
Figure S7.3 Optimal intervention profiles (TPPs) for transmission-blocking vaccines under various deployment regimes to achieve a *Pf*PR$_{0\text{-}99}$ reduction of at least 70%. 91
Figure S7.4 Optimal intervention profiles (TPPs) for attractive targeted sugar baits under various deployment regimes to achieve a *Pf*PR$_{0\text{-}99}$ reduction of at least 70%. 92

1560 Figure S7.5 Optimal intervention profiles (TPPs) for eave tubes to achieve a *Pf*PR$_{0\text{-}99}$ reduction
1561 of at least 70%. 93
1562
1563

1564 **1 Disease model**
1565

Name and *references*	Description of core assumptions
Key modelled epidemiological processes (base model)	
Malaria infection of humans *(99) and eq. 1-4 of Appendix 1 in (60)*	- Determined by EIR which is a model input and affects the force of infection in the simulated setting - Considers an age-dependent exposure of human hosts to mosquitoes (correlating with body-surface area) - The relationship between infection rates and EIR is defined and fitted with data from The Gambia, Nigeria and Kenya in (99)
Infection progression in humans: asexual parasite densities and immunity *(60, 94, 99, 118) and eq. 5-15 of Appendix 1 in (60)*	- Blood-stage parasite density depends on the time since infection and is affected by naturally acquired immunity. Acquired immunity reduces parasite density of subsequent infections. - The duration of infection follows a log-normal distribution and is estimated from a malaria therapy dataset ((118) and eq. 1 in (94)) - Immunity (both pre-erythrocytic and blood-stage) develops progressively following consequent episodes of exposure to infection and total parasitemia seen by an individual in their lifetime. - Super-infection is possible with cumulative parasite densities - The parasite density in a host at a given time is defined and fitted with data from Ghana, Nigeria and Tanzania in (94)
Transmission from infected humans to mosquitoes *(60, 95, 119) and eq. 16-21 of Appendix 1 in (60)*	- Infectivity to mosquitoes depends on the density of parasites present in the human (including a time-lag for gametocyte development) - The fraction of resulting infected mosquitoes after feeding on a human host follows a binomial distribution and is - The relationship between infectivity to mosquitoes and parasite density was defined and fitted in (95) with data from malaria therapy collected in Georgia between 1940 and 1963 and available from (118) - The age-specific contribution to overall infectiousness to mosquitoes was validated in (95) against field data collected from Liberia, The Gambia, Tanzania, Kenya, Papua New Guinea and Cameroon.
Clinical illness, morbidity, mortality and anemia *(60, 80, 96, 120) and eq. 22-32 of Appendix 1 in (60)*	- Acute clinical illness depends on human host parasite densities and their pyrogenic threshold which evolves over time depending on the individual exposure history - Acute morbidity episodes can be uncomplicated or evolve to severe episodes; a proportion of the severe episodes leads to deaths - The probability of a clinical malaria episode was defined and fitted with data from Senegal in (96) - The probabilities that a clinical episode becomes severe and the risk of mortality for a severe episode are defined and fitted to field data from over 10 African countries in (80)
Modelled characteristics of the transmission setting	
Population age structure *(80, 100)*	- Informed by health and demographic surveillance data from Tanzania

Transmission seasonality *(64, 99)*	-	Seasonally-forced, the same transmission pattern is reproduced each year in absence of interventions, displayed in Fig. S2.1. Seasonal patterns are inputs to the model and users can define any patterns as needed e.g, perennial, one or two peak seasonal patterns, etc.
Case management *(79)*	-	Modelled through a comprehensive decision tree-based model defined and validated in (79) which determines the corresponding treatment implications depending on the occurring clinical events such as fevers and seeking of care
	-	Its representation includes specification of access to official or non-official care, access to hospital for severe cases, diagnostic tests (use, specificity, sensitivity and threshold of detection), treatments for first, second line and non-official care, effects of treatment, case fatality rate, case sequelae and cure rates
Entomological setting *(93)*	-	Comprehensive simulation of the mosquito lifecycle and behavior towards human and animal hosts (biting, resting) embedded in a dynamic entomological model of the mosquito feeding cycle defined in (93)
	-	Multiple vector species can be simulated simultaneously
Modelled interventions and their action		
Vector control *(59, 63, 121)*	-	Acts on the availability of the protected human hosts to mosquitoes (deterrence), on the probability that a mosquito bites a protected human host (preprandial effect) and on the probability that a mosquito survives host feeding (postprandial effect)
Drugs and Vaccines *(55, 122)*	-	Act at various levels of the parasite life cycle (transmission blocking, anti-infective, blood-stage clearance) and their action is defined by their initial efficacy, half-life and decay
Deployment characteristics	-	Interventions can be deployed for several rounds to a targeted group of individuals and specified coverages (proportion of the population covered by the intervention)
Simulation regimes and model variants		
Time steps	-	Simulation outputs are tracked every 5 days
Model variants (91)	-	Varying assumptions in immunity decay, treatment and heterogeneity of transmission are covered in 14 model variants described in (91). In the present study, we use the base model (parameterization described in Table 2 in (91) under the denomination R0001)
Software availability and documentation		
-	Source code and wiki page available on GitHub: https://github.com/SwissTPH/openmalaria/	

Table S1.1
Overview of the OpenMalaria model components.
The OpenMalaria individual based, stochastic model of malaria transmission in humans was originally developed in 2003-2006 (60), with mosquito dynamics updated in 2008 (92) and an additional 13 structural model variants developed and parameterized in 2012 (91). In this table we summarize the key model components and assumptions and reference the previous studies where these assumptions have been quantified, fitted and validated using field epidemiological data.

Parameter	Estimated value from (91) (model R0001)
Lower limit of success probability of inoculations at high EIR	0.049
Critical value of EIR	0.032 inoculations/person-night
Lower limit of success probability of inoculations in immune individuals	0.14
Critical value of cumulative number of entomological inoculations	1’514.4 inoculations
Steepness of relationship between success of inoculation and the critical value of cumulative number of entomological inoculations	2.04
Variation between hosts on parasite densities (variance of log-normal distribution)	10.174
Critical value of cumulative number of parasite days	3.52 parasite-days/μl x 10^{-7}
Critical value of cumulative number of infections	97.3 infections
Maternal protection at birth	0.90
Decay of maternal protection	2.53 per year
Fixed variance component for densities	0.66 $[\ln(\text{parasites}/\mu l)]^2$
Critical value of cumulative number of infections for variance in parasite densities	0.92 infections
Critical value in determining an increase of the pyrogenic threshold	6’502.3 parasites/μL
Factor determining an increase in the pyrogenic threshold	143’000 $\text{parasites}^2 \mu l^{-2} \text{day}^{-1}$
Density bias (non Garki)	0.177
Mass action parameter	1
Case fatality for severe episodes in the community compared to hospital	2.09
Co-morbidity intercept relevant to indirect mortality	0.019
Non-malaria intercept for infant mortality rate	49.5 deaths/1000 live births
Density bias (Garki)	4.796

Parasitemia threshold for severe episodes type B_1	784’000 parasites/μL
Immune penalty	1
Immune effector decay	1
Prevalence of co-morbidity/susceptibility at birth relevant to severe episodes	0.092
Decay rate of the pyrogenic threshold	2.5 per year
Critical value of parasite density in determining an increase in the pyrogenic threshold	0.6 parasites/μl
Asexual immunity decay	0
Pyrogenic threshold at birth	296.302 parasites/μl
Idete multiplier	2.798
Critical age of co-morbidity	0.117

Table S2.2
Estimated core parameters of OpenMalaria describing the natural history of the disease in human hosts.
These parameters have been previously estimated in (60) and (91) through model calibration (see Section 2 of Materials and Methods and Table S.1.1) and were kept unchanged during all the simulations in the present study. EIR stands for entomological inoculation rate.

Parameter	Value
Duration of the period when a mosquito is resting	3 days
Extrinsic incubation period (time required for sporozoite development)	11 days
Proportion of mosquitoes which are host seeking on same day as oviposition	0.313
Maximum proportion of the day that a mosquito spends host-seeking	0.33
Probability that a mosquito survives the feeding cycle	0.623
Probability that a mosquito successfully bites the chosen human host	0.95
Probability that a mosquito escapes the human host and finds a resting place after biting	0.95
Probability that a mosquito successfully rests after finding a resting site	0.99
Probability that a mosquito successfully lays eggs given that it has rested	0.88
Human blood index: the proportion of resting mosquitoes which fed on human blood during their last feed	0.5

Table S1.3
OpenMalaria model parameters describing the dynamics of the mosquito feeding cycle.
These parameters have been previously estimated in (92) and were kept unchanged during all the simulations in the present study.

2 Disease scenarios

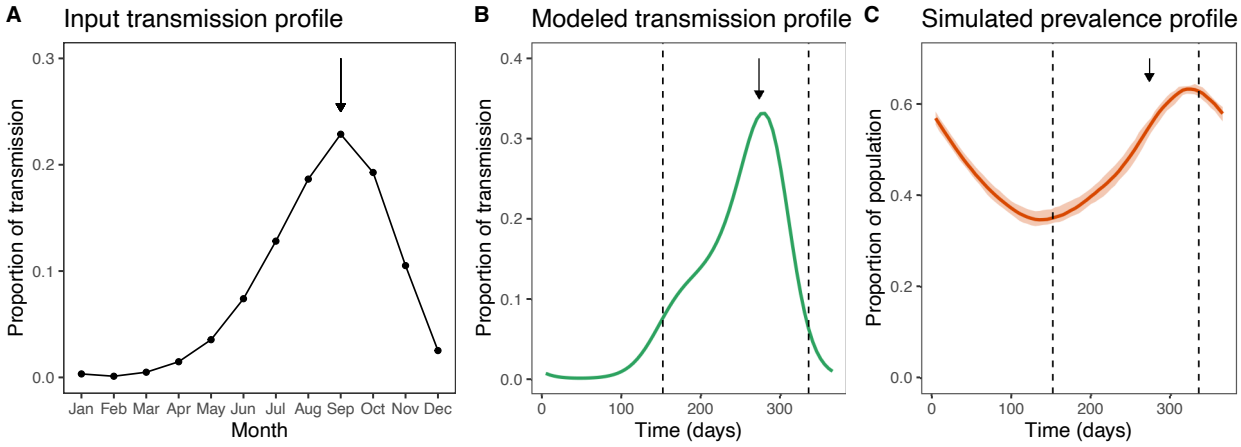

Figure S2.1
Illustration of the yearly malaria transmission and prevalence patterns in simulated seasonal settings.

(A) Observed, normalized, monthly seasonal pattern of malaria EIR in Namawala, Tanzania extracted from (80). **(B)** Corresponding input, 5-day seasonal EIR pattern used in OpenMalaria simulations, obtained by scaling and extrapolating the monthly seasonality profile from (80) to 5-day time steps. For this example, the simulated input EIR was 7.78 infectious bites per person per year. **(C)** Resulting simulated yearly *Pf*$PR_{0\text{-}99}$ profile. In all figures, the arrows indicate the month of September, the peak of transmission and show the delay between the peak of transmission and the resulting peak in malaria prevalence. The dotted vertical lines on figures **(B)** and **(C)** indicate the deployment times of first and second rounds of malaria interventions when applicable.

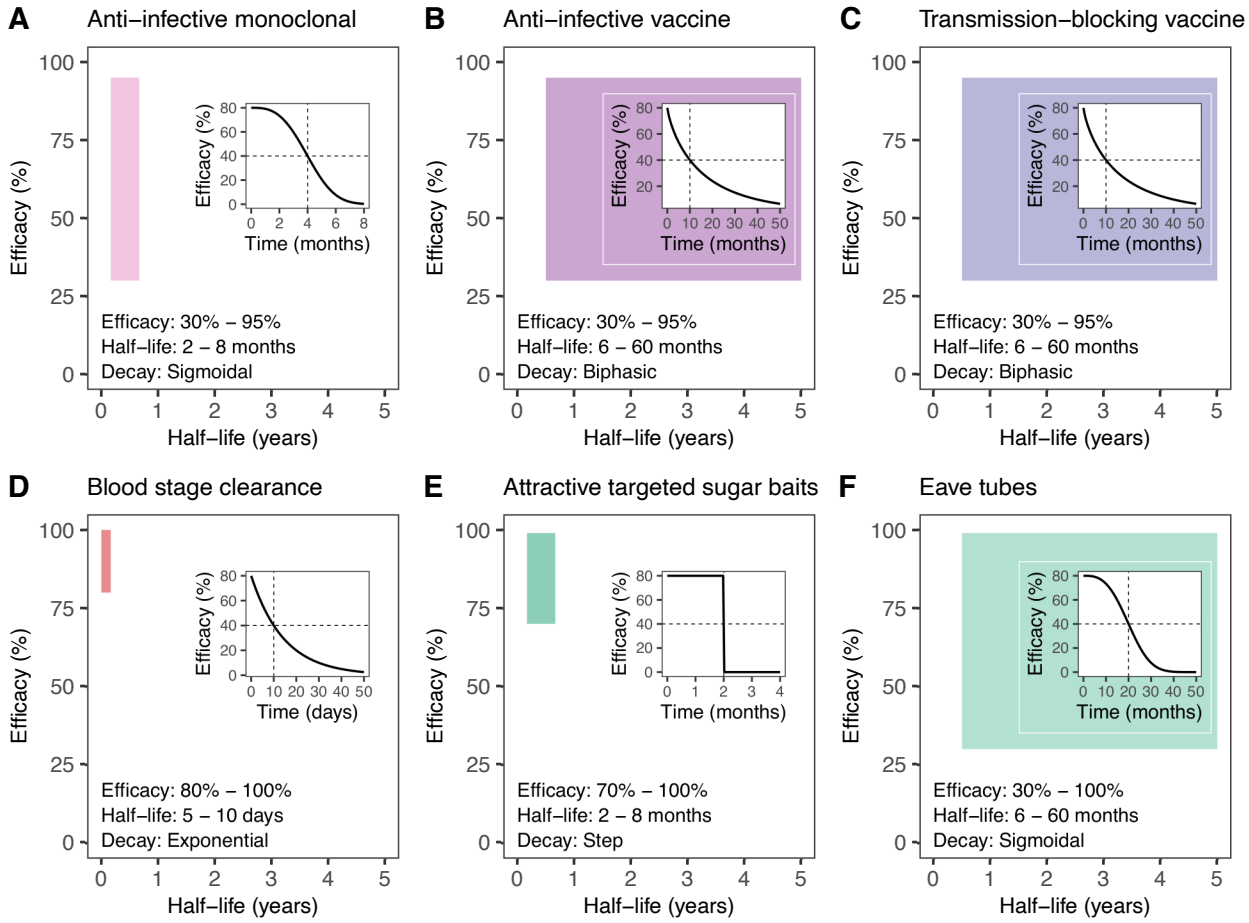

Figure S2.2

Representation of decay and the range of efficacy and half-life against different parasite or vector targets for intervention-agnostic malaria interventions.

The simulated malaria interventions (**A – F**) were modeled in terms of their targets in the malaria transmission cycle. The effect of each intervention is represented through the half-life of its decay (x axis) as well as the initial efficacy (y axis). The color blocks represent the range of parameter space of efficacy and half-life of decay considered in the current analysis for each intervention. The half-life and the color block do not represent the entire duration of effect, as that depends on the decay shape chosen for each intervention. The decay shape for each intervention is displayed in the right side insert of each plot where the dotted lines specify the half-life and corresponding half of the intervention efficacy. The definitions of all the parameter ranges for all interventions are provided in each figure on the lower left side and detailed in Table S2.1.

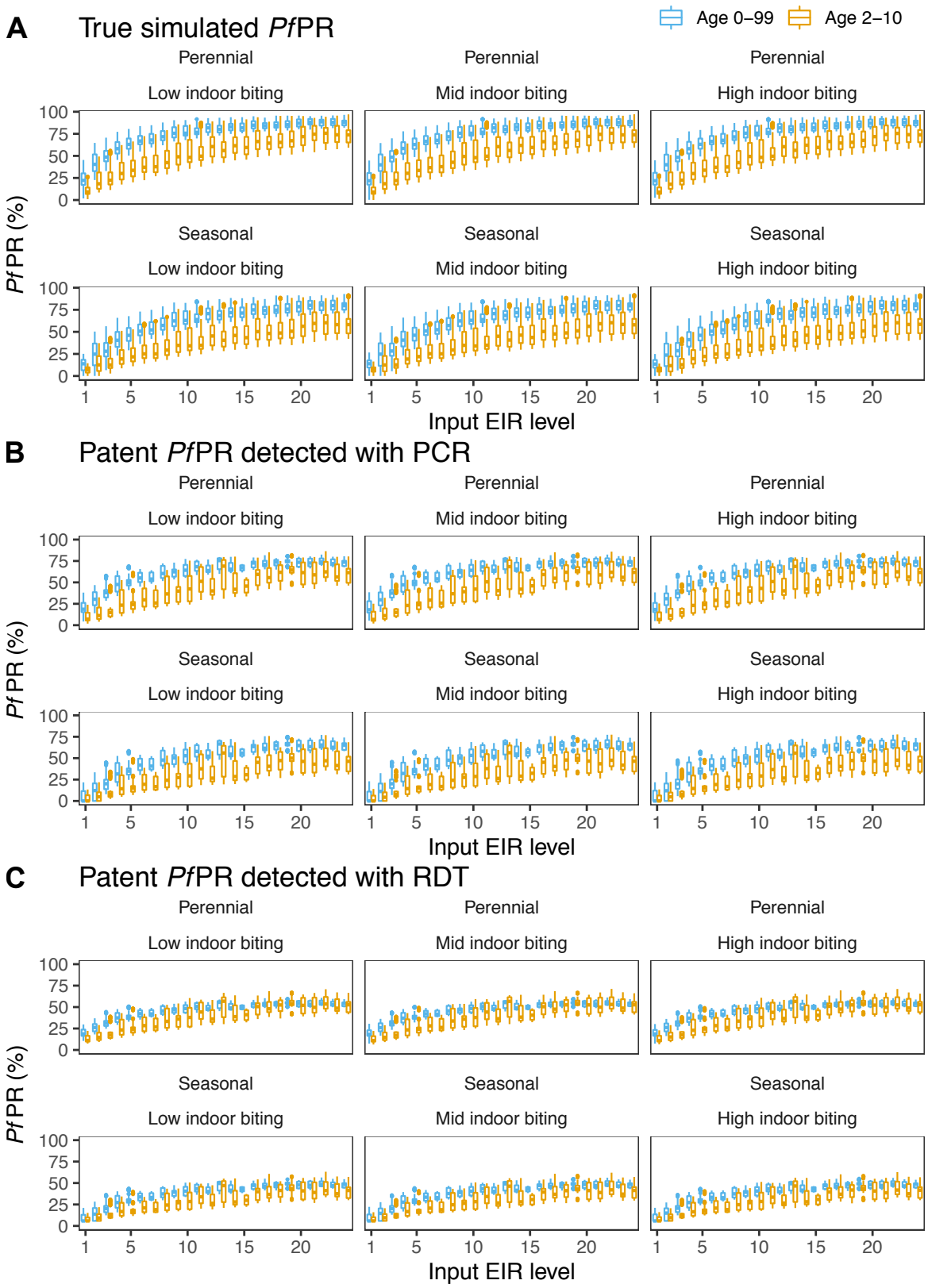
A
True simulated *Pf*PR
Age 0–99
Age 2–10
Perennial
Low indoor biting
Mid indoor biting
High indoor biting
Seasonal
*Pf*PR (%)
Input EIR level
B
Patent *Pf*PR detected with PCR
C
Patent *Pf*PR detected with RDT

1614

1615 **Figure S2.3**
1616 **Simulated distributions of true and patent (detected with PCR or RDT) *Pf*PR$_{0\text{-}99}$ and**
1617 ***Pf*PR$_{2\text{-}10}$ for various input EIR levels in absence of interventions.**
1618 The input entomological inoculation rate (EIR) defines the simulated malaria transmission level.
1619 In every simulation experiment, EIR was uniformly sampled from the interval [1, 25]. In figures
1620 (A) – (C), each panel corresponds to a simulated setting and presents the distributions of true **(A)**,
1621 patent with PCR **(B)** and patent with RDT **(C)** *Plasmodium falciparum* prevalence (*Pf*PR, shown
1622 with boxplots, blue for 0-99 years old and orange for 2-10 years old) at varying EIR levels (x axis).
1623 The 6 represented settings are defined by the seasonality pattern (perennial shown in the first row,
1624 or seasonal shown in the second row of each figure) and mosquito indoor biting behavior (low-
1625 shown in the first column, mid- shown in the second column or high-indoor biting shown in the
1626 third column of each figure). Each EIR level on the x axis is defined as a set of continuous input
1627 EIR values which range between the current level and the current level - 1, e.g., an input EIR level
1628 of 1 contains EIR values in the interval (0, 1]. For each EIR level and setting, the case management
1629 levels, i.e., the probability of seeking care (access to treatment) within 5 days from the onset of
1630 fever (E_5), was varied within the interval [0.04 - 0.5]. PCR stands for polymerase chain reaction
1631 and RDT stands for rapid diagnostic test.
1632

Intervention	Minimized profile	Intervention properties constraints	Specifications of combination therapies
Anti-infective monoclonal antibody (Sigmoidal decay)	Coverage	Coverage ∈ [0 .. 80%] Efficacy = 85% Half-life = 4 months	Blood stage drug: Efficacy = 90% Half-life = 10 days
	Efficacy	Coverage = 60% Efficacy ∈ [30% .. 95%] Half-life = 4 months	
	Half-life	Coverage = 60% Efficacy = 85% Half-life ∈ [2 .. 8 months]	
Anti-infective vaccine (Biphasic decay)	Coverage	Coverage ∈ [0 .. 80%] Efficacy = 85% Half-life = 7 months	Blood stage drug: Efficacy = 90% Half-life = 10 days
	Efficacy	Coverage = 60% Efficacy ∈ [30% .. 95%] Half-life = 7 months	
	Half-life	Coverage = 60% Efficacy = 85% Half-life ∈ [2 months .. 5 years]	
Transmission-blocking vaccine (Biphasic decay)	Coverage	Coverage ∈ [0 .. 80%] Efficacy = 85% Half-life = 7 months	Blood stage drug: Efficacy = 90% Half-life = 10 days
	Efficacy	Coverage = 60% Efficacy ∈ [30% .. 95%] Half-life = 7 months	
	Half-life	Coverage = 60% Efficacy = 85% Half-life ∈ [2 months .. 5 years]	
Attractive targeted sugar baits (Step decay)	Coverage	Coverage ∈ [0 .. 80%] Efficacy = 85% Half-life = 4 months	Not applicable
	Efficacy	Coverage = 60% Efficacy ∈ [70% .. 99%] Half-life = 4 months	
	Half-life	Coverage = 60% Efficacy = 85% Half-life ∈ [2 .. 8 months]	
Eave tubes (Sigmoidal decay)	Coverage	Coverage ∈ [0 .. 80%] Efficacy = 85% Half-life = 3 years	Not applicable
	Efficacy	Coverage = 60% Efficacy ∈ [30% .. 99%] Half-life = 3 years	
	Half-life	Coverage = 60% Efficacy = 85% Half-life ∈ [6 months .. 5 years]	

Table S2.1

Specifications of the optimization procedure for TPP development.

For each intervention, we successively identified the minimum profiles of the intervention coverage, efficacy, and half-life. Precisely, we optimized each parameter separately (column "Minimized profile"), according to its feasibility constraints while setting the two other parameters

1638 to the specified fixed values (column “Intervention properties constraints”). When deployed in
1639 combination with other drugs or vaccines, the additional interventions had fixed properties as well
1640 (column “Specifications of combination therapies”).
1641

3 Results: Disease model simulations

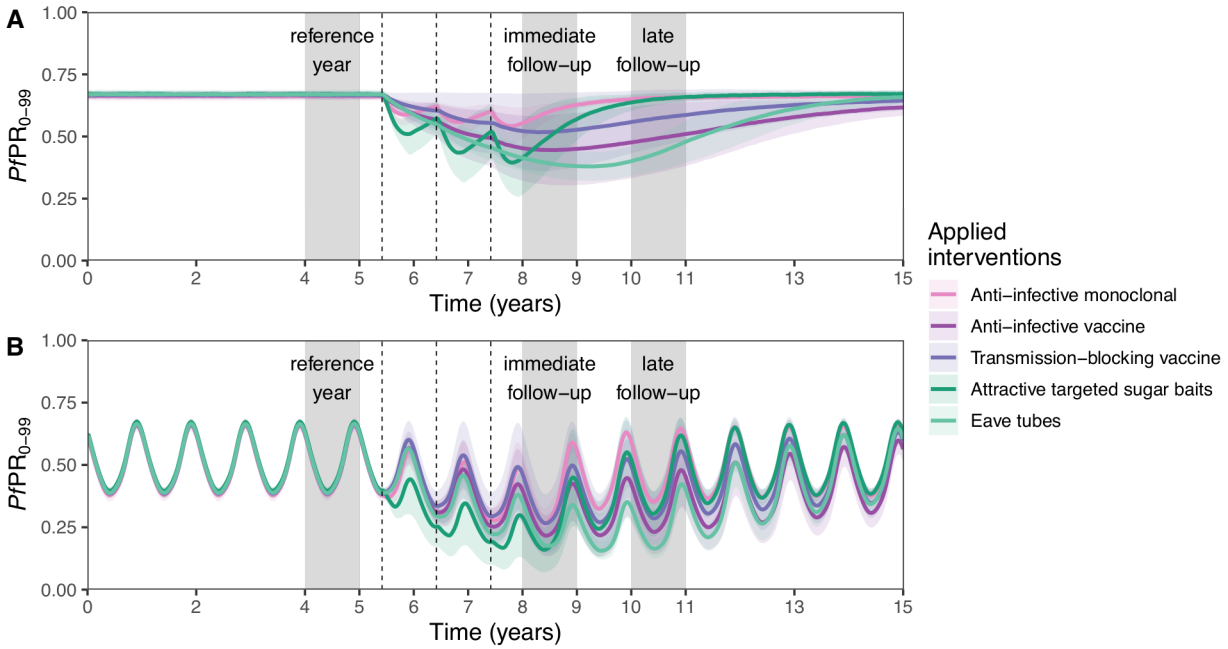

Figure S3.1.
Examples of OpenMalaria simulation outputs.

Time series of simulated malaria *Pf*PR$_{0\text{-}99}$ in a perennial **(A)** and seasonal **(B)** setting. Both figures display the prevalence of malaria cases, *Pf*PR$_{0\text{-}99}$, (y axis) across time (x axis). Interventions targeting different stages in the malaria transmission cycle (different colors) are applied once per year at the beginning of June (vertical dotted lines, in this example for three years of deployment). The effect of each intervention is assessed by evaluating the *Pf*PR$_{0\text{-}99}$ reduction in all ages relative to the year prior deployment (first grey block). Two outcomes are assessed, following an immediate and late follow-up (second and third grey blocks), depending on whether the average prevalence is calculated across the next year after deployment, or across the third year after deployment, respectively.

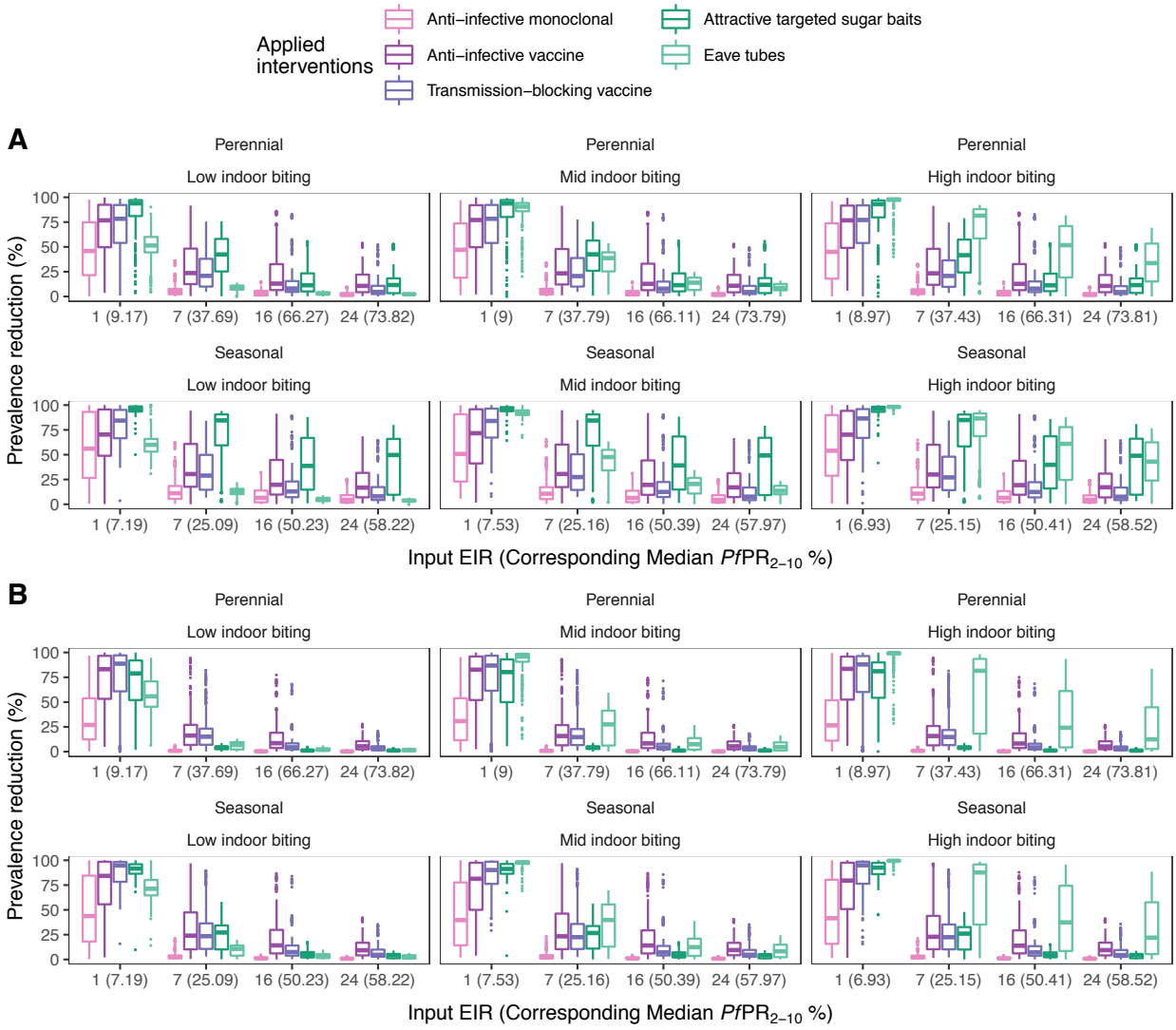

Figure S3.2.

Distributions of prevalence reduction following yearly deployment of single interventions.

Prevalence reduction was calculated by comparing the initial prevalence in the year before any interventions were deployed to the yearly prevalence obtained in the following year (short follow-up, panel **A**) and in the third year (long follow-up, panel **B**) after deployment of interventions. Each individual figure corresponds to a simulated setting and presents the distributions of $Pf\mathrm{PR}_{0\text{-}99}$ reduction (shown with boxplots) at varying EIR as well as corresponding simulated $Pf\mathrm{PR}_{2\text{-}10}$ levels (x axis). Each boxplot displays the interquartile range (box), the median value (horizontal line), the largest and smallest values within 1.5 times the interquartile range (whiskers), and the remaining outside values (points). The 6 represented settings in each panel are defined by the seasonality pattern (perennial or seasonal) and mosquito indoor biting behavior (low, mid or high indoor biting). Each EIR level on the x axis is defined as a set of continuous input EIR values which range between the current level and the current level - 1, e.g., an input EIR level of 1 contains all EIR values in the interval (0, 1]. The definitions and ranges of all the EIR levels is included in Table S2.1.

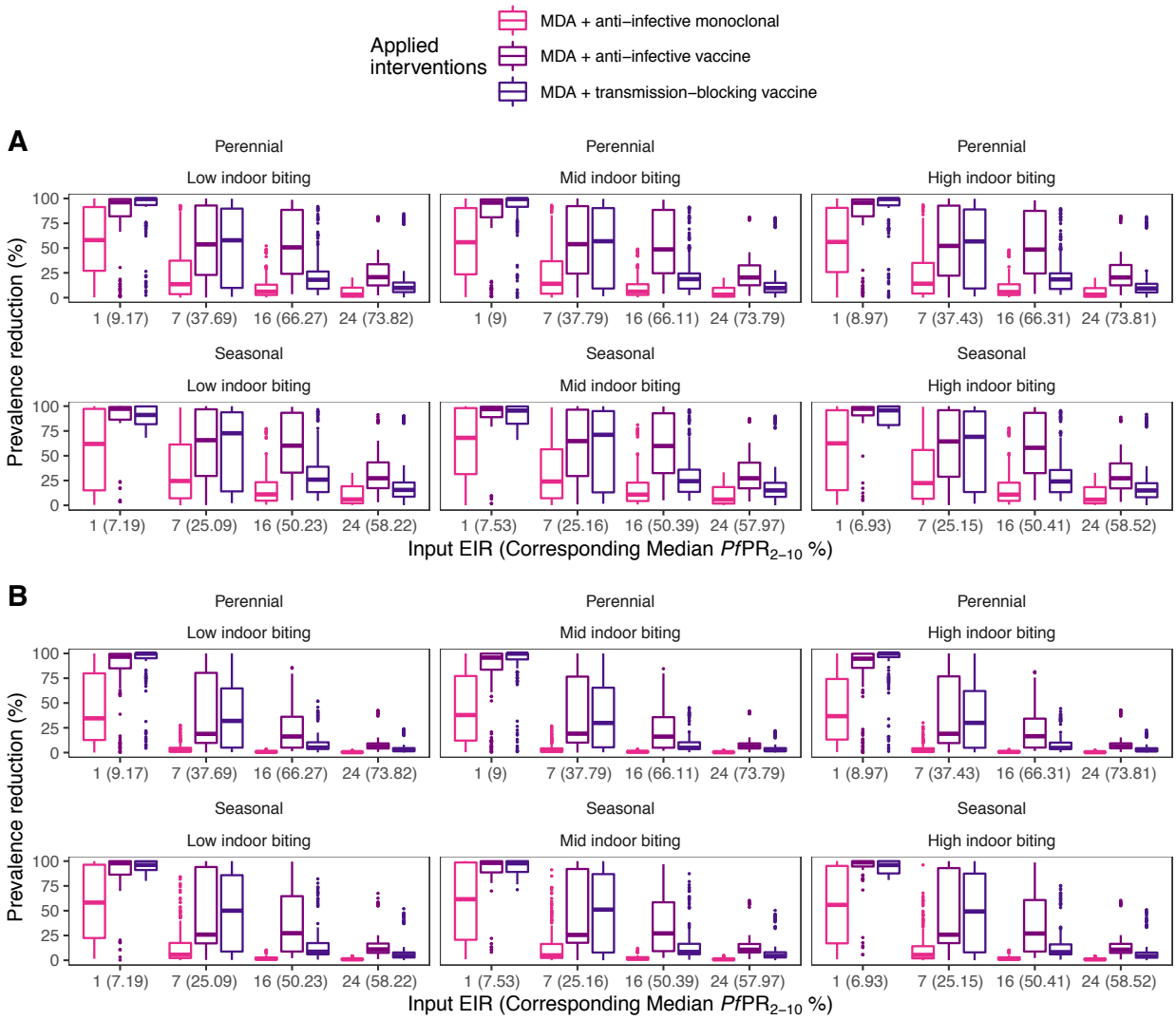

Figure S3.3.
Distributions of prevalence reduction following yearly deployment of combinations of interventions.

Prevalence reduction was calculated by comparing the initial prevalence in the year before any interventions were deployed to the yearly prevalence obtained in the following year (short follow-up, panel **A**) and in the third year (long follow-up, panel **B**) after deployment of interventions. Each individual figure corresponds to a simulated setting and presents the distributions of $Pf\mathrm{PR}_{0\text{-}99}$ reduction (shown with boxplots) at varying EIR as well as the corresponding simulated $Pf\mathrm{PR}_{2\text{-}10}$ levels (x axis). Each boxplot displays the interquartile range (box), the median value (horizontal line), the largest and smallest values within 1.5 times the interquartile range (whiskers), and the remaining outside values (points). The 6 represented settings in each panel are defined by the seasonality pattern (perennial or seasonal) and mosquito indoor biting behavior (low, mid or high indoor biting). Each EIR level on the x axis is defined as a set of continuous input EIR values which range between the current level and the current level - 1, e.g., an input EIR level of 1 contains EIR values in the interval (0, 1]. The definitions and ranges of all the EIR levels are included in Table S2.1. MDA stands for mass drug administration.

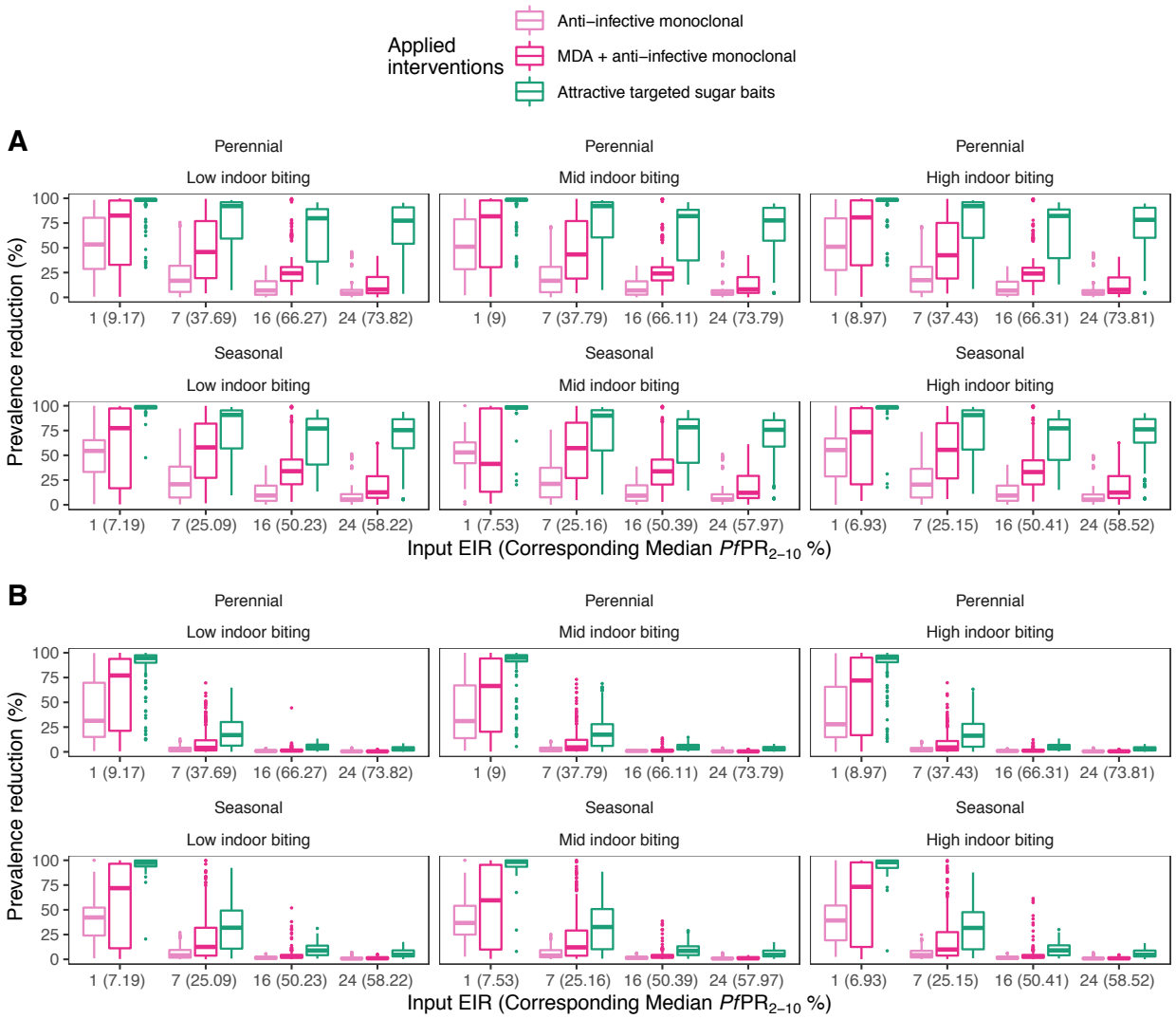

Figure S3.4.

Distributions of prevalence reduction following deployment of single and combinations of interventions twice per year.

Prevalence reduction was calculated by comparing the initial prevalence in the year before any interventions were deployed to the yearly prevalence obtained in the following year (short follow-up, panel **A**) and in the third year (long follow-up, panel **B**) after deployment of interventions. Each individual figure corresponds to a simulated setting and presents the distributions of $Pf\mathrm{PR}_{0\text{-}99}$ reduction (shown with boxplots) at varying EIR as well as corresponding simulated $Pf\mathrm{PR}_{2\text{-}10}$ levels (x axis). Each boxplot displays the interquartile range (box), the median value (horizontal line), the largest and smallest values within 1.5 times the interquartile range (whiskers), and the remaining outside values (points). The 6 represented settings in each panel are defined by the seasonality pattern (perennial or seasonal) and mosquito indoor biting behavior (low, mid or high indoor biting). Each EIR level on the x axis is defined as a set of continuous input EIR values which range between the current level and the current level - 1, e.g., an input EIR level of 1 contains EIR values in the interval (0, 1]. The definitions and ranges of all the EIR levels for all simulated settings is included in Table S2.1. MDA stands for mass drug administration.

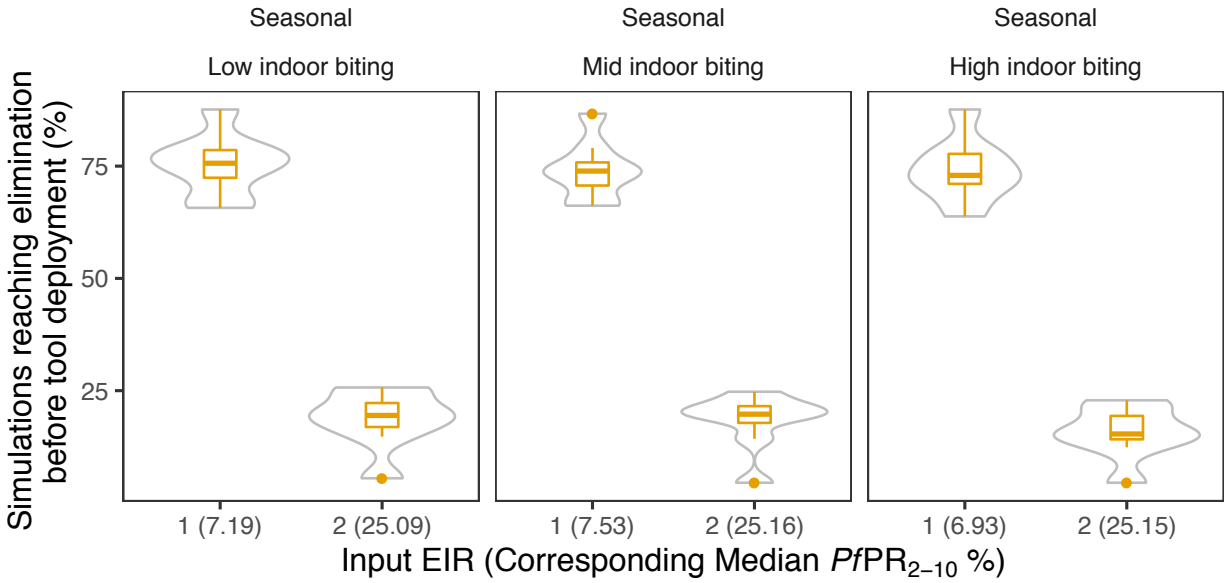

Figure S3.5.

Simulations reaching malaria elimination before intervention deployment.

The violin plots and boxplots in each panel present the distributions of the percentage of simulations reaching malaria elimination ($Pf\mathrm{PR}_{0\text{-}99} = 0$) before intervention deployment (this can arrive due to case management and only occurs in seasonal settings), across all simulated interventions and intervention combinations.

4 Results: Emulator performance

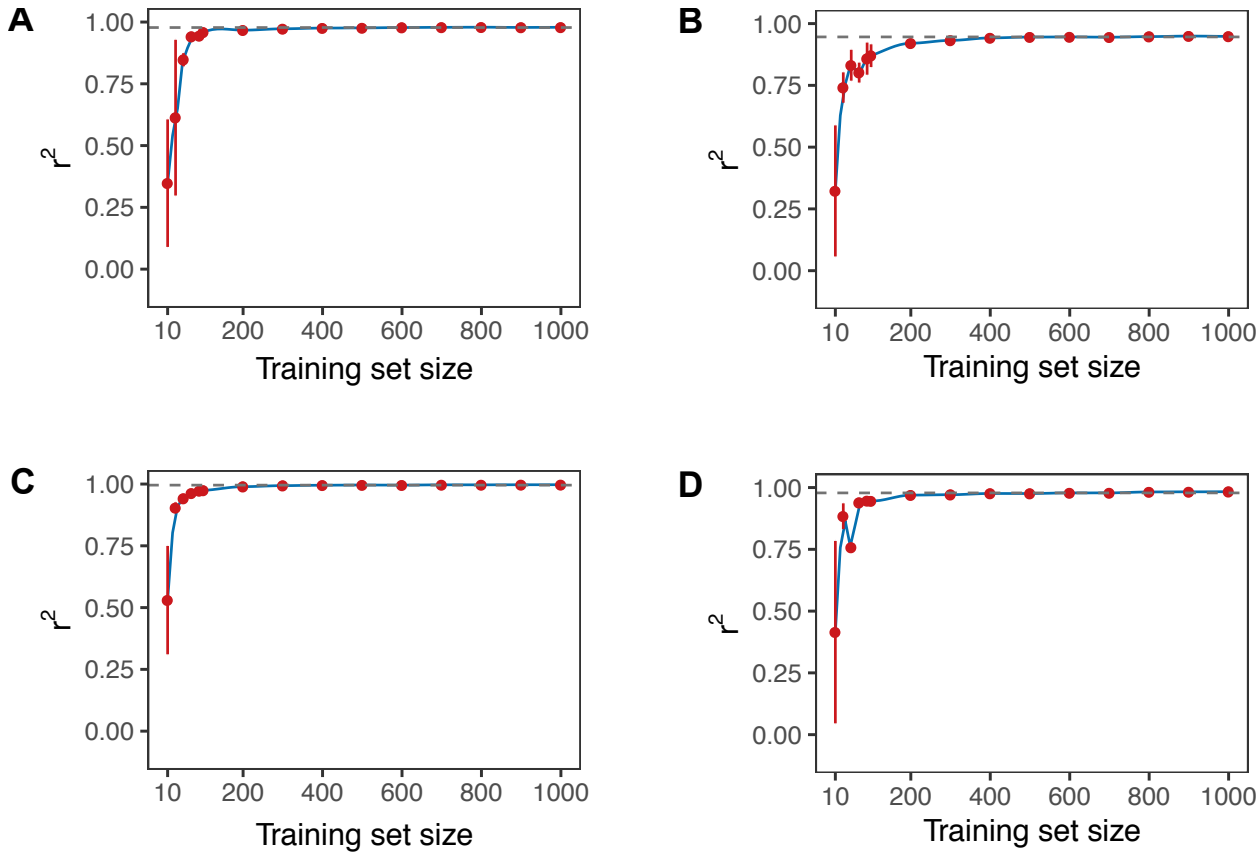

Figure S4.1.
Assessment of the performance of the trained GP depending on the training set size.
Each figure presents the Pearson correlation coefficient r^2 between true and predicted values on a broad range of out-of-sample test sets of varying length, when simulating deployment of an anti-infective monoclonal antibody deployed once per year **(A)** or twice per year **(B)** as well as in combination with a blood-stage drug once **(C)** or twice per year **(D)**.

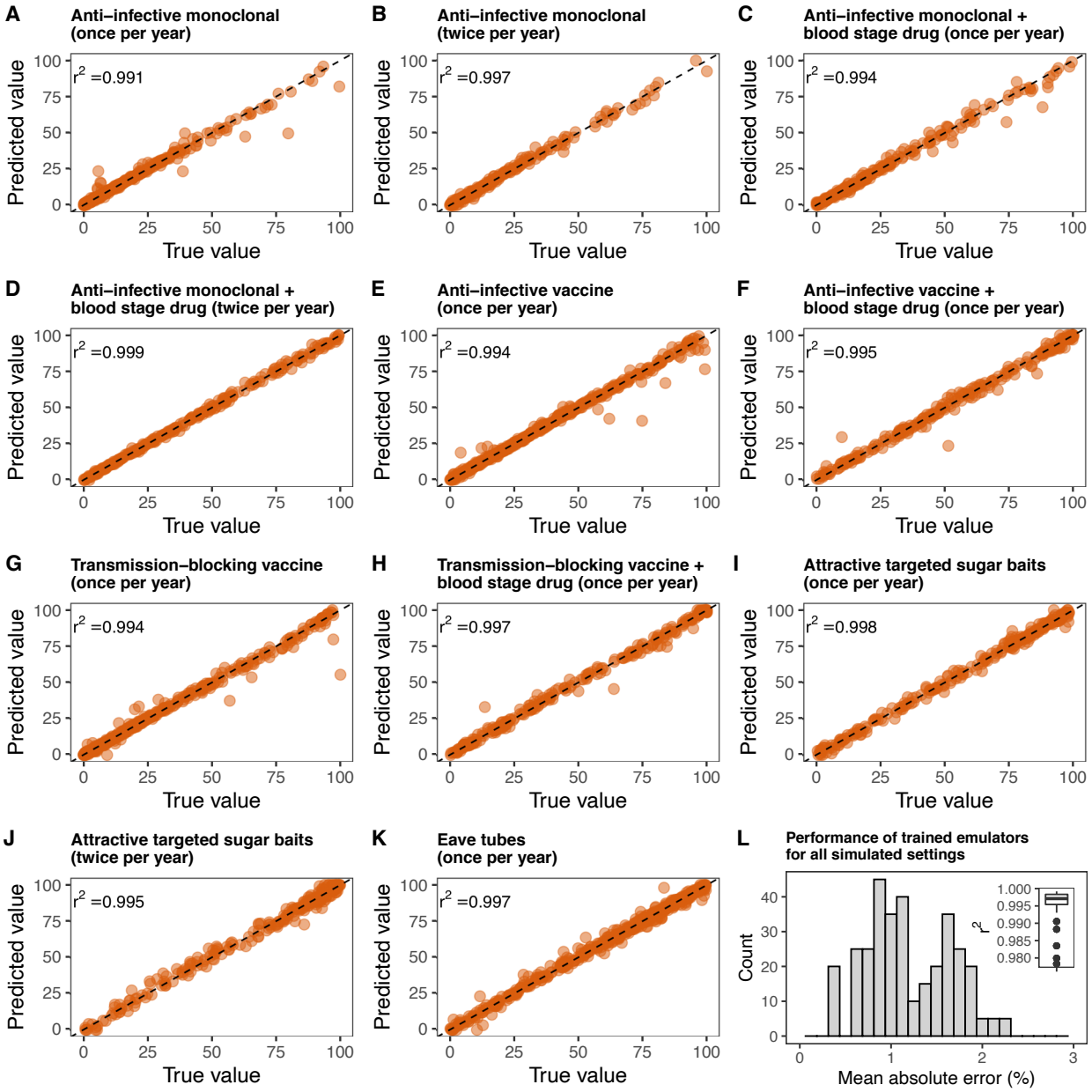

Figure S4.2.

Performance of the trained GP emulators predicting immediate intervention impact.

For a wide range of deployed interventions and transmission settings (see Materials and Methods), GP emulators were trained to predict the immediate impact of each intervention, i.e., the resulting average *Pf*PR$_{0\text{-}99}$ reduction in the year following deployment of the intervention. The performance of the trained emulators was assessed by inspecting the Pearson correlation coefficient (r^2) and the mean absolute error between true and predicted values on an out-of-sample test set. Figures **(A) – (K)** display the true and predicted values of each trained emulator across all deployed interventions in a seasonal transmission setting with high indoor biting. Figure **(L)** summarizes r^2 and the mean absolute error of all the trained emulators for all simulated transmission settings and interventions (the simulated settings were defined by seasonality and mosquito biting patterns, see Table S2.1 for detailed values per setting).

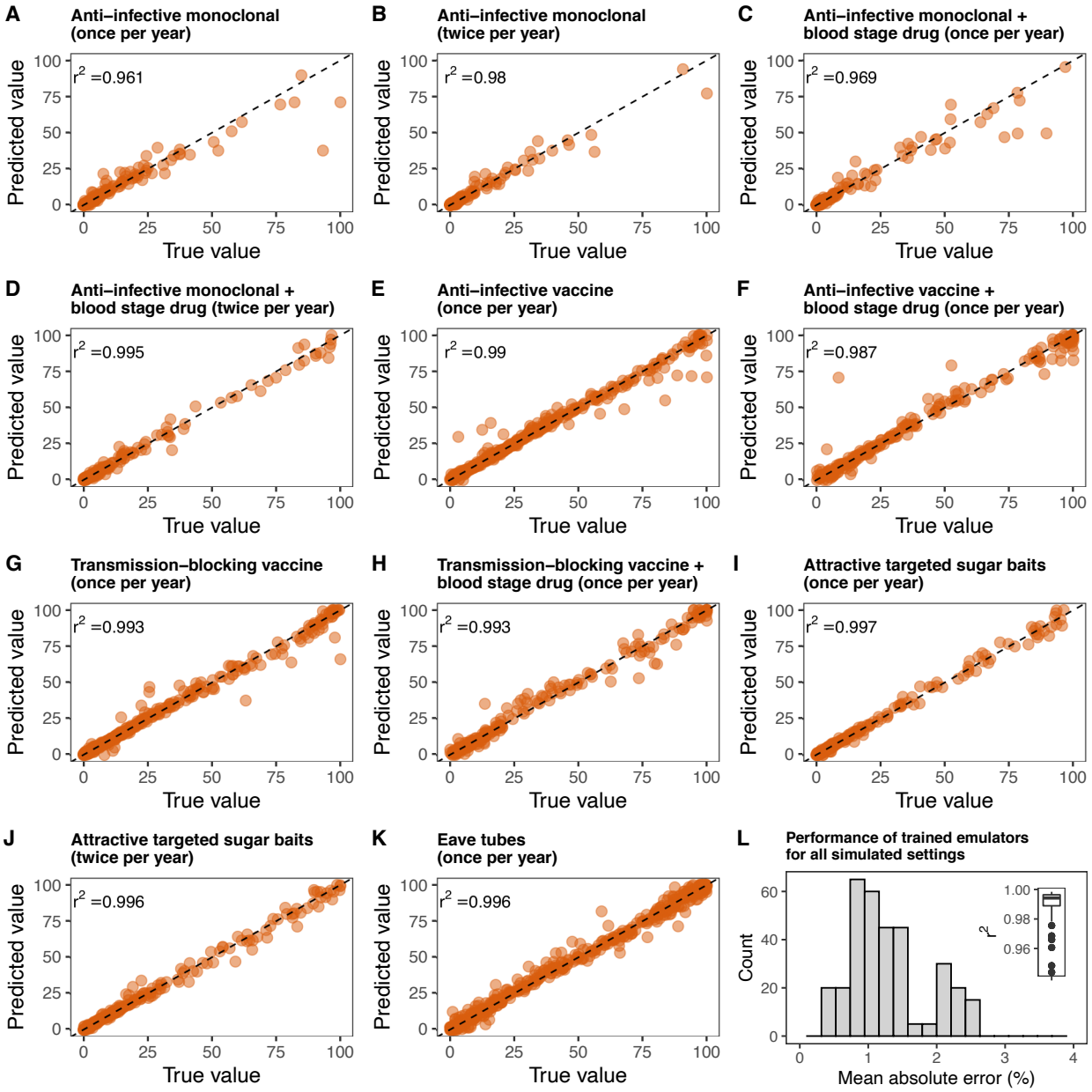

Figure S4.3.

Performance of the trained GP emulators predicting long-term intervention impact.

For a wide range of deployed interventions and transmission settings (see Methods), GP emulators were trained to predict the immediate impact of each intervention, i.e., the resulting average *Pf*PR$_{0\text{-}99}$ reduction in the third year following deployment of the intervention. The performance of the trained emulators was assessed by inspecting the Pearson correlation coefficient (r^2) and the mean absolute error between true and predicted values on an out-of-sample test set. Figures **(A) – (K)** display the true and predicted values of each trained emulator across all deployed interventions in a seasonal transmission setting with high indoor biting. Figure **(L)** summarizes r^2 and the mean absolute error of all the trained emulators for all simulated transmission settings and interventions (the simulated settings were defined by seasonality and mosquito biting patterns, see Table S2.1 for detailed values per setting).

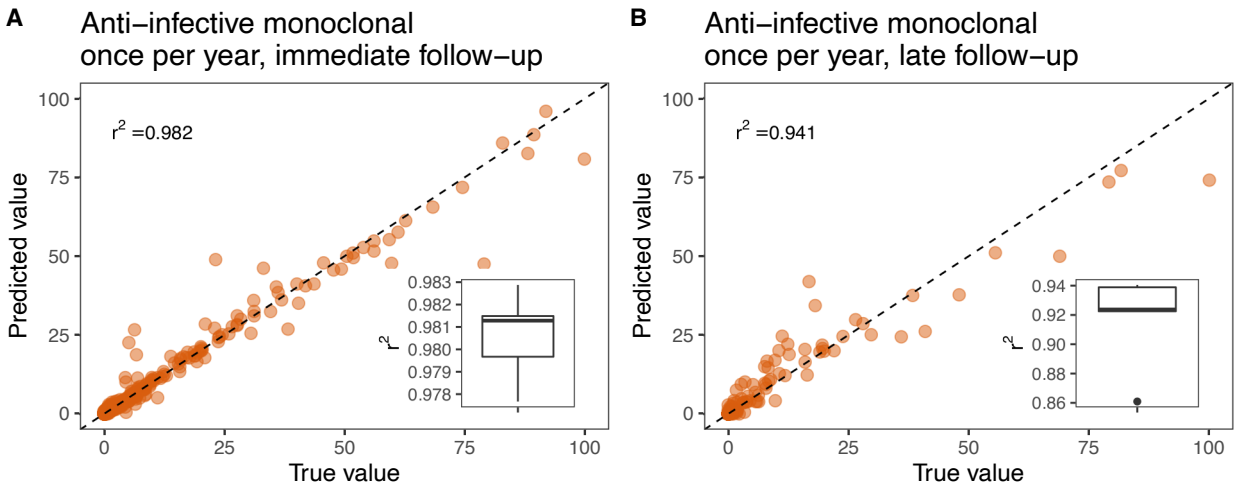

Figure S4.4

Performance of trained GP emulators predicting incidence reduction

Plasmodium falciparum malaria incidence reduction in all ages in the first **(A)** and third **(B)** year following deployment of a monoclonal antibody intervention. The performance of the trained emulators was assessed by inspecting the Pearson correlation coefficient (r^2) in a cross-validation scheme (lower right boxplot displays the distribution of r^2 obtained on the left-out test sets during cross-validation) as well as on an out-of-sample test set (upper left corner).

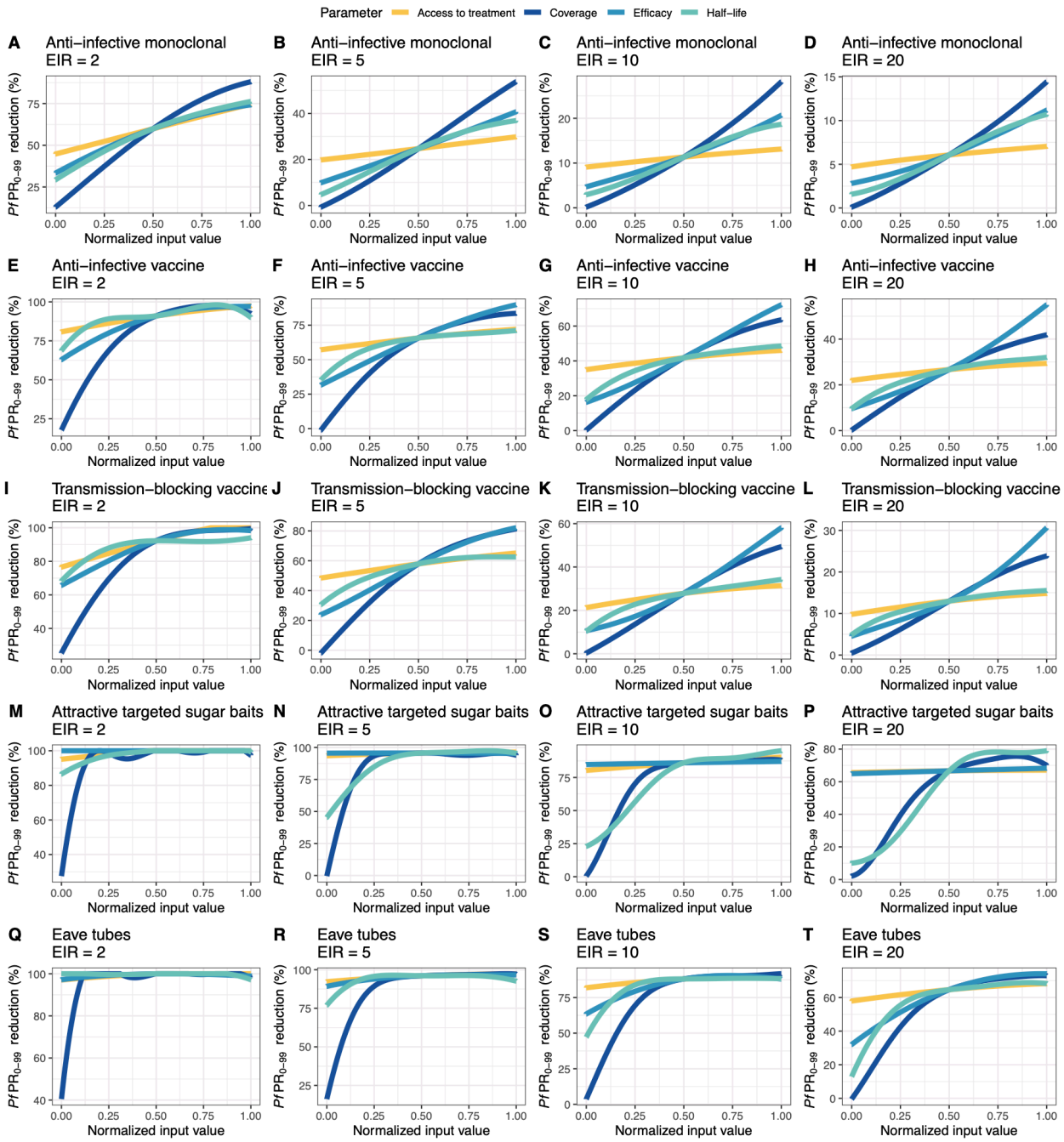

Figure S4.5

Relationships between input intervention parameters and the predicted immediate *Pf*PR$_{0\text{-}99}$ reduction with the trained GP emulator

Each parameter (intervention characteristic) was varied in turn across its defined range (parameter ranges are defined in Table 1) while the remaining parameters were set to their average values. The figures display the immediate *Pf*PR$_{0\text{-}99}$ reduction predicted with the GP emulator. A min-max normalization was used to display the varying input values of each of the parameters.

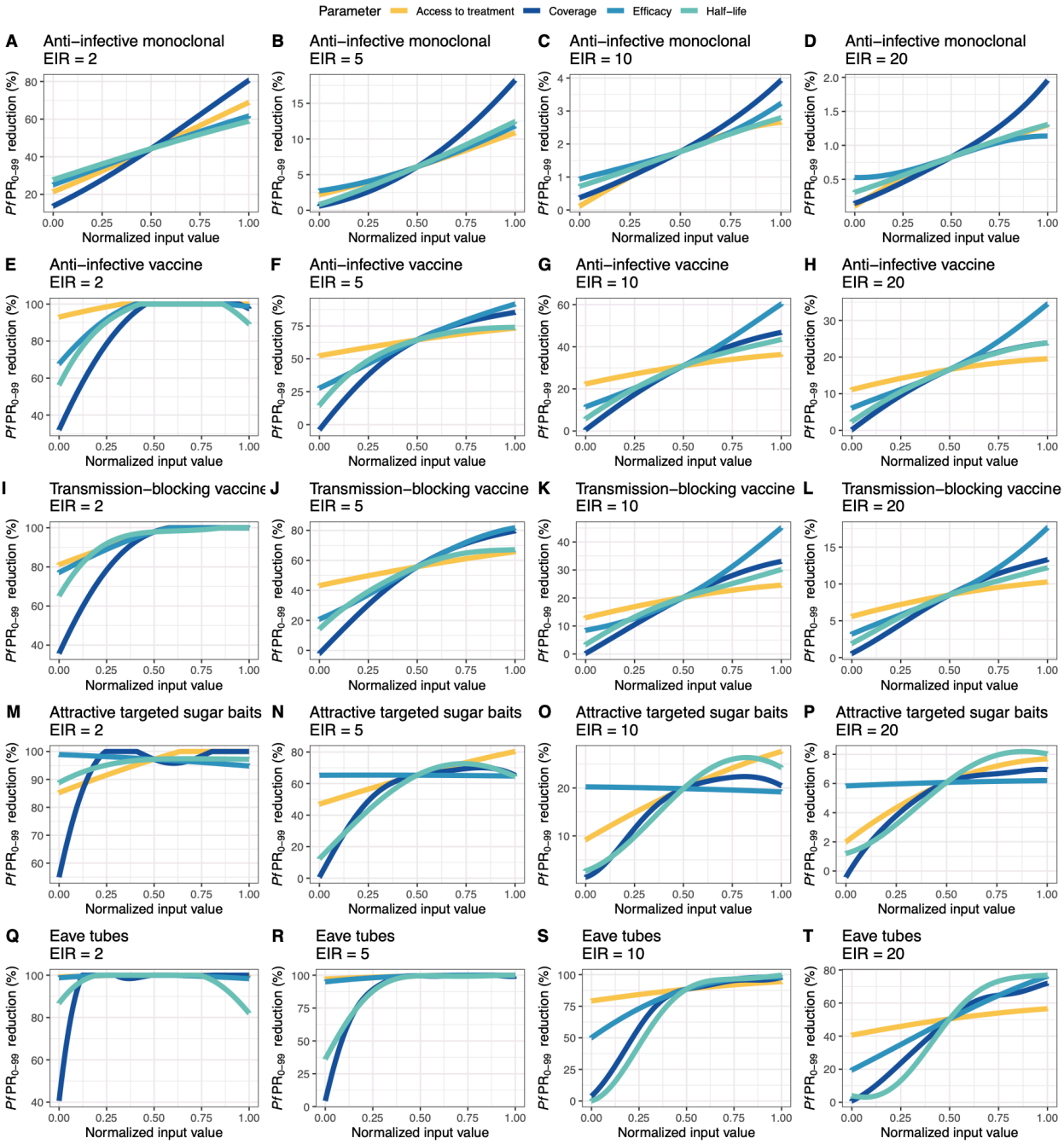

Figure S4.6

Relationships between input intervention parameters and the predicted long-term *Pf*PR$_{0\text{-}99}$ reduction with the trained GP emulator

Each parameter (intervention characteristic) was varied in turn across its defined range (parameter ranges are defined in Table 1) while the remaining parameters were set to their average values. The figures display the long-term *Pf*PR$_{0\text{-}99}$ reduction predicted with the GP emulator. A min-max normalization was used to display the varying input values of each of the parameters.

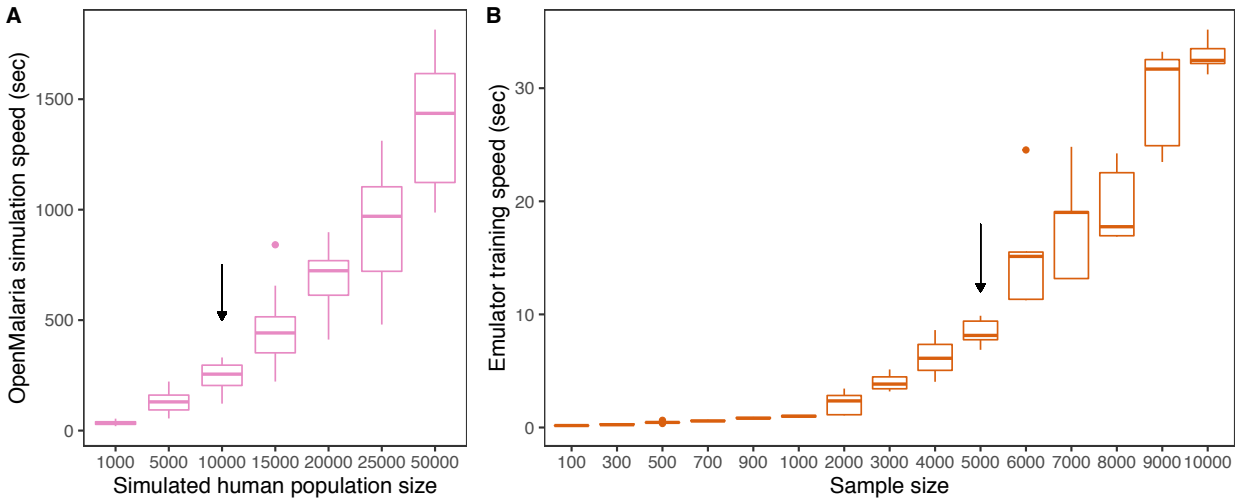

Figure S4.7

Execution time of OpenMalaria simulations and GP emulator training

(A) CPU execution time of a single OpenMalaria simulation for varying population size. The arrow indicates the population size of 10000 human hosts used in the present study. **(B)** CPU time required for training the GP emulator using training sets of OpenMalaria simulations of varying size. The arrow indicates the typical sample size used in the present analysis. In both figures, execution times were estimated 5 times in each case and the resulting distribution was displayed (boxplots).

Intervention(s) (deployment)	Training set size	Test set size	Cross-validation r^2 and (mean error)	Test set r^2 and (mean error)
Anti-infective monoclonal antibody (once/year)	10000	5000	**Immediate:** 0.99 (1.02%) **Long:** 0.96 (1.15%)	**Immediate:** 0.99 (0.63%) **Long:** 0.97 (0.68%)
Anti-infective monoclonal antibody (twice/year)	5000	2500	**Immediate:** 0.99 (1.11%) **Long:** 0.97 (1.32%)	**Immediate:** 0.99 (0.91%) **Long:** 0.99 (0.83%)
Anti-infective monoclonal antibody + Blood stage drug (once/year)	10000	5000	**Immediate:** 0.99 (1.34%) **Long:** 0.96 (1.74%)	**Immediate:** 0.99 (1.18%) **Long:** 0.98 (1.05%)
Anti-infective monoclonal antibody + Blood stage drug (twice/year)	5000	2500	**Immediate:** 0.99 (1.26%) **Long:** 0.97 (1.98%)	**Immediate:** 0.99 (0.98%) **Long:** 0.99 (1.12%)
Anti-infective vaccine (once/year)	10000	5000	**Immediate:** 0.99 (1.08%) **Long:** 0.99 (1.3%)	**Immediate:** 0.99 (0.99%) **Long:** 0.99 (1.16%)
Anti-infective vaccine + Blood stage drug (once/year)	5000	2500	**Immediate:** 0.99 (1.18%) **Long:** 0.99 (1.63%)	**Immediate:** 0.99 (1.57%) **Long:** 0.99 (2.25%)
Transmission-blocking vaccine (once/year)	10000	5000	**Immediate:** 0.99 (1.13) **Long:** 0.99 (1.25%)	**Immediate:** 0.99 (0.89%) **Long:** 0.99 (1.07%)
Transmission-blocking vaccine + Blood stage drug (once/year)	5000	2500	**Immediate:** 0.99 (1.25%) **Long:** 0.99 (1.53%)	**Immediate:** 0.99 (1.68%) **Long:** 0.99 (2.23 %)
Attractive targeted sugar baits (once/year)	5000	2500	**Immediate:** 0.99 (1.26%) **Long:** 0.98 (1.71%)	**Immediate:** 0.99 (1.98%) **Long:** 0.99 (1.19%)
Attractive targeted sugar baits (twice/year)	5000	2500	**Immediate:** 0.99 (1.09%) **Long:** 0.99 (1.98%)	**Immediate:** 0.99 (1.03%) **Long:** 0.99 (1.29%)
Eave tubes (once/year)	10000	5000	**Immediate:** 0.99 (1.11%) **Long:** 0.99 (1.3%)	**Immediate:** 0.99 (0.89%) **Long:** 0.99 (1.26%)

Table S4.1.
Performance of the trained GP emulators predicting immediate and long-term intervention impact.

For each modelled transmission setting defined by case management level and mosquito biting patterns and for each intervention (Table S2.1), a comprehensive set of simulation scenarios was built by sampling uniformly the parameter space (defined in Table S2.1) and simulation with OpenMalaria. In this manner, a training and a test set were constructed. The training set was used to train, for each setting and intervention, a Heteroskedastic GP model in a 5-fold cross-validation procedure. The performance of the trained GP was assessed by computing the Pearson correlation coefficient r^2 as well as the mean error between the true and predicted outcomes on both out-of-sample cross-validation and test sets. For each intervention and follow-up (immediate or long-term), the average r^2 and mean error for all the GP models trained across 6 settings (seasonal or perennial, high, medium or low mosquito indoor biting) are reported.

5 Results: Key determinants of impact

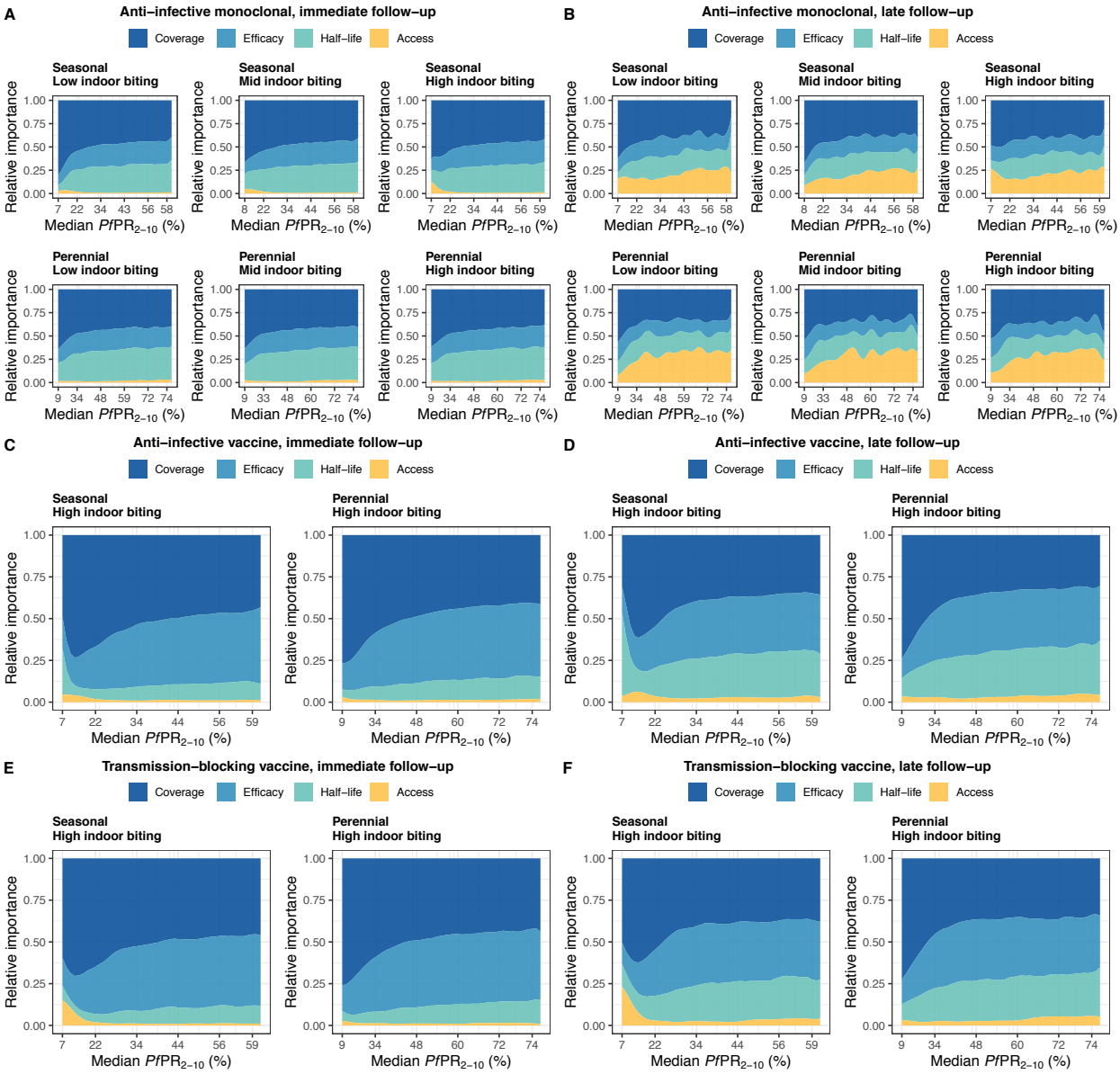

Figure S5.1.

Key drivers of impact for immunological malaria interventions across different transmission settings.

Results of sensitivity analysis identifying the determinants of intervention impact on *Pf*PR$_{0\text{-}99}$ reduction for anti-infective monoclonal antibodies **(A, B)**, anti-infective vaccines **(C, D)** and transmission-blocking vaccines **(E, F)**. The distinct colors represent proportions of the GP emulator output variance (relative importance) attributable to intervention efficacy, half-life, deployment coverage, as well as health system access. Determinants of impact are shown for both immediate and late follow-up, when interventions are applied once per year for three years in different transmission settings (see full intervention specifications in the Methods section). The transmission settings are defined by two seasonal settings (seasonal and perennial) and three types of mosquito biting patterns (low, medium and high indoor biting). The mosquito biting patterns

had little to no effect on the results of the sensitivity analysis for these immunological interventions (see results for all settings for monoclonal antibodies in figures A and B). Therefore, only the results for seasonal and perennial settings with high indoor mosquito biting are displayed for the vaccine interventions.

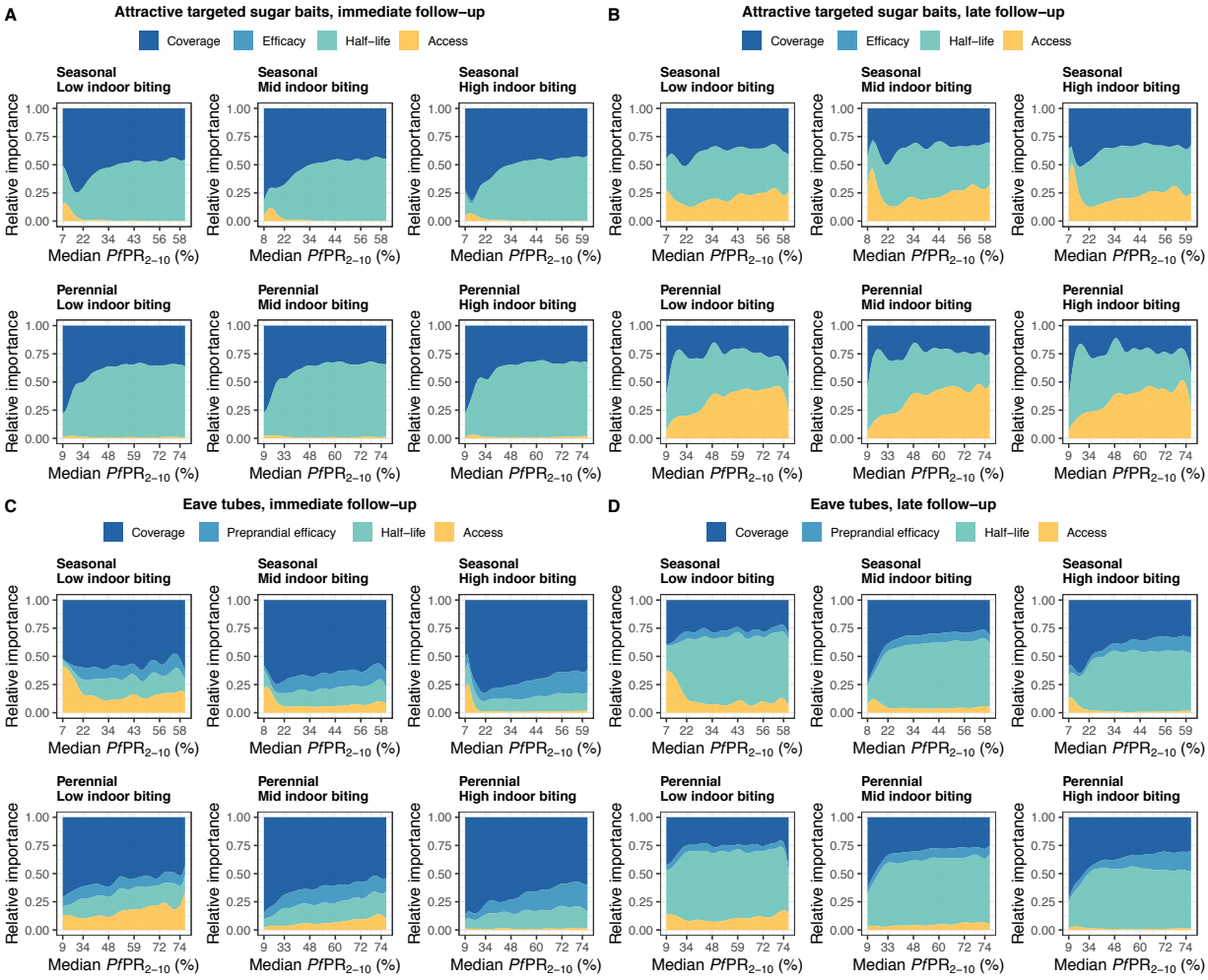

Figure S5.2.
Key drivers of impact for vector control malaria interventions across different transmission settings.

Results of sensitivity analysis identifying the determinants of intervention impact on *Pf*PR$_{0\text{-}99}$ reduction for attractive targeted sugar baits **(A, B)** and eave tubes **(C, D)**. The distinct colors represent proportions of the GP emulator output variance (relative importance) attributable to intervention efficacy, half-life, deployment coverage, as well as health system access. Determinants of impact are shown for both immediate and late follow-up, when interventions are applied once per year for three years in different transmission settings (see full intervention specifications in the Methods section). The transmission settings are defined by two seasonal settings (seasonal and perennial) and three types of mosquito biting patterns (low, medium and high indoor biting). Like for the immunological interventions in the previous figure, we see limited difference between key drivers for attractive targeted sugar baits in different biting settings as mosquitoes sugar feed before indoor or outdoor biting. In contrast, we observe that intervention properties of eave tubes rather than health system access to treatment are larger drivers of impact in indoor biting settings, as mosquitoes in those settings will be more likely to contact the eave tube.

6 Results: Feasible landscapes of optimal, constrained intervention profiles

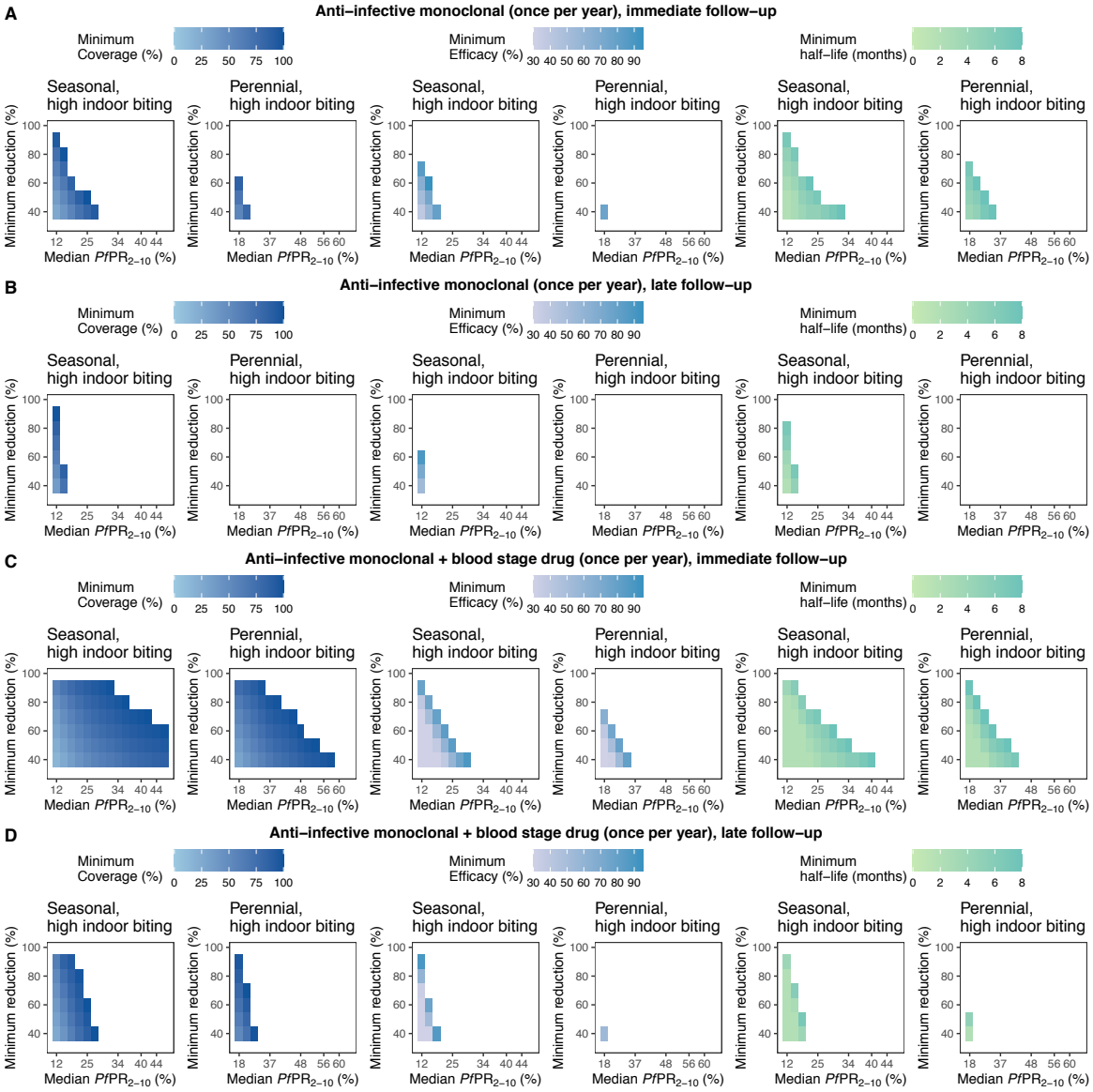

Figure S6.1.

Feasible landscapes of optimal, constrained intervention profiles (TPPs) for an anti-infective monoclonal antibody deployed once per year.

The heatmaps represent landscapes of optimal, constrained intervention characteristic profiles (minimum coverage, efficacy, and half-life) required to achieve various health goals (quantified by minimal reduction in $Pf\mathrm{PR}_{0\text{-}99}$, y axis) across different simulated true $Pf\mathrm{PR}_{2\text{-}10}$ settings (rounded values, x axis) with seasonal transmission and high indoor mosquito biting. Each intervention characteristic was minimized in turn, while keeping the other characteristics fixed (fixed parameter values for each optimization are specified in Table S2.2). Results are shown for an anti-infective monoclonal antibody delivered alone and assessing immediate **(A)** and late **(B)** follow up, as well as when delivered in combination with a blood stage drug assessing immediate **(C)** and late **(D)** follow-up. The simulated case management level (E_5) for all the displayed optimization analyses was assumed 25%.

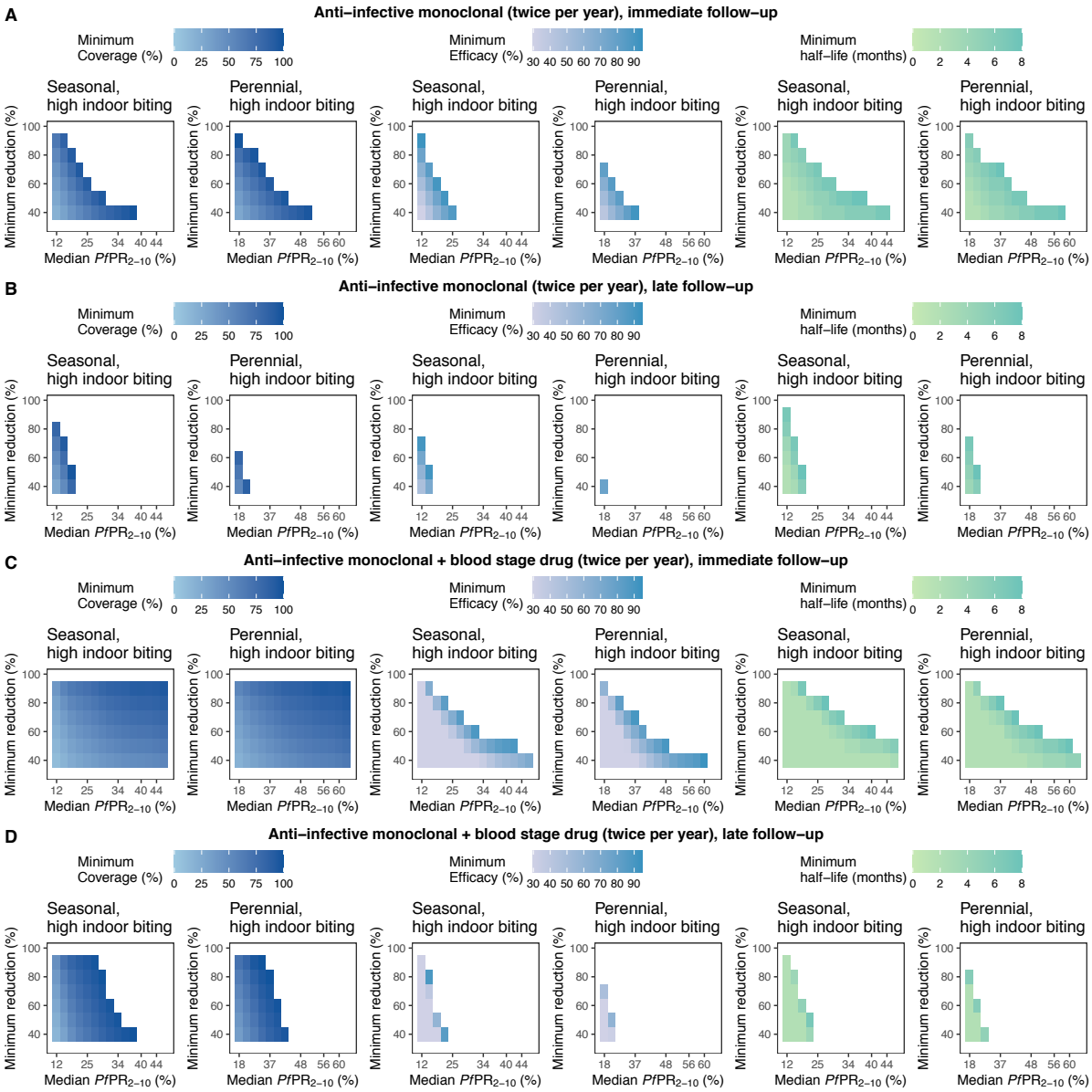

Figure S6.2.

Feasible landscapes of optimal, constrained intervention profiles (TPPs) for an anti-infective monoclonal antibody deployed twice per year.

The heatmaps represent landscapes of optimal, constrained intervention characteristic profiles (minimum coverage, efficacy, and half-life) required to achieve various health goals (quantified by minimal reduction in *Pf*PR$_{0\text{-}99}$, y axis) across different simulated true *Pf*PR$_{2\text{-}10}$ settings (rounded values, x axis) with seasonal transmission and high indoor mosquito biting. Each intervention characteristic was minimized in turn, while keeping the other characteristics fixed (fixed parameter values for each optimization are specified in Table S2.2). Results are shown for an anti-infective monoclonal antibody delivered alone and assessing immediate **(A)** and late **(B)** follow up, as well as when delivered in combination with a blood stage drug assessing immediate **(C)** and late **(D)** follow-up. The simulated case management level (E_5) for all the displayed optimization analyses was assumed 25%.

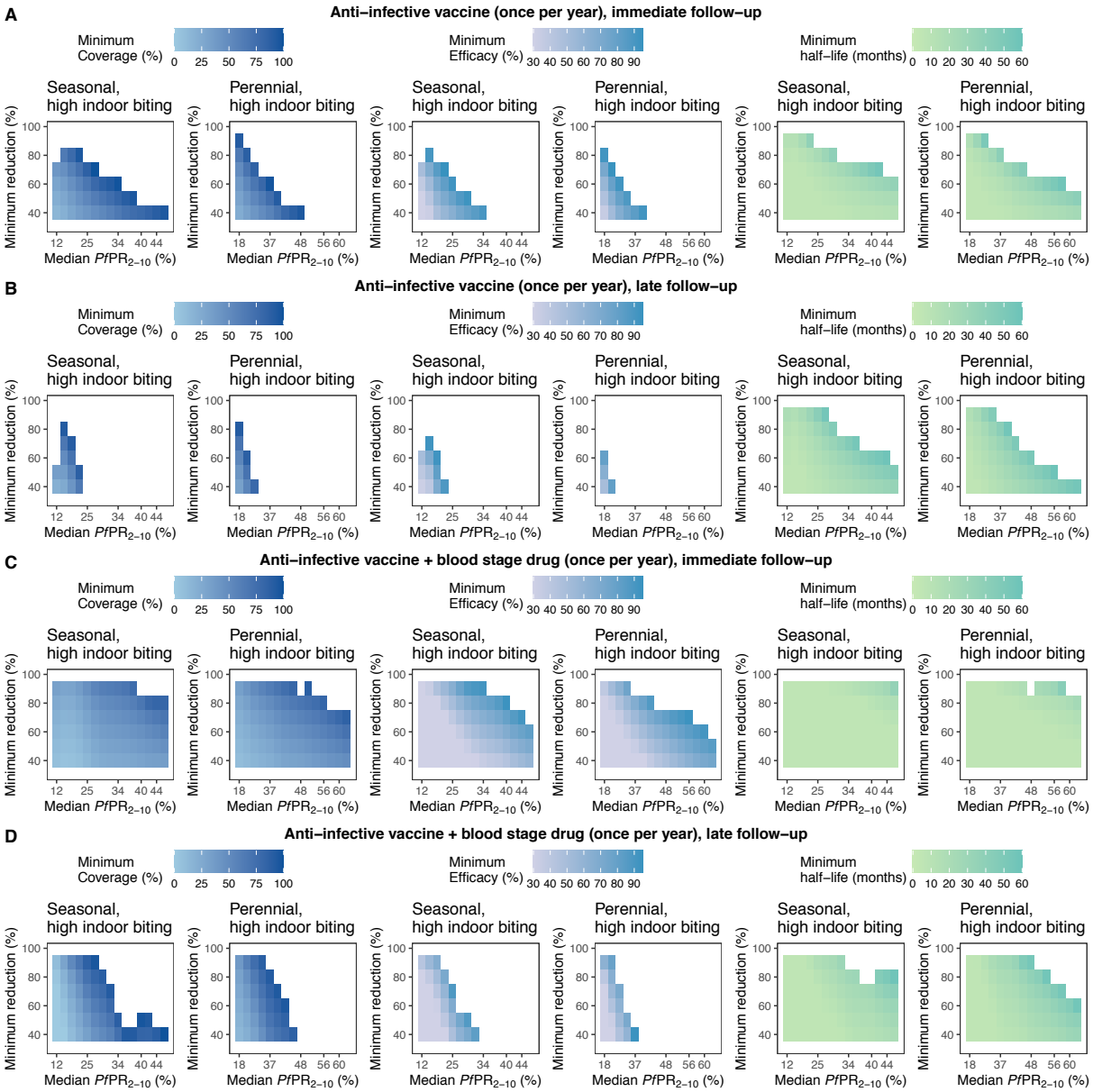

Figure S6.3

Feasible landscapes of optimal, constrained intervention profiles (TPPs) for an anti-infective vaccine deployed once per year.

The heatmaps represent landscapes of optimal, constrained intervention characteristic profiles (minimum coverage, efficacy, and half-life) required to achieve various health goals (quantified by minimal reduction in *Pf*PR$_{0\text{-}99}$, y axis) across different simulated true *Pf*PR$_{2\text{-}10}$ settings (rounded values, x axis) with seasonal transmission and high indoor mosquito biting. Each intervention characteristic was minimized in turn, while keeping the other characteristics fixed (fixed parameter values for each optimization are specified in Table S2.2). Results are shown for an anti-infective vaccine delivered alone and assessing immediate **(A)** and late **(B)** follow up, as well as when delivered in combination with a blood stage drug assessing immediate **(C)** and late **(D)** follow-up. The simulated case management level (E_5) for all the displayed optimization analyses was assumed 25%.

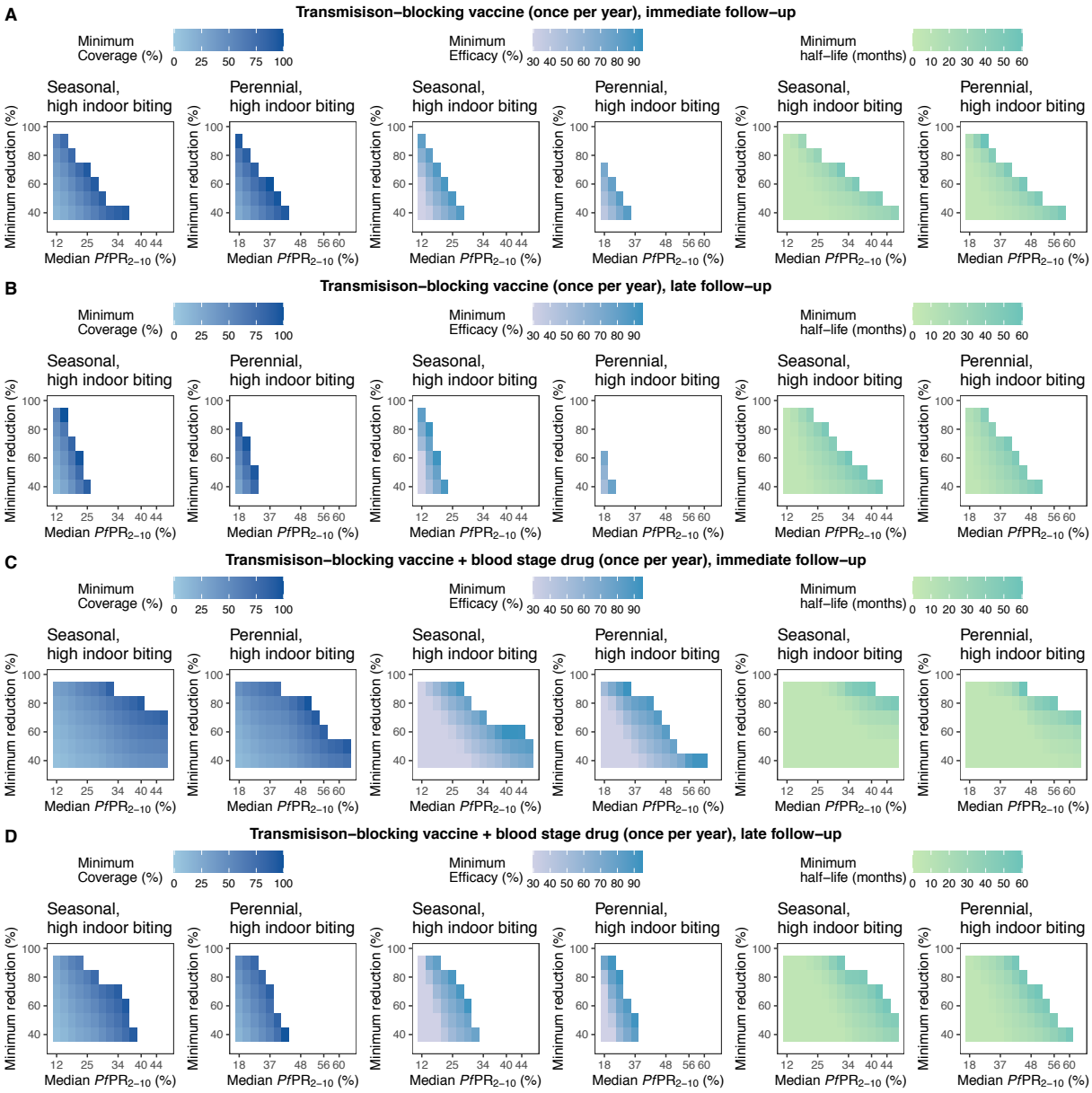

Figure S6.4.

Feasible landscapes of optimal, constrained intervention profiles (TPPs) for a transmission-blocking vaccine deployed once per year.

The heatmaps represent landscapes of optimal, constrained intervention characteristic profiles (minimum coverage, efficacy, and half-life) required to achieve various health goals (quantified by minimal reduction in $Pf\mathrm{PR}_{0\text{-}99}$, y axis) across different simulated true $Pf\mathrm{PR}_{2\text{-}10}$ settings (rounded values, x axis) with seasonal transmission and high indoor mosquito biting. Each intervention characteristic was minimized in turn, while keeping the other characteristics fixed (fixed parameter values for each optimization are specified in Table S2.2). Results are shown for a transmission-blocking vaccine delivered alone and assessing immediate **(A)** and late **(B)** follow up, as well as when delivered in combination with a blood stage drug assessing immediate **(C)** and late **(D)** follow-up. The simulated case management level (E_5) for all the displayed optimization analyses was assumed 25%.

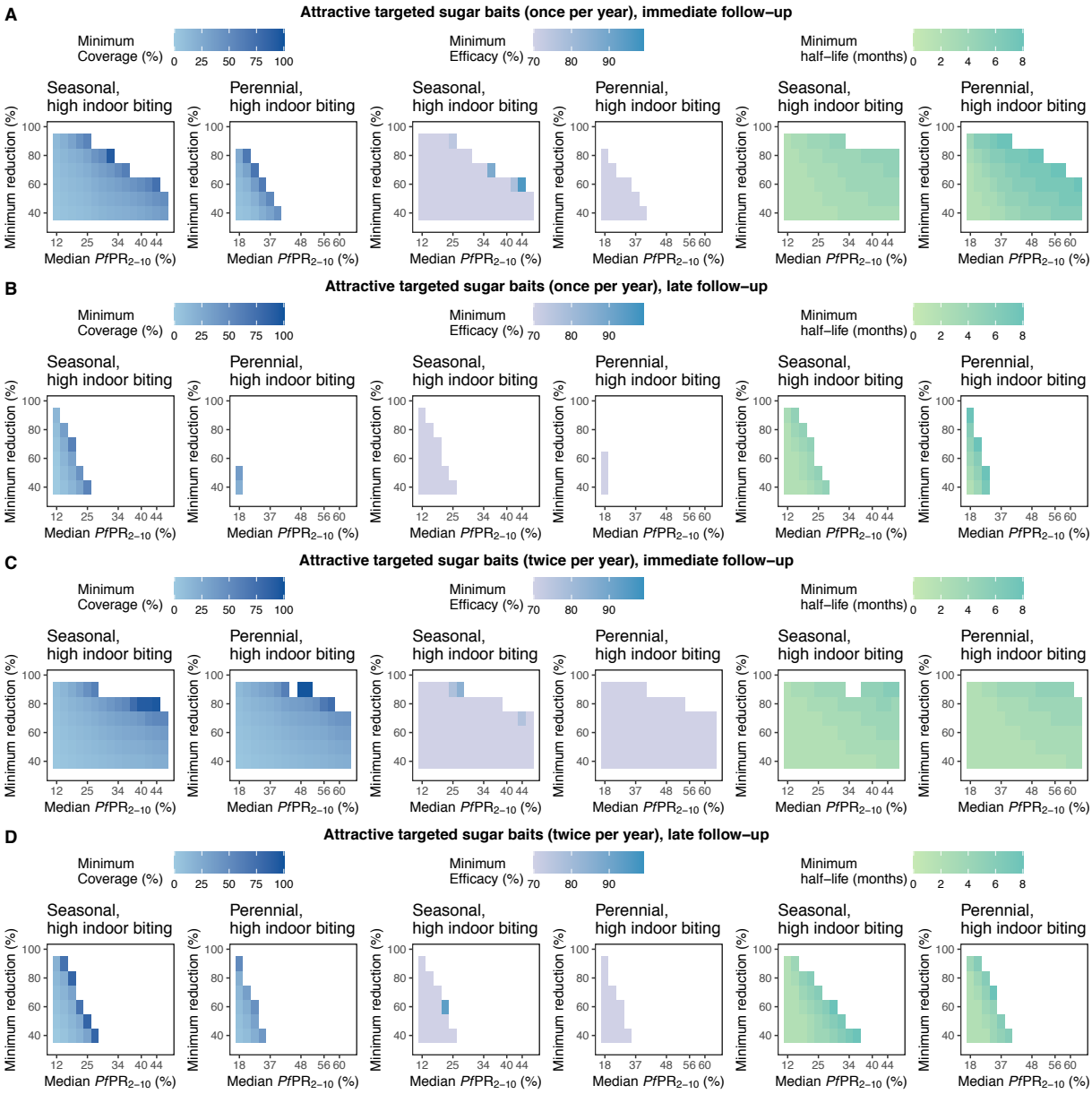

Figure S6.5.

Feasible landscapes of optimal, constrained intervention profiles (TPPs) for attractive targeted sugar baits deployed once or twice per year.

The heatmaps represent landscapes of optimal, constrained intervention characteristic profiles (minimum coverage, efficacy, and half-life) required to achieve various health goals (quantified by minimal reduction in *Pf*PR$_{0\text{-}99}$, y axis) across different simulated true *Pf*PR$_{2\text{-}10}$ settings (rounded values, x axis) with seasonal transmission and high indoor mosquito biting. Each intervention characteristic was minimized in turn, while keeping the other characteristics fixed (fixed parameter values for each optimization are specified in Table S2.2). Results are shown for attractive targeted sugar baits delivered alone once per year and assessing immediate **(A)** and late **(B)** follow up, as well as when delivered twice per year assessing immediate **(C)** and late **(D)** follow-up. The simulated case management level (E_5) for all the displayed optimization analyses was assumed 25%.

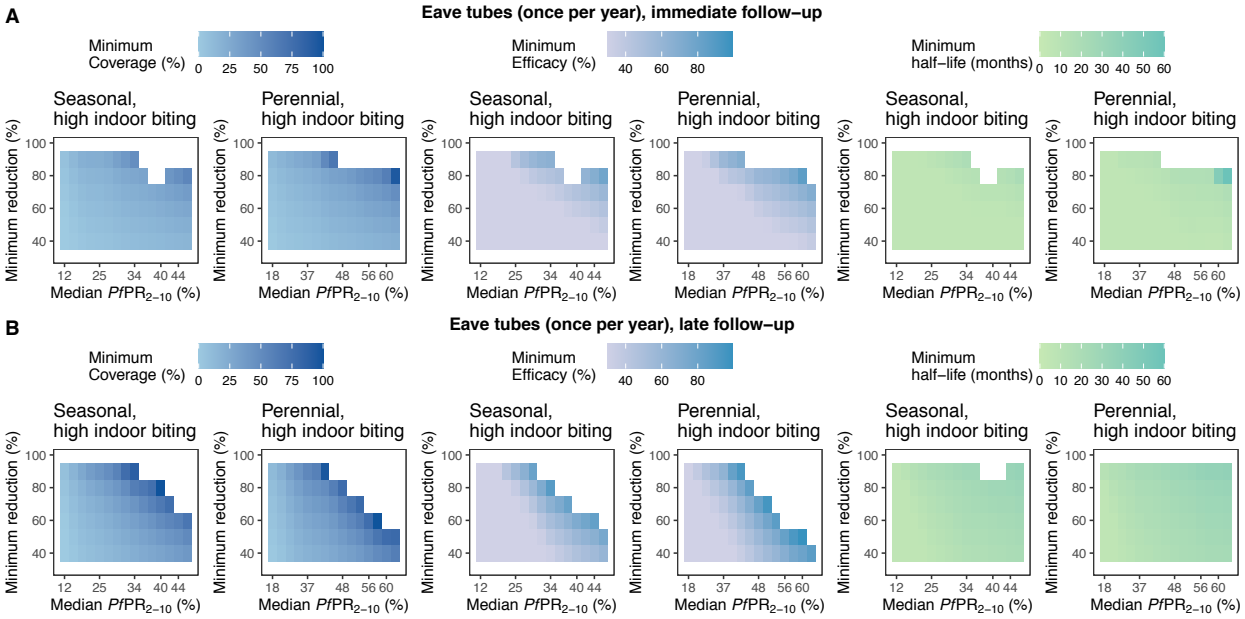

Figure S6.6.

Feasible landscapes of optimal, constrained intervention profiles (TPPs) for eave tubes deployed once per year.

The heatmaps represent landscapes of optimal, constrained intervention characteristic profiles (minimum coverage, efficacy, and half-life) required to achieve various health goals (quantified by minimal reduction in $Pf\mathrm{PR}_{0\text{-}99}$, y axis) across different simulated true $Pf\mathrm{PR}_{2\text{-}10}$ settings (rounded values, x axis) with seasonal or perennial transmission and high indoor mosquito biting (results for other biting patterns not shown as they are similar). Each intervention characteristic was minimized in turn, while keeping the other characteristics fixed (fixed parameter values for each optimization are specified in Table S2.2). Results are shown for eave tubes delivered alone and assessing immediate **(A)** and late **(B)** follow up. The simulated case management level (E_5) for all the displayed optimization analyses was assumed 25%.

7 Results: Optimal intervention profiles

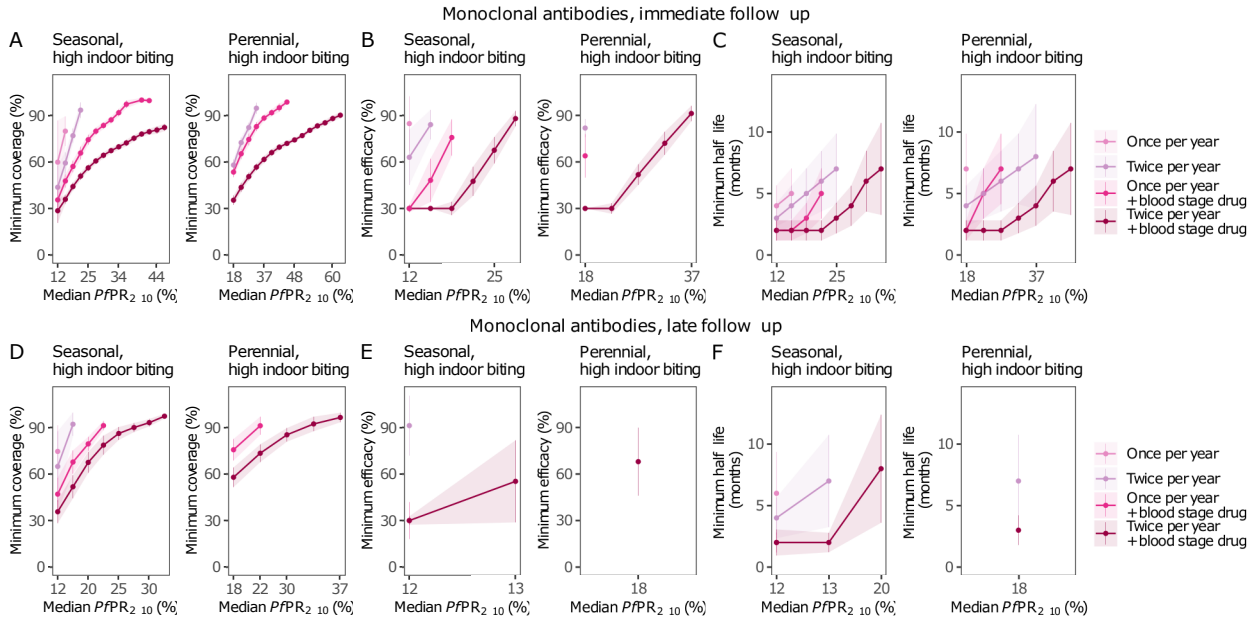

Figure S7.1

Optimal intervention profiles (TPPs) for anti-infective monoclonal antibodies under various deployment regimes to achieve a *Pf*PR$_{0\text{-}99}$ reduction of at least 70%.

Each figure displays minimum, constrained intervention characteristic profiles (minimum coverage, efficacy, and half-life, y axis) required to achieve a minimal reduction in *Pf*PR$_{0\text{-}99}$ of 70% across different simulated true *Pf*PR$_{2\text{-}10}$ settings (rounded values, x axis) with seasonal transmission and high indoor mosquito biting. Each intervention characteristic was minimized in turn, while keeping the other characteristics fixed (fixed parameter values for each optimization are specified in Table S2.2). Results are shown when assessing *Pf*PR$_{0\text{-}99}$ reduction at immediate **(A - C)** and late **(D - F)** follow up. The simulated case management level (E_5) for all the displayed optimization analyses was assumed 25%.

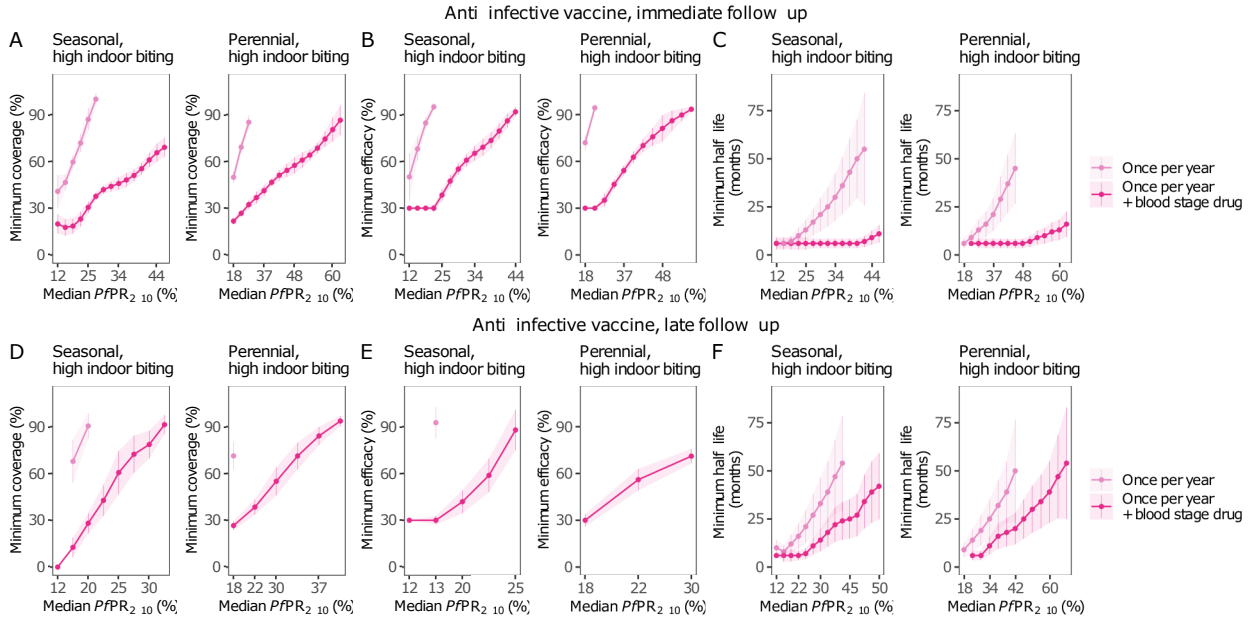

Figure S7.2

Optimal intervention profiles (TPPs) for anti-infective vaccines under various deployment regimes to achieve a *Pf*PR$_{0\text{-}99}$ reduction of at least 70%.

Each figure displays minimum, constrained intervention characteristic profiles (minimum coverage, efficacy, and half-life, y axis) required to achieve a minimal reduction in *Pf*PR$_{0\text{-}99}$ of 70% across different simulated true *Pf*PR$_{2\text{-}10}$ settings (rounded values, x axis) with seasonal transmission and high indoor mosquito biting. Each intervention characteristic was minimized in turn, while keeping the other characteristics fixed (fixed parameter values for each optimization are specified in Table S2.2). Results are shown when assessing *Pf*PR$_{0\text{-}99}$ reduction at immediate **(A - C)** and late **(D - F)** follow up. The simulated case management level (E_5) for all the displayed optimization analyses was assumed 25%.

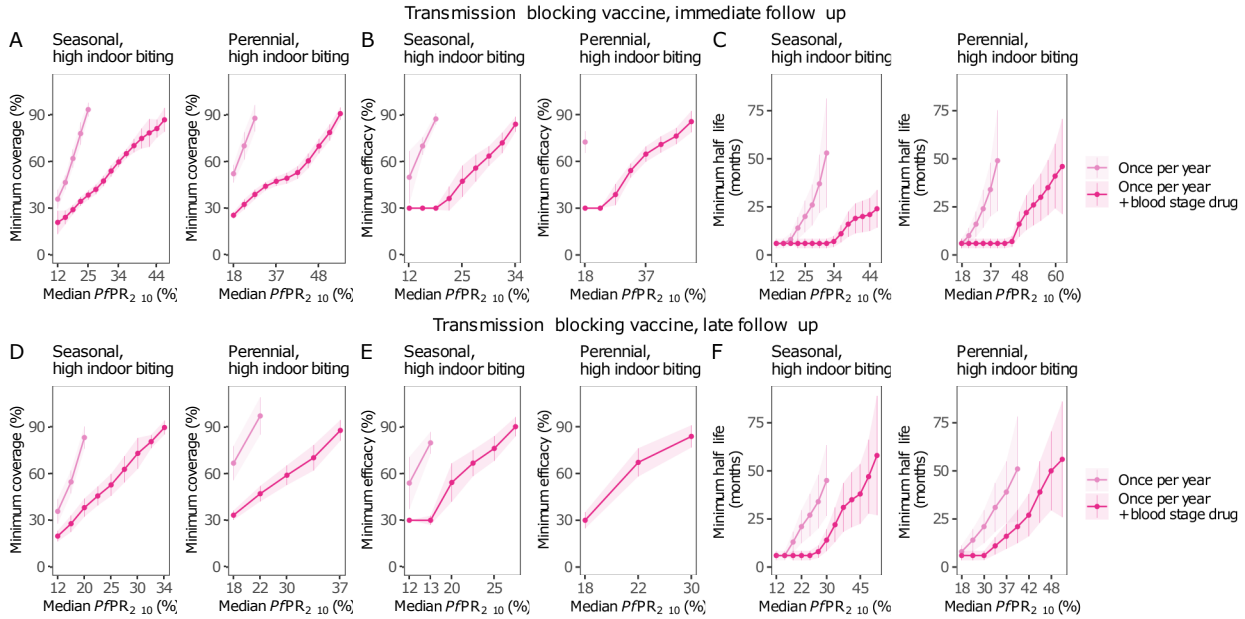

Figure S7.3

Optimal intervention profiles (TPPs) for transmission-blocking vaccines under various deployment regimes to achieve a *Pf*PR$_{0\text{-}99}$ reduction of at least 70%.

Each figure displays minimum, constrained intervention characteristic profiles (minimum coverage, efficacy, and half-life, y axis) required to achieve a minimal reduction in *Pf*PR$_{0\text{-}99}$ of 70% across different simulated true *Pf*PR$_{2\text{-}10}$ settings (rounded values, x axis) with seasonal transmission and high indoor mosquito biting. Each intervention characteristic was minimized in turn, while keeping the other characteristics fixed (fixed parameter values for each optimization are specified in Table S2.2). Results are shown when assessing *Pf*PR$_{0\text{-}99}$ reduction at immediate **(A - C)** and late **(D - F)** follow up. The simulated case management level (E_5) for all the displayed optimization analyses was assumed 25%.

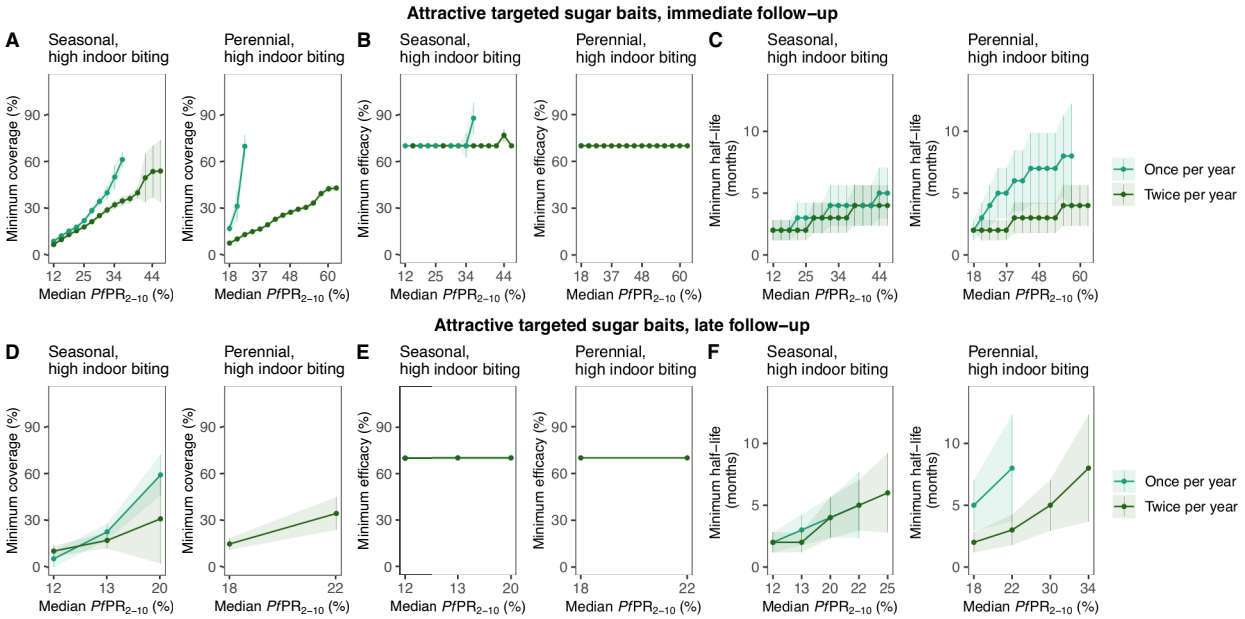

Figure S7.4

Optimal intervention profiles (TPPs) for attractive targeted sugar baits under various deployment regimes to achieve a *Pf*PR$_{0\text{-}99}$ reduction of at least 70%.

Each figure displays minimum, constrained intervention characteristic profiles (minimum coverage, efficacy, and half-life, y axis) required to achieve a minimal reduction in *Pf*PR$_{0\text{-}99}$ of 70% across different simulated true *Pf*PR$_{2\text{-}10}$ settings (rounded values, x axis) with seasonal transmission and high indoor mosquito biting. Each intervention characteristic was minimized in turn, while keeping the other characteristics fixed (fixed parameter values for each optimization are specified in Table S2.2). Results are shown when assessing *Pf*PR$_{0\text{-}99}$ reduction at immediate **(A - C)** and late **(D - F)** follow up. The simulated case management level (E_5) for all the displayed optimization analyses was assumed 25%.

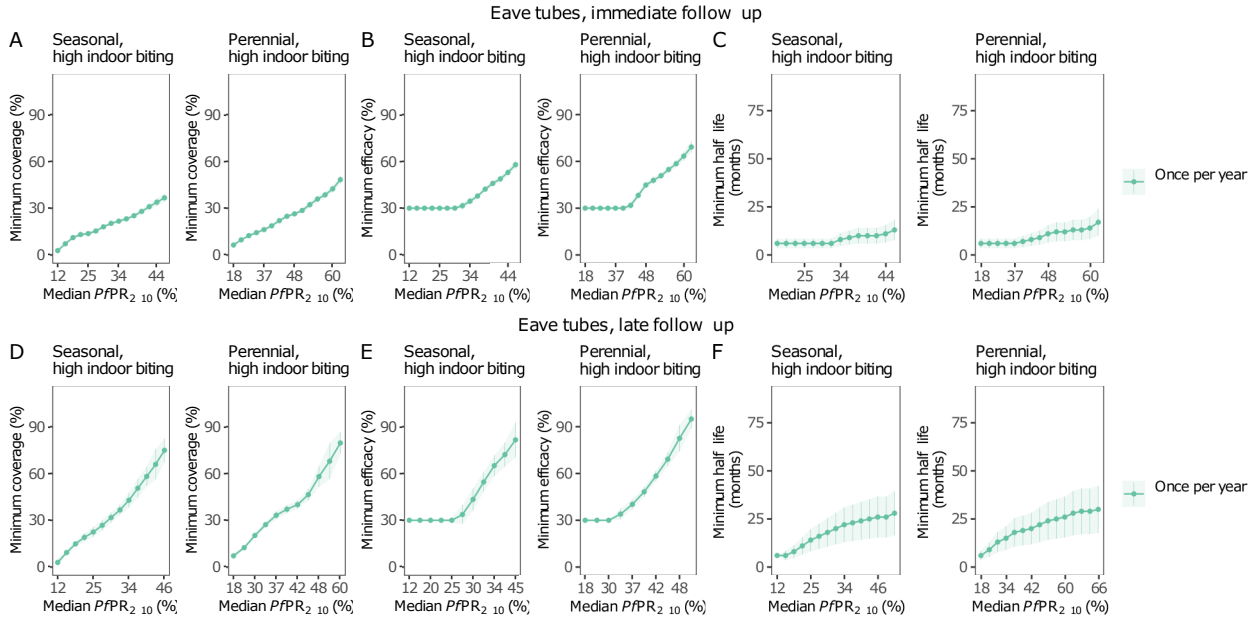

Figure S7.5

Optimal intervention profiles (TPPs) for eave tubes to achieve a *Pf*PR$_{0\text{-}99}$ reduction of at least 70%.

Each figure displays minimum, constrained intervention characteristic profiles (minimum coverage, efficacy, and half-life, y axis) required to achieve a minimal reduction in *Pf*PR$_{0\text{-}99}$ of 70% across different simulated true *Pf*PR$_{2\text{-}10}$ settings (rounded values, x axis) with seasonal transmission and high indoor mosquito biting. Each intervention characteristic was minimized in turn, while keeping the other characteristics fixed (fixed parameter values for each optimization are specified in Table S2.2). Results are shown when assessing *Pf*PR$_{0\text{-}99}$ reduction at immediate **(A - C)** and late **(D - F)** follow up. The simulated case management level (E_5) for all the displayed optimization analyses was assumed 25%.